

Development of Superpave 5 Asphalt Mix Designs for Minnesota Pavements

Mihai Marasteanu, Principal Investigator

Department of Civil, Environmental, and Geo- Engineering
University of Minnesota

JUNE 2022

Research Report
Final Report 2022-18

To request this document in an alternative format, such as braille or large print, call [651-366-4718](tel:651-366-4718) or [1-800-657-3774](tel:1-800-657-3774) (Greater Minnesota) or email your request to ADArequest.dot@state.mn.us. Please request at least one week in advance.

Technical Report Documentation Page

1. Report No. MN 2022-18	2.	3. Recipients Accession No.	
4. Title and Subtitle Development of Superpave 5 Asphalt Mix Designs for Minnesota Pavements		5. Report Date June 2022	
		6.	
7. Author(s) Tianhao Yan, Mihai Marasteanu, Jia-Liang Le, Mugurel Turos, and Kristen Cash		8. Performing Organization Report No.	
9. Performing Organization Name and Address Department of Civil, Environmental, and Geo- Engineering University of Minnesota - Twin Cities 500 Pillsbury Drive, Minneapolis, MN		10. Project/Task/Work Unit No. CTS #2020009	
		11. Contract (C) or Grant (G) No. (c) 1003325 (wo) 106	
12. Sponsoring Organization Name and Address Minnesota Department of Transportation Office of Research & Innovation 395 John Ireland Boulevard, MS 330 St. Paul, Minnesota 55155-1899		13. Type of Report and Period Covered Final Report 2019-2022	
		14. Sponsoring Agency Code	
15. Supplementary Notes https://www.mndot.gov/research/reports/2022/202218.pdf			
16. Abstract (Limit: 250 words) High field density is desired for improving the durability of asphalt pavements. This research aims to develop Superpave 5 mixtures (more compactable than traditional Superpave mixtures) by using locally available materials to improve the field density in Minnesota. First, previous projects in Minnesota were investigated. The mean and standard deviation of field density in Minnesota were about 93.5 % G_{mm} and 1.5 % G_{mm}, respectively. Significant correlations were identified between field density and mix design indices, i.e., N_{design}, NMAS, and fine aggregate angularity (FAA). Four traditional Superpave mixtures were then selected and modified to Superpave 5 mixtures by adjusting their aggregate gradations while maintaining the asphalt binder content. Laboratory performance tests were performed to check the mechanical properties of the modified mixtures. The results showed it was feasible to design Superpave 5 mixtures (more compactable mixtures) by adjusting aggregate gradations, and the improved compactability of the mixtures did not adversely affect the performance of the mixtures for rutting, stiffness, and cracking resistance. Therefore, Superpave 5 mixtures can increase field density as well as other performances of asphalt pavements if implemented.			
17. Document Analysis/Descriptors Field density, Compaction, Asphalt, Mix design, Superpave		18. Availability Statement No restrictions. Document available from: National Technical Information Services, Alexandria, Virginia 22312	
19. Security Class (this report) Unclassified	20. Security Class (this page) Unclassified	21. No. of Pages 155	22. Price

DEVELOPMENT OF SUPERPAVE 5 ASPHALT MIX DESIGNS FOR MINNESOTA PAVEMENTS

FINAL REPORT

Tianhao Yan
Mihai Marasteanu
Jia-Liang Le
Mugurel Tuross
Kristen Cash
Department of Civil, Environmental, and Geo- Engineering
University of Minnesota

June 2022

Published by:

Minnesota Department of Transportation
Office of Research & Innovation
395 John Ireland Boulevard, MS 330
St. Paul, Minnesota 55155-1899

This report represents the results of research conducted by the authors and does not necessarily represent the views or policies of the Minnesota Department of Transportation and/or the University of Minnesota. This report does not contain a standard or specified technique.

The authors, the Minnesota Department of Transportation, and/or the University of Minnesota do not endorse products or manufacturers. Trade or manufacturers' names appear herein solely because they are considered essential to this report.

ACKNOWLEDGMENTS

The authors gratefully acknowledge the financial support provided by the Minnesota Department of Transportation. The guidance provided by the project's Technical Advisory Panel and, in particular, the guidance and technical support provided by Chelsea Bennett, John Garrity, and Gregory Johnson, and the logistical support provided by Project Coordinator David Glycer are acknowledged.

Also acknowledged are Ray Betts, Michael Skurdalsvold, and Joseph Voels from Office of Materials & Road Research (OMRR) for performing part of the experimental work and our colleagues at the North Central Superpave Center for providing some of the materials and sharing the compaction curves for some of the Superpave 5 mixtures used in this study.

Special thanks to Ervin Dukatz and Gerry Huber for providing their expert opinion during the entire duration of the project.

TABLE OF CONTENTS

CHAPTER 1: Introduction	1
1.1 Background	1
1.2 Objective	1
1.3 Organization of the Report	1
CHAPTER 2: Literature Review	2
2.1 Superpave Mix Design	2
2.1.1 Introduction of Superpave Mixture Design	2
2.1.2 Evaluation of Superpave Mix Design	4
2.1.3 Summary	4
2.2 New Developments of mix design after superpave	5
2.2.1 Superpave 5	5
2.2.2 Regressing Air Void	6
2.2.3 Balanced mix design	6
2.2.4 Summary	7
2.3 Compactability of mixtures	7
2.3.1 Compactability Evaluation	8
2.3.2 Effects of Binder Viscosity on Compactability	8
2.3.3 Effects of Binder Lubricity on Compaction	10
2.3.4 Effects of Binder Content on Compaction	11
2.3.5 Effects of Aggregate Gradation on Compactability	11
2.3.6 Effects of Other Aggregate Properties on Compaction	13
2.4 Field Compaction	14
2.4.1 Randomness in Field Density	14
2.4.2 Traffic Compaction	15

2.4.3 Lift Thickness	15
2.4.4 Field Compaction Equipment.....	16
2.5 Implementation of Superpave 5 in Minnesota	17
2.5.1 Current MnDOT Standards	17
2.5.2 Superpave 5 Mix Design at Indiana DOT	20
2.5.3 Possible Changes.....	23
CHAPTER 3: Data Analyses of 2018~2019 projects	25
3.1 Mix Design Information	25
3.2 Aggregate Gradation and Angularity.....	27
3.2.1 Gradation Curves.....	27
3.2.2 Gradation Characterization.....	28
3.2.3 Aggregate Angularity.....	30
3.3 Field Density Data.....	31
3.3.1 Field Density Data for MnDOT Mixtures.....	31
3.3.2 Field Density Data for Indiana Superpave 5 Mixtures	34
3.4 Statistical Analysis OF MnDOT Field Density data.....	34
3.4.1 Analysis of Variance (ANOVA).....	34
3.5 Correlation Analysis between Material Properties and Field Densities	40
3.6 Conclusions	45
CHAPTER 4: Data Analyses of 2020 Projects	47
4.1 mixture Information	47
4.2 Aggregate Gradation and Angularity.....	47
4.2.1 Gradation Curves.....	47
4.2.2 Gradation Characterization.....	49
4.2.3 Aggregate Angularity.....	50

4.3 Field Density Data.....	51
4.3.1 Field Density Data for MnDOT Mixtures.....	51
4.4 Statistical Analysis of MnDOT Field Density Data	55
4.4.1 Analysis of Variance (ANOVA).....	55
4.4.2 Correlation Analysis between Material Properties and Field Densities	56
4.5 Laboratory Gyratory Compaction of Loose mixtures	59
4.6 Conclusions	62
CHAPTER 5: Data Analyses of Superpave 5 projects.....	63
5.1 Mixture Information	63
5.2 Aggregate Gradation and Angularity.....	63
5.2.1 Gradation Curves.....	63
5.2.2 Gradation Characterization.....	65
5.2.3 Aggregate Angularity.....	66
5.3 Field Density.....	67
5.3.1 Field Density Distribution	67
5.3.2 Comparison between Superpave 5 Projects	69
5.4 Comparison between Superpave 5 and Traditional Superpave Projects	70
5.4.1 Comparison of Field Densities.....	70
5.4.2 Comparison of Material Properties.....	73
5.4.3 Comparison of VMA	78
5.5 Performance Tests.....	79
5.5.1 Semi-Circular Bending (SCB) Test.....	80
5.5.2 Flow Number.....	82
5.5.3 Diametral Dynamic Modulus E* 	82
5.6 Conclusions	84

CHAPTER 6: Development of Superpave 5 Mix Designs	85
6.1 Mixture Information	85
6.2 Development of Superpave 5 Mix Designs	86
6.2.1 Project 1 (MSP4-1).....	88
6.2.2 Project 2 (MSP4-2).....	90
6.2.3 Project 3 (MSP4-3).....	92
6.2.4 Project 4 (MSP4-4).....	94
6.2.5 Comparison of Bailey Method Parameters.....	96
6.3 Performance Tests at UMN.....	98
6.3.1 Sample Preparation.....	99
6.3.2 The Semi-Circular Bending (SCB) Test	99
6.3.3 Diametral Dynamic Modulus (E^*) Test	103
6.3.4 Flow Number Test	105
6.3.5 Comparison between SP4 and MSP4	107
6.3.6 Comparison between MSP4 and SP5	110
6.3.7 Comparison between SP4 and SP5.....	113
6.4 Performance Tests at OMRR.....	116
6.4.1 IDEAL-CT.....	116
6.4.2 Hamburg Wheel Tracking Test	118
6.4.3 Disc-shaped Compact Tension Test.....	120
6.5 Consistence of Sample PREPARATION between the two Laboratories.....	121
6.5.1 UMN Test OMRR Samples	121
6.5.2 OMRR Test UMN Samples	123
6.6 Conclusions	125
CHAPTER 7: Summary, Conclusions, and Recommendations	127

LIST OF FIGURES

Figure 2.1 Four steps of Superpave mix design (FHWA, 2000) 2

Figure 2.2 Frequencies of the changes made to the Superpave by different State DOTs. (West et al., 2018)..... 5

Figure 2.3 The relationship between stability and durability with respect to asphalt content (Federal Aviation Administration, 2013) 7

Figure 2.4 Stribeck curve: the relationship between sliding speed and coefficient of friction (Ingrassia, 2018)..... 10

Figure 2.5 Table 2360-7 of the MnDOT construction standard 2360..... 17

Figure 2.6 Table 2360-19 of the MnDOT construction standard 2360..... 18

Figure 2.7 Table 2360-22 of the MnDOT construction standard 2360..... 18

Figure 2.8 Table 2360-23 of the MnDOT construction standard 2360..... 18

Figure 2.9 Table 2360-24 of the MnDOT construction standard 2360..... 19

Figure 2.10 Table 2360-25 of the MnDOT construction standard 2360..... 19

Figure 2.11 Table 3139-2 of the MnDOT construction standard 3139..... 19

Figure 2.12 Design air void ratio in Indiana standard (Indiana DOT, 2019) 20

Figure 2.13 Gyratory compaction effort in the new Indiana standard (Indiana DOT, 2019)..... 20

Figure 2.14 VMA requirements in the new Indiana standard (Indiana DOT, 2019)..... 21

Figure 2.15 Requirements of volume of effective binder in the new Indiana standard (Indiana DOT, 2019) 21

Figure 2.16 Requirements of VFA in the new Indiana standard (Indiana DOT, 2019) 21

Figure 2.17 Pay factor of V_{be} in the new Indiana standard (Indiana DOT, 2019)..... 22

Figure 2.18 Pay factor of design air voids in the new Indiana standard (Indiana DOT, 2019) 22

Figure 2.19 Pay factor of in-place density in the new Indiana standard (Indiana DOT, 2019) 23

Figure 2.20 Recommended field compaction operation in the new Indiana standard (Indiana DOT, 2019)	23
Figure 3.1 Gradation curves of mixtures with NMAAS = 9.5 mm (3/8in)	27
Figure 3.2 Gradation curves of mixtures with NMAAS = 12.5 mm (1/2in)	28
Figure 3.3 Aggregate properties requirements in MnDOT specification (2018)	30
Figure 3.4 Frequency distribution of field cores density data.	31
Figure 3.5 Normal distribution q-q plot for cores density data	32
Figure 3.6 Cumulative distribution function of cores density data	33
Figure 3.7 Frequency distribution of longitudinal joint densities.	33
Figure 3.8 Box plot of the core density data for all projects	35
Figure 3.9 95% confidence intervals for all projects	36
Figure 3.10 Comparison between different NMAAS levels. A stands for 9.5mm (3/8in) and B stands for 12.5mm (1/2in).	38
Figure 3.11 Comparison between different traffic levels.	38
Figure 3.12 Comparison of different NMAAS and traffic levels.	39
Figure 3.13 Correlation between field density and N_{design} .	41
Figure 3.14 Correlations of FAA with N_{design} and field density.	42
Figure 3.15 Correlations between fine aggregate angularity and gradation.	43
Figure 3.16 Correlation between coarse aggregate angularity and nominal maximum aggregate size	44
Figure 3.17 Correlations between gradation properties.	45
Figure 4.1 Gradation curves of type A mixtures with NMAAS = 9.5 mm (3/8in)	48
Figure 4.2 Gradation curves of type B mixtures with NMAAS = 12.5 mm (1/2in)	49
Figure 4.3 Frequency distribution of field cores density data.	52
Figure 4.4 Normal distribution q-q plot for cores density data	52
Figure 4.5 Cumulative distribution function of cores density data	53
Figure 4.6 Boxplot of field density data of each mixture.	53

Figure 4.7 Frequency distribution of longitudinal joint densities (including both confined and unconfined sides).....	54
Figure 4.8 Effect of NMAS on field density.	56
Figure 4.9 Effect of traffic level on field density.	56
Figure 4.10 Diagram of the identified significant correlations.	58
Figure 4.11 Gyratory compaction curves of mix-1 loose mixture.	59
Figure 4.12 Gyratory compaction curves of mix-1 loose mixture.	60
Figure 4.13 Gyratory compaction curves of mix-1 loose mixture.	60
Figure 4.14 Schematic diagram of computing N_{equ} (ρ represents field density).....	61
Figure 4.15 Compaction curves and N_{equ} for mix-1	61
Figure 5.1 Gradation curves of type A mixtures with NMAS = 9.5 mm (3/8in)	64
Figure 5.2 Gradation curves of type B mixtures with NMAS = 12.5 mm (1/2in)	65
Figure 5.3 Frequency distribution of field cores density data.	67
Figure 5.4 Normal distribution q-q plot for cores density data	68
Figure 5.5 Cumulative distribution function of cores density data	68
Figure 5.6 Boxplot of field density data of each mixture.	69
Figure 5.7 Tukey method multiple comparison of different Superpave 5 projects.	70
Figure 5.8 Comparison of the field density distribution between SP5 and traditional SP4 projects.	71
Figure 5.9 Comparison of between the cumulative probability distributions of field densities of SP4 and SP5 projects.	71
Figure 5.10 Comparison of field density distribution between SP5 B3 projects and SP4 B3 projects.	72
Figure 5.11 Comparison of the field density distribution between SP5 A3 projects and SP4 A3 projects.	73
Figure 5.12 Comparison of gradation curves of B3 projects between SP4 and SP5.	74
Figure 5.13 Comparison of gradation curves of A4 projects between SP4 and SP5.	74
Figure 5.14 Comparison of gradation parameters (the error bar indicates the range of the corresponding values).....	76

Figure 5.15 Comparison of asphalt binder content (error bar indicates the range of the corresponding values).....	77
Figure 5.16 Comparison of aggregate angularity (the error bar indicates the range of the corresponding values).....	77
Figure 5.17 Comparison of G_{mm} (the error bar indicates the range of the corresponding values).....	78
Figure 5.18 Comparison of VMA (the error bar indicates the range of the corresponding values).	79
Figure 5.19 Comparison of fracture energy of different mixtures at different temperatures (the error bar indicates the standard error of the mean computed based on three replicates).	81
Figure 5.20 Comparison of fracture toughness of different mixtures at different temperatures (the error bar indicates the standard error of the mean computed based on three replicates).	81
Figure 5.21 Comparison of the flow numbers of different mixtures (the error bar indicates the standard error of the mean computed based on three replicates).....	82
Figure 5.22 $ E^* $ master curves.	83
Figure 6.1 Gradation curves of the SP4 mixtures.....	86
Figure 6.2 Procedure for developing SP5 mix designs.....	87
Figure 6.3 The 0.45 gradation chart for the trial blends of MSP4-1.....	89
Figure 6.4 Compaction curves for MSP4-1 trial blend specimens.	90
Figure 6.5 The 0.45 gradation chart for the trial blends of MSP4-2.....	91
Figure 6.6 Compaction curves for MSP4-2 trial blend specimens.	92
Figure 6.7 The 0.45 gradation chart for the trial blends of SP4-3.....	93
Figure 6.8 Compaction curves for MSP4-3 trial blend specimens.	94
Figure 6.9 The 0.45 gradation chart for the trial blends of MSP4-4.....	95
Figure 6.10 Compaction curves for MSP4-4 trial blend specimens.....	96
Figure 6.11 CA ratio of the SP4 and MSP4 mix designs	97
Figure 6.12 FAc ratio of the SP4 and MSP4 mix designs.....	97
Figure 6.13 FAF ratio of the SP4 and MSP4 mix designs	98
Figure 6.14 Comparison of fracture energy of the different mixture groups, SP4, MSP4, and SP5, at their respective actual low temperature and -12°C.	101

Figure 6.15 Comparison of fracture toughness of different mixture groups, SP4, MSP4, and SP5, at their respective actual low temperature and -12°C.	102
Figure 6.16 Master curves for each mixture group at the reference temperature of 12°C.	105
Figure 6.17 Comparison of the flow numbers of the different mixture groups at 49°C.	107
Figure 6.18 Comparison of fracture energy between SP4 and MSP4 at -12°C and the lowest temperature.	108
Figure 6.19 Comparison of fracture toughness between SP4 and MSP4 at -12°C and the lowest temperature.	108
Figure 6.20 Comparison of $ E^* $ values between SP4 and MSP4 groups. 12°C was the reference temperature that was chosen.	109
Figure 6.21 Comparison of flow numbers between SP4 and MSP4 group at 49°C.	110
Figure 6.22 Comparison of fracture energy between MSP4 and SP5 at -12°C and the lowest temperature.	111
Figure 6.23 Comparison of fracture toughness between MSP4 and SP5 at -12°C and the lowest temperature.	111
Figure 6.24 Comparison of $ E^* $ values between MSP4 and SP5 groups. 12°C was the reference temperature that was chosen.	112
Figure 6.25 Comparison of flow numbers between the MSP4 and SP5 groups at 49°C.	113
Figure 6.26 Comparison of fracture energy between SP4 and SP5 at -12°C and the lowest temperature.	114
Figure 6.27 Comparison of fracture toughness between SP4 and SP5 at -12°C and the lowest temperature.	114
Figure 6.28 Comparison of $ E^* $ values between SP4 and SP5 groups. 12°C was the reference temperature that was chosen.	115
Figure 6.29 Comparison of flow numbers between the MSP4 and SP5 groups at 49°C.	116
Figure 6.30 Displacement vs. stability results of a replicate of SP41.	117
Figure 6.31 Comparison of fracture energy of SP4 and MSP4 mixtures.	118
Figure 6.32 Comparison of CT-index of SP4 and MSP4 mixtures.	118
Figure 6.33 Hamburg wheel tracking test results of SP41.	119

Figure 6.34 DCT fracture energy of MSP44 and SP44 mixtures.....	120
Figure 6.35 Comparison of E* master curves of UMN and OMRR samples of SP44.	121
Figure 6.36 Comparison of flow numbers of UMN and OMRR samples of SP44.....	122
Figure 6.37 Comparison of the SCB Gf and K _{1c} of UMN and OMRR samples of SP44.....	122
Figure 6.38 Comparison of the CTindex of UMN and OMRR samples of SP44.....	123
Figure 6.39 Comparison of the DCT Gf of UMN and OMRR samples of SP44.	123
Figure 6.40 Hamburg wheel track test results of the OMRR samples of SP44.	124
Figure 6.41 Hamburg wheel track test results of the UMN samples of SP44.....	125

LIST OF TABLES

Table 2.1 Superpave compaction effort (AASHTO R35, 2012).....	3
Table 2.2 Volumetric requirements at different critical gyration numbers (AASHTO M 323, 2005)	3
Table 2.3 Summary of the Bailey Method	13
Table 3.1 Summary of MnDOT mixtures with NMAS = 9.5mm (3/8in)	25
Table 3.2 Summary of MnDOT mixtures with NMAS = 12.5 mm (1/2in)	26
Table 3.3 Summary of Indiana Superpave 5 mixtures.....	26
Table 3.4 Bailey Method Parameters for MnDOT mixtures with NMAS = 9.5mm (3/8in)	29
Table 3.5 Bailey Method Parameters for MnDOT mixtures with NMAS = 12.5mm (1/2in)	29
Table 3.6 Bailey Method Parameters for Indiana Superpave 5 mixtures.....	29
Table 3.7 Aggregate angularity	31
Table 3.8 Basic statistics of field cores density data	32
Table 3.9 Basic statistics of longitudinal joint density data	34
Table 3.10 One-Way ANOVA of the all projects.....	35
Table 3.11 Estimated values of mean and standard error by Tukey method.....	36
Table 3.12 Two-Way ANOVA for all projects	37

Table 3.13 Estimated values of mean and standard error of projects grouped by NMAAS.	38
Table 3.14 Estimated value of means and standard errors of projects grouped by traffic levels.	39
Table 3.15 Estimated value of means and standard errors of projects grouped by NMAAS and traffic levels.	40
Table 3.16 P-values for the correlation analysis	40
Table 3.17 Correlation coefficients	41
Table 4.1 Summary of the mixtures used in the ten 2020 MnDOT projects	47
Table 4.2 Bailey Method Parameters for 2020 MnDOT mixtures.	50
Table 4.3 Aggregate angularity	51
Table 4.4 Basic statistics of field cores density data	51
Table 4.5 Mean and standard deviation (std.) of field density data for each mixture.....	54
Table 4.6 Basic statistics of longitudinal joint density data	54
Table 4.7 Anova results	55
Table 4.8 p-values for the correlation analysis	57
Table 4.9 Coefficients of correlation	57
Table 4.10 Air voids at N_{design} and N_{equ} values	60
Table 5.1 Summary of the Superpave 5 mixtures	63
Table 5.2 Summary of the aggregate gradations of the Superpave 5 mixtures	64
Table 5.3 Bailey Method Parameters for Superpave 5 mixtures.	66
Table 5.4 Aggregate angularity	66
Table 5.5 Basic statistics of field cores density data	67
Table 5.6 Mean and standard deviation (std.) of field density data for each mixture.....	69
Table 5.7 ANOVA table of the comparison between different Superpave 5 projects	69
Table 5.8 Comparison of the basic statistics of field densities between SP5 and traditional SP4 projects.	71
Table 5.9 ANOVA table of the comparison between field densities of SP5 and SP4 projects.	72

Table 5.10 Comparison of basic statistics of field densities between SP5 and SP4 projects in B3 category.	72
Table 5.11 ANOVA table of the comparison between field densities of SP5 and SP4 projects in the B3 category.	72
Table 5.12 Comparison of the basic statistics of field densities between SP5 and traditional SP4 projects in the A4 category.	73
Table 5.13 ANOVA table of the comparison between field densities of SP5 and SP4 projects in the A4 category.	73
Table 5.14 Material properties of B3 projects.	75
Table 5.15 Material properties of A4 projects.	75
Table 5.16 VMA of B3 mixtures.	78
Table 5.17 VMA of A4 mixtures.	78
Table 5.18 Air voids and number of gyrations for the gyratory compacted samples.	79
Table 5.19 Test temperature and replicates.	80
Table 5.20 SCB fracture energy.	80
Table 5.21 SCB fracture toughness.	80
Table 5.22 Flow number.	82
Table 5.23 $ E^* $ test results.	83
Table 6.1 Basic information for the selected SP4 projects.	85
Table 6.2 Summary of aggregate angularity values for the selected SP4-4 projects.	86
Table 6.3 Weight percentage of aggregate sources and virgin binder content for MSP4-1 trial blends ...	88
Table 6.4 Gradations for MSP4-1 trial blends.	88
Table 6.5 Compaction data for MSP4-1 trials.	89
Table 6.6 Weight percentage of aggregate sources and virgin binder content for MSP4-2 trial blends ...	90
Table 6.7 Gradations for MSP4-2 trial blends.	91
Table 6.8 Compaction data for MSP4-2 trials.	91
Table 6.9 Weight percentage of aggregate sources and virgin binder content for MSP4-3 trial blends ...	92

Table 6.10 Gradations for MSP4-3 trial blends	93
Table 6.11 Compaction data for MSP4-3 trials	93
Table 6.12 Weight percentage of aggregate sources and virgin binder content for MSP4-4 trial blends .	94
Table 6.13 Gradation and aggregate packing fraction for MSP4-4 trial blends.....	95
Table 6.14 Compaction data for MSP4-4 trials	95
Table 6.15 Bailey method parameters of the SP4 and MSP4 mix designs	97
Table 6.16 Summary of the Superpave 5 mixtures	98
Table 6.17 Test temperatures for performance tests	99
Table 6.18 SCB fracture energy.....	100
Table 6.19 SCB fracture toughness.....	100
Table 6.20 E* test results	103
Table 6.21 Flow number	106
Table 6.22 IDEAL- CT results	117
Table 6.23 Hamburg wheel tracking test results.....	119

EXECUTIVE SUMMARY

Field density is essential for the durability of asphalt pavements. This research aims to develop Superpave 5 mixtures (more compactable than traditional Superpave mixtures) by using locally available materials to improve the field density in Minnesota.

First, field density and material properties data of previous projects were analyzed. It was found that the field densities of these projects exhibited considerable randomness. They approximately followed normal distributions, while consistently exhibiting left-skewed and leptokurtic features. The mean field density and standard deviation of the previous projects in Minnesota were about 93.5 % G_{mm} and 1.5 % G_{mm} , respectively. The correlation analysis showed that 1) mixtures designed for a higher traffic level tended to have lower field density; 2) mixtures with larger aggregate size (NMAS) tended to have lower field density; 3) mixtures harder to compact in the laboratory (designed by higher N_{design}) tended to have lower field density; and 4) mixtures with higher fine aggregate angularity (FAA) tended to have lower field density. Gyratory compaction tests of loose mixtures from constructed projects showed that, regardless of the traffic level, 30 gyrations approximately represented the field compaction effort in Minnesota, and thus can be used as the N_{design} for the Superpave 5 mix design.

Four traditional Superpave mixtures in Minnesota were selected and then modified to Superpave 5 mixtures by changing their aggregate gradations while keeping their binder contents unchanged. The results showed that it was feasible to improve the compactability of mixtures by adjusting aggregate gradation, and therefore to design Superpave 5 mixtures. Performance tests on the rutting, stiffness, and cracking resistance of mixtures were also conducted. The results showed that, in general, the Superpave 5 mixtures performed better than the traditional Superpave mixtures.

This research demonstrated a feasible approach to designing Superpave 5 mixtures using local materials and small changes in the gradation of the aggregates currently used in the traditional Superpave design.

CHAPTER 1: INTRODUCTION

1.1 BACKGROUND

Recent studies have shown that the air void ratio of hot mix asphalt (HMA) has a significant effect on the durability and long-term performance of asphalt pavements. MnDOT HMA pavements are typically constructed with air voids close to 7% in the mat and often exceeding 10% over the longitudinal construction joints. Recent efforts in Indiana have shown that a new mix design method, called Superpave 5, can be used to design mixtures at 5% air voids and to successfully compact them in the field at the same 5% air voids, a significant decrease compared to current practice. According to a study performed for the Wisconsin Department of Transportation (WSDOT), each 1% increase in air voids results in about 10% loss in pavement service life (Willoughby and Mahoney, 2007).

1.2 OBJECTIVE

The objective of this research is to develop Superpave 5 mix designs for various traffic levels using local aggregates to improve the field density in Minnesota.

1.3 ORGANIZATION OF THE REPORT

First, a comprehensive literature review is conducted in Chapter 2, summarizing the previous research efforts on compaction and field density of asphalt mixtures. In Chapter 3, field density and material properties of previous projects constructed in 2018 and 2019 are investigated to reveal the current situation of field density in Minnesota. Correlations between field density and material properties are identified from the data. Similar analyses are performed in Chapter 4 for ten additional projects constructed in 2020. Chapter 5 investigates the field density and material properties of three Superpave 5 projects constructed in Minnesota in 2020. In Chapter 6, four traditional Superpave mixtures are selected to be modified to Superpave 5 mixtures by adjusting their aggregate gradations. Laboratory performance tests are performed to check the mechanical properties of the modified mixtures. Chapter 7 consists of a summary of the work followed by conclusions and recommendations.

CHAPTER 2: LITERATURE REVIEW

In this chapter, a comprehensive literature review was performed related to field and laboratory compaction. The review includes MnDOT Standard specifications 2360 and 3139 to identify the most significant items that would be proposed for change in the currently being developed MnDOT Superpave 5 mix design. Information about the Superpave 5 mix design currently used in Indiana is also included.

2.1 SUPERPAVE MIX DESIGN

2.1.1 Introduction of Superpave Mixture Design

To address the increased deterioration of asphalt pavements in the late 1970s and the 1980s, in 1987 the US Congress established a 5-year, \$150 million research program aimed at improving the performance, durability, safety, and efficiency of the Nation's highway system. The program was called Strategic Highway Research Program (SHRP). Its main objectives were to develop a performance-based asphalt binder specification, a performance-based asphalt mixture specification, and a mixture design system.

The performance-based (PG) asphalt binder specification, was very successful and was implemented in the United States as well as other countries. The performance-based mixture specification, known as Superpave (SUperior PERforming Asphalt PAVements), was less successful. Though performance tests and prediction models were developed, the system was too difficult to implement, and was never used in practice (Huber, 2013).

Instead, the Superpave mix design remained a volumetric design method that consists of four basic steps: 1) materials selection; 2) design of aggregate structure; 3) determining design binder content; and 4) check moisture sensitivity, as shown in Figure 2.1.

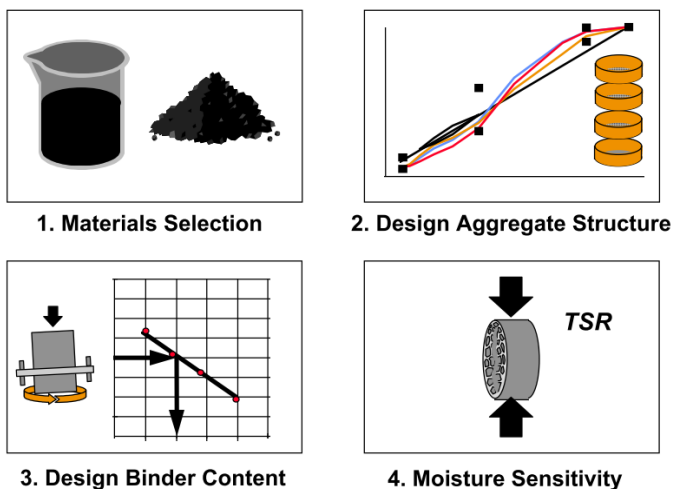


Figure 2.1 Four steps of Superpave mix design (FHWA, 2000)

The Superpave gyratory compactor (SGC) was widely adopted as the laboratory compaction method, since the gyratory loading better simulated the densification process of mixture in the field (McDaniel et al., 2011).

In Superpave, it is assumed that the mixture is designed to its ultimate density in the field, which is achieved usually after 2 to 3 years of traffic compaction. As a consequence, the laboratory compaction effort (N_{design}) was chosen to reflect both the construction compaction and the traffic compaction. Table 2.1 shows the critical gyration numbers ($N_{initial}$, N_{design} , and $N_{maximum}$) for roads with different traffic levels. They are determined from a linear regression between the logarithm of ESAL (equivalent single axle load) and the logarithm of gyration number (Blankenship et al, 1994). The idea of relating the laboratory compaction effort to traffic volume originated from Marshall mix design, where the blow number of Marshall compactor was related to the traffic volume (White, 1985).

Table 2.1 Superpave compaction effort (AASHTO R35, 2012)

Design 20-year Traffic level (million ESALs)	Compaction Parameter		
	$N_{initial}$	N_{design}	$N_{maximum}$
<0.3	6	50	75
0.3 to <3.0	7	75	115
3.0 to <30.0	8	100	160
>30.0	9	125	205

Superpave is a volumetric design method. The volumetric properties are determined by their relation with pavement performance. If in-place density of the pavement is too low (<93% G_{mm}), it will result in increased permeability to water and excessive binder oxidization, causing moisture damage, cracking, and raveling. If in-place density is too high (>97% G_{mm}), the pavements will tend to bleed, rut, and have less skid resistance (Linden et al., 1989; Brown, 1990; Cooley et al., 2001). Table 2.2 shows the volumetric requirements of Superpave at different critical gyration numbers. As shown, a 96% G_{mm} is the design ultimate density that is required to be achieved at N_{design} . The other requirement of density and VMA (Voids in mineral aggregate) are mainly for preventing tender mixtures that are prone to rutting. For example, a maximum density is also required at the $N_{initial}$, and $N_{maximum}$ respectively, and a minimum VMA is required at N_{design} .

Table 2.2 Volumetric requirements at different critical gyration numbers (AASHTO M 323, 2005)

Design 20-year Traffic level (million ESALs)	% G_{mm}			Min. VMA at N_{design}						VFA at N_{design}	Dust to Binder Ratio
	$N_{initial}$	N_{design}	$N_{maximum}$	NMAS mm							
				37.5	25	19	12.5	9.5	4.75		
<0.3	≤91.5	96	≤98	11	12	13	14	15	16	70-80	0.6-1.2
0.3 to <3.0	≤90.5	96	≤98	11	12	13	14	15	16	65-78	0.6-1.2
3.0 to <10.0	≤89	96	≤98	11	12	13	14	15	16	65-75	0.6-1.2
3.0 to <30.0	≤89	96	≤98	11	12	13	14	15	16	65-75	0.6-1.2
>30.0	≤89	96	≤98	11	12	13	14	15	16	65-75	0.6-1.2

2.1.2 Evaluation of Superpave Mix Design

After SHRP, many studies have been conducted to evaluate the validity of Superpave mix design. Mixtures designed by Superpave are generally shown to have sufficient resistance to rutting distress. However, some mixtures were designed too dry (too low asphalt binder content) and were hard to compact and had durability issues (FHWA, 2010; Prowell and Brown, 2007). This is understandable, because at the time when Superpave was developed, rutting was the most prevalent distress, and the main focus was on preventing rutting.

In Superpave, the philosophy is to match the laboratory design density of mixtures to the ultimate density in the field, whereas the as-constructed density of mixture is not designed or controlled in the mix design process. As a result, higher than desired as-constructed air voids have been reported in many field studies (Prowell and Brown, 2007; Brown et al., 2004; Harmelink and Aschenbrener, 2002). The as-constructed state should be of equal importance as the ultimate state. Mixtures should perform as designed immediately after construction. The high as-constructed air voids is likely to cause premature distress related to durability (water damage, cracking, and raveling) even before the mixture reaches the ultimate density.

A number of studies showed that the N_{design} level was chosen higher than needed and should be reduced. A study conducted by Colorado DOT indicated that the in-place air voids after 5 to 6 years of traffic were higher than those obtained at N_{design} by SGC (Harmelink and Aschenbrener, 2002). In an NCHRP report, Prowell and Brown (2007) showed that 55% of the 40 projects studied had as-constructed densities less than 92% of G_{mm} , and 78% projects had as-constructed densities less than desired (93% of G_{mm}). The average ultimate density was 94.6% of G_{mm} , which was also less than the design density, 96% of G_{mm} . This research recommended a reduction of N_{design} , which the authors believed, if adopted, would lead to more compactable mixture and increased durability. Federal Highway Administration (FHWA) evaluated the recommendation of reducing N_{design} , but did not adopt the suggestion, because the data was too variable for a blanket national acceptance of the proposed N_{design} tables. Instead, FHWA suggested state highway agencies should perform independent evaluations to make adjustments to the N_{design} level (FHWA, 2010). A field density investigation in Minnesota showed that the average field density is about 93.5% G_{mm} (Yan et al., 2021b) and the compaction effort is equivalent to about 30 gyrations in laboratory gyratory compaction (Yan et al., 2022b).

2.1.3 Summary

The Superpave mix design has been shown to be effective in preventing rutting distress, however, it also produced stiffer and dryer mixtures which resulted in inadequate compaction and in durability issues. These issues are not addressed in the current Superpave mix design, and the main reason is the design does not have a minimum as-constructed density requirement.

2.2 NEW DEVELOPMENTS OF MIX DESIGN AFTER SUPERPAVE

After the implementation of Superpave in the 1990s, many agencies have reported that, although rutting distress has been virtually eliminated, the durability related distresses, e.g. cracking, moisture damage and raveling, have become the primary factors controlling the service life of asphalt pavements.

Changes have been made to Superpave by Highway agencies to improve mixtures' durability. The following are the most commonly used methods:

1. Lowering gyration levels (N_{design});
2. Increasing the minimum VMA;
3. Lowering air void ratio;
4. Performing air voids regression (add 0.5~1.0% binder).

The results of these changes are nothing more than either increasing binder content or changing aggregate gradation to get a denser packing of aggregates.

A survey on the changes to the Superpave made by different State DOTs has been conducted by National Center of Asphalt Technology (NCAT). The frequencies of these changes (and the changes related to RAP and RAS) are shown in Figure 2.2 (West et al., 2018).

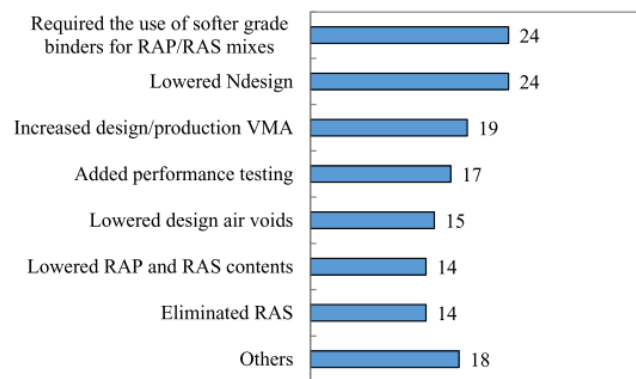


Figure 2.2 Frequencies of the changes made to the Superpave by different State DOTs. (West et al., 2018)

Three representative approaches to modify Superpave are reviewed in this section. They are Superpave 5, Regressing Air Voids, and the Balanced Mix Design Method.

2.2.1 Superpave 5

Superpave 5 was developed by Indiana DOT and Purdue University in the past five years (Hekmatfar et al., 2015; Huber et al., 2016). In the traditional Superpave design, a mixture is designed at 4% air voids, but usually it is compacted to about 7~8% air voids during construction. In Superpave 5, the mix is designed at 5% air voids and is also compacted to 5% air voids during construction. It is assumed that the reduction of as-constructed air voids improves durability of pavements.

Compared to traditional Superpave, Superpave 5 significantly decreases N_{design} , increases design air voids by 1% from 4% to 5%, and the VMA also increases by 1% to maintain the effective binder content typically used in the traditional Superpave. The reduction of N_{design} is achieved by adjusting aggregates gradation to be closer to the maximum density line to make the mixture more compactable (Huber et al., 2016).

Unlike the traditional Superpave, in which N_{design} is related to the design traffic volume, in Superpave 5 the mixture is compacted directly to the ultimate density during construction, and the N_{design} is related to the construction compaction efforts rather than the design traffic volume. Such a design philosophy of Superpave 5 was inspired by the LCPC (Laboratoire Central des Ponts et Chaussées) mixture design method developed in France (Huber et al., 2016).

Superpave 5 was validated by performance tests for rutting and cracking. It was shown that at the as-constructed state, properties of Superpave 5 mixtures (5% air voids) performed better than or at least as well as the traditional Superpave mixtures (7% air voids) (Hekmatfar et al., 2015). The field trial section also showed that mixtures designed by Superpave 5 can be compacted to 5% air voids in the field without any change in the current compaction operations.

Superpave 5 shows a lot of promise, however, there are still a few questions that remain unanswered. For example, if 5% air voids represent the optimum in-place field density, and if the reduction in N_{design} would adversely affect the rutting resistance of the mixtures.

2.2.2 Regressing Air Void

Another method to improve durability was proposed by Wisconsin DOT (WisDOT), called “regressing air voids”. This method starts with the traditional Superpave which designs a mix for 4.0% air voids, which is the current WisDOT practice, and then predicts the amount of additional asphalt binder needed to achieve an air-void ratio of 3.5% or 3.0%, which typically results in a 0.3 to 0.4% increase in binder content (West and Hefel, 2018).

A number of studies investigated the effect on mechanical properties of mixtures designed with this method, such as cracking, rutting, and moisture damage resistance. The performance tests included the Illinois Flexibility Index Test to evaluate intermediate temperature cracking resistance, the Disc-Shaped Compacted Tension for low-temperature cracking resistance, and the Hamburg Wheel Tracking Test for rutting and moisture resistance. The results indicate that the regressed air voids concept can improve mixture cracking resistance without compromising the rutting resistance of asphalt mixes (West et al., 2018).

2.2.3 Balanced mix design

In the Balanced Mix Design, the mixture is designed to balance between rutting resistance and cracking resistance. The relationship between stability and durability with the changing of binder content is illustrated in Figure 2.3. An optimum asphalt content is achieved to balance stability and durability performance (West et al., 2018).

Balanced Mix Design emphasized the limitation of volumetric design method and the importance of incorporating performance-based tests into mixture design.

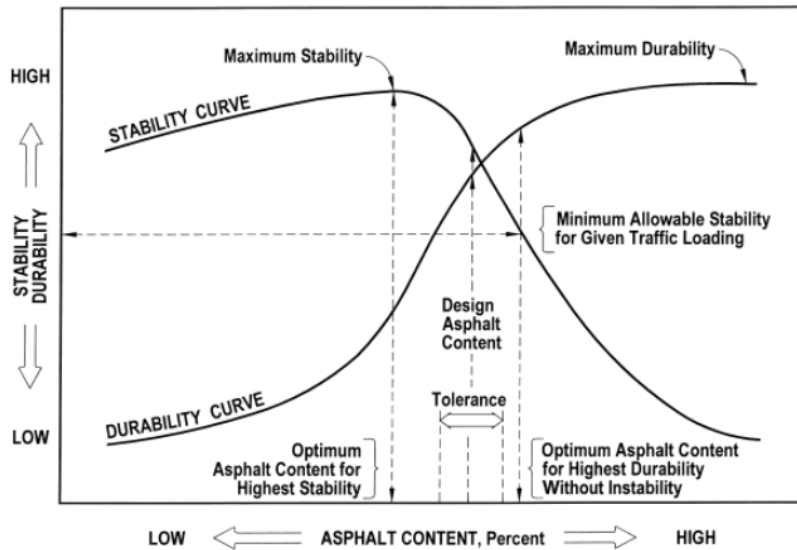


Figure 2.3 The relationship between stability and durability with respect to asphalt content (Federal Aviation Administration, 2013)

2.2.4 Summary

After the implementation of Superpave, the most common pavement distress changed from rutting to distresses related to durability, e.g., cracking, raveling and water damage.

Many modifications to Superpave have been proposed to improve durability. Most of these modifications relied in either an increase in binder content, or a change in aggregate gradation, or a combination of both. For example, Superpave 5 changes aggregate gradation. Regressing Air Voids and the Balanced Mix Design optimize binder content.

2.3 COMPACTABILITY OF MIXTURES

The durability of mixtures is affected not only by mixture design, but also by compaction during construction. A mediocre mix that is well-constructed usually performs better than a good mix that is poorly constructed. Compaction has a significant effect on pavements performance, and affects all major distresses commonly observed in asphalt pavements (Finn and Epps, 1980; Hughes, 1989; Linden et al., 1989; Vivar and Haddock, 2006; Willoughby and Mahoney, 2007, Marasteanu et al., 2019). Therefore, improving compaction is the key in improving durability. The compaction of mixture is affected by two aspects: the compactability of mixture and field compaction operations. This section focuses on the current studies on the compactability of mixtures. Research on field compaction is covered in the next section.

2.3.1 Compactability Evaluation

Many research efforts were performed with the goal to understand the compaction process. As part of these research efforts, different indices were proposed to interpret the compaction curves obtained from the Superpave Gyratory Compactor (SGC). The first was the slope of the compaction curve in the semi-logarithmic plot, as a result of the linear relationship between density and the logarithm of the gyrations number found by Moutier (1974). This index is widely used as an indicator of the overall compactability.

Another proposed index is the “locking point”. A closer look at the compaction curve in the semi-logarithmic plot shows that it is not entirely linear. Rather, it begins to level off at a certain number of gyrations. This number is defined as the locking point, which has the physical meaning of aggregates locking together, at which point further compaction of the mixture becomes very hard (Vavrik and Carpenter, 1998). Slightly different definitions of locking point have been proposed (Pine, 1997; Vavrik and Carpenter, 1998; Shamsi and Mohammad, 2010), but they all share the same physical interpretation—compaction becomes limited when aggregates begin locking together.

In the Superpave mix design (AASHTO R35, 2015), the shape of the compaction curve is controlled by three critical gyration numbers (N_{initial} , N_{design} , and N_{max}). These gyration numbers were originally proposed to relate laboratory compaction effort to traffic volume (Blankenship et al., 1994) and not to evaluate compactability.

In addition to the change of density, studies have been also focused on the shear resistance of the mixtures during compaction. A device was developed, called Gyratory Load Plate Assembly (GLPA), to monitor the shear resistance during compaction (Guler et al., 2000). Based on that, compaction energy indices were proposed to characterize the compactability of mixtures (Stakston and Bahia, 2003; Faheem and Bahia, 2004; Dessouky et al., 2004). The energy indices were shown to have good correlations with the compactability and stability of mixtures (Leiva and West, 2008; Anderson et al., 2002; Dessouky, 2015; Yeung et al., 2016). Other studies have been focused on exploring the physical mechanisms of compaction. Aggregate rearrangements and binder-aggregate interaction have been proposed as the main physical mechanisms to explain the change of density and shear resistance during the compaction process (Yan et al., 2021a). Based on the physical mechanism of aggregate rearrangements, analytical models have been proposed to characterize gyratory compaction curves (Yan et al., 2022a, Yan et al., 2022c). The parameters of the models provide a good means of characterizing compactability of asphalt mixtures.

2.3.2 Effects of Binder Viscosity on Compactability

Binder viscosity is one of the most significant factors that affects compaction. Since it is very sensitive to temperature, viscosity of binder during construction is typically controlled by temperature. Requiring a minimum temperature for mixing and compaction to ensure a relatively low viscosity of binder during compaction is one of the most effective ways to control the compaction quality. It has been shown that inadequate compaction temperature usually results in poor compaction with excessive air voids.

Asphalt Institute (AI) presented the first recommendation of the appropriate viscosity ranges for compaction and mixing of HMA (1962), which are 140 ± 15 seconds Saybolt-Furol and 85 ± 10 seconds Saybolt-Furol for mixing and compaction respectively. Compaction and mixing temperatures are then determined to achieve the proposed viscosity range. In 1974, AI changed the viscosity measurements from the units of Saybolt-Furol to units of centistokes (cSt) (Asphalt Institute, 1974). The required viscosity values for compaction and mixing are 280 ± 30 cSt and 170 ± 20 cSt respectively. For the Superpave mix design, the basic concept of equi-viscous method remained unchanged. Only the units changed from cSt to Pascal-seconds (Pa-s) and the viscosity is measured using the Rotational Viscometer. The recommended viscosity values for compaction and mixing are $0.28 \pm .03$ Pa-s and 0.17 ± 0.02 Pa-s respectively.

The equi-viscous method works well for unmodified binders, however, a number of issues were reported when it was used on modified binder. The equi-viscous method requires an excessively high temperature (e.g. 180°C) for modified binders (Bahia et al., 2001; Yildirim et al., 2000), which it is unacceptable because it may cause excessive oxidation and increase of energy cost, while, in reality, a temperature around 160°C is typically enough for most modified binders to be well compacted (Bahia et al., 2001; Yildirim et al., 2000). The reason has been attributed to the shear thinning phenomenon (Bahia et al., 2001), responsible for viscosity decreases with increase in shear rate. Thus, in order to determine the compaction temperature for modified binders, the required viscosity for compaction and mixing must be related to the shear rates at which compaction or mixing occur (Bahia et al., 2006; Shenoy, 2001).

In 2000, the high shear rate viscosity method (HSV) was developed by the researchers at the University of Texas (Yildirim et al., 2000). In this method, the viscosity at a high shear rate is used to determine the compaction temperature. The shear rate of compaction was estimated at 500s^{-1} . By using HSV, the compaction and mixing temperature for the modified binder were reduced by 10 to 30°C compared to the equi-viscous method. Later on (Yildirim et al., 2006), the recommended viscosity ranges for mixing and compaction at the high shear rate were centered at 0.275 and 0.550 Pa s, respectively.

In 2001, researchers at University of Wisconsin developed another method called the zero shear rate method (ZSV) (Khatri, 2001). This method uses the viscosity when the shear rate is zero, which based on statistical analyses was found to correlate best with mixture compactability. The target values of ZSV for mixing and compaction were recommended as 3.0 Pa s and 6.0 Pa s, respectively. The result showed that the compaction temperature was, on average, 40°C lower than the equi-viscous method. Researchers at Indiana verified the ZSV method by comparing this method with their empirical method (Tang and Haddock, 2006).

In 2001, the research group at the University of Wisconsin simplified ZSV method to low shear rate viscosity method (LSV). Compared to ZSV, LSV simplified the interpolation process. Rather than using the viscosity at a shear rate of zero, the viscosity at the shear rate of 0.001s^{-1} was used to determine the compaction and mixing temperature. It was reported that LSV is simpler but can get the same result as ZSV (Bahia et al., 2001; Bahia et al., 2006).

2.3.3 Effects of Binder Lubricity on Compaction

The binder lubricity received considerable attention as part of the research on Warm Mix Asphalt (WMA) technology. WMA improves the workability of the mixture, that cannot be explained by the reduction of viscosity, since some types of WMA increase binder viscosity (Kataware and Singh, 2018; Mo et al., 2012).

Hanz and Bahia (2013) were among the first to suggest that the increase in binder lubricity was the reason for the improvement of compaction after adding WMA. During compaction, the distance between aggregate particles decreases. In thin films or when particles are in contact, the concept of rheology does not apply, and it becomes necessary to investigate thin film behavior through the use of tribology. As found by Kavehpour and McKinley (2004), for two surfaces separated by a viscous fluid, rheology governs the transmission of stress when the distance between the two surfaces is large, while tribology begins to play a more important role as the distance decreases. Different configurations have been used to obtain binder lubricity, and it was found that the friction coefficient is a function of test speed, viscosity and normal load (Canestrari et al., 2017). At a controlled viscosity and normal load, the lubrication effect of binder can be expressed as a function of the sliding speed. Their relationship is expressed by the Stribeck curve in tribology, as shown in Figure 2.4 (Ingrassia, 2018).

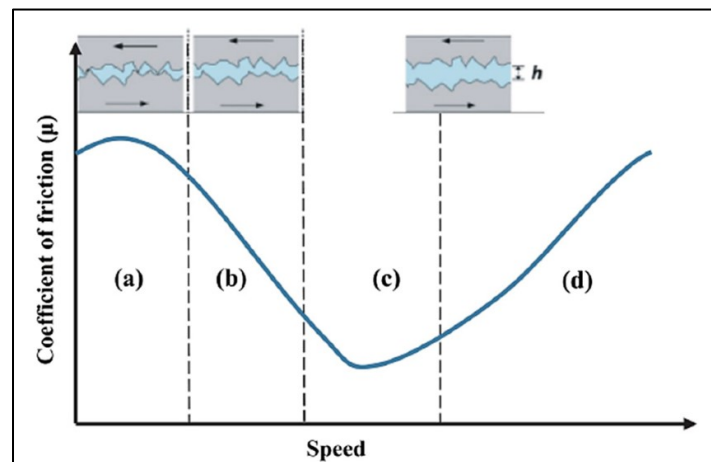


Figure 2.4 Stribeck curve: the relationship between sliding speed and coefficient of friction (Ingrassia, 2018)

According to the Stribeck curve, the lubrication properties can be divided into four regions: “(1) the boundary regime, in which friction is mainly caused by the interaction of the asperities of the two solids; (2) the mixed regime, where a reduction of friction occurs, because the direct contact between the solids is reduced by the hydrodynamic pressure of the lubricant; (3) the elasto-hydrodynamic regime, in which the surfaces of the solids are no longer in contact and therefore the minimum friction, which is related only to the lubricant properties, is reached; (4) the hydrodynamic regime, where friction increases because of the increase in the viscous drag of the lubricant.” (Ingrassia, 2018).

In addition to WMA, the lubricating effect of binder has been used to explain the increased compactability of Graphite Nanoplatelets (GNP) modified asphalt mixtures (Yan et al., 2020)

2.3.4 Effects of Binder Content on Compaction

As already mentioned, adding more binder helps compaction. This is the basis for the “regressing air voids” method developed in Wisconsin (West et al., 2018). However, adding more binder is more expensive and may have a negative impact on the stability of mixtures.

2.3.5 Effects of Aggregate Gradation on Compactability

The effect of aggregate gradation on compaction has long been recognized. For many years, aggregates have been chosen to have gradation curves close to the maximum density line based on the 0.45 power law. However, it is not clear how the distance between the gradation curve and maximum density line affects the compactability of mixtures.

2.3.5.1 Bailey Method

The Bailey method was proposed by Robert D. Bailey at Illinois Department of Transportation in the early 1980s. It provided a systematic way of designing and adjusting aggregate gradation (Vavrik et al., 2002). The idea of the Bailey method is to design the interlock of the aggregates directly. A good interlocked aggregate skeleton is required for good rutting resistance. In the Bailey method, a number of parameters are used to characterize the gradation. The relationship between those parameters and the workability and volumetric of asphalt mixtures are provided, which greatly helps engineers to adjust the gradation to achieve the desired volumetric properties and compactability.

In the Bailey method, it is assumed that the coarse aggregates form the interlock and fine aggregates fill the voids of the coarse aggregates. Coarse and fine aggregates are separated by the primary control sieve (PCS), which is defined as the sieve size that equals $0.22 \cdot \text{NMPS}$ (normal maximum particle size). The value 0.22 was determined by 2D and 3D packing analysis of differently shaped particles. The unit weight of coarse aggregates is used to describe the degree of interlocking. Unit weight means the weight of aggregates that fills a unit volume. The loose unit weight (LUW) is the unit weight of aggregates without any compaction. This condition represents the beginning of the aggregate interlock. The rodded unit weight (RUW) is the unit weight with compaction effort applied. This condition represents the fully developed aggregate interlock. Thus, we can control the degree of interlock by choosing an appropriate unit weight. If the chosen unit weight (CUW) is 95~105% of LUW, the mixture is called coarse-graded mixture. If CUW is less than 90% of LUW, it is called fine-graded mixture. Usually, RUW equals 110% of LUW; SMA mixtures have a CUW larger than 110% of LUW. Thus, the heavier the CUW the better interlocking the mixture will be. Since the probability of degradation and the compaction effort both increase, an excessive high CUW should be avoided. CUW has a significant effect on the volumetric properties. An increase in CUW over LUW will increase the air voids and VMA, while for the fine-graded mixture (CUW less than 90%), the effect of CUW on air voids and VMA is not significant.

To determine how gradation affects VMA and compactability, the gradation is separated into three portions—the coarse aggregate (sieve size larger than PCS), the coarse portion of fine aggregate (sieve

size larger than SCS but smaller than PCS), and the fine portion of fine aggregate (sieve size smaller than SCS).

The packing of each portion is characterized by a ratio. They are Coarse Aggregate Ratio (CA Ratio), Fine Aggregate Coarse Ratio (FA_c Ratio), and Fine Aggregate Fine Ratio (FA_f Ratio) respectively.

$$CA\ Ratio = \frac{(\% \text{ Passing Half Sieve} - \% \text{ Passing PCS})}{(100\% - \% \text{ Passing Half Sieve})}$$

$$FA_c\ Ratio = \frac{\% \text{ Passing SCS}}{\% \text{ Passing PCS}}$$

$$FA_f\ Ratio = \frac{\% \text{ Passing TCS}}{\% \text{ Passing SCS}}$$

where Half Sieve is the sieve size equals $0.5 \cdot PCS$. SCS is secondary control sieve which equals $0.22 \cdot PCS$. Similarly, TCS is called tertiary control sieve which equals $0.22 \cdot SCS$.

CA Ratio describes the packing characteristics of the coarse aggregate portion. Coarse particles that are smaller than the half sieve size but larger than PCS are called “interceptors”, so CA Ratio shows the proportion of the interceptors in the coarse aggregate portion. Interceptors are too large to fill the voids of coarse aggregates, and therefore, an increase in the CA Ratio will increase the difficulty of compaction and increase the air voids and VMA as well. However, if the proportion of interceptors is too low (CA Ratio is too low) the mixture becomes gap-graded and will be prone to segregation.

FA_c Ratio describes the packing characteristics of the coarse portion of the fine aggregate. As this ratio increases, the fine aggregates become denser and the VMA decreases. Noticeably, this ratio typically has the most significant effect on VMA. A similar trend of effect can be seen in FA_f .

In summary, the influence of CUW, CA Ratio, FA_c Ratio, and FA_f Ratio on the VMA and workability is summarized in Table 2.3.

Table 2.3 Summary of the Bailey Method

Bailey Method indices	VMA	workability
CUW: Chosen Unit Weight	An increase of 5% in the chosen unit weight will increase VMA by 0.5 to 1.0%. For fine-graded mixtures, the effect is not significant.	An increase in CUW will decrease compactability
CA Ratio: Coarse Aggregate Ratio	An increase of 0.2 in the CA Ratio will result in an increase of 0.5 to 1.0% VMA.	A decrease in CA Ratio will increase compactability, but also segregation.
FA _c Ratio: Fine Aggregate Coarse Ratio	A decrease of 0.05 in the FA _c Ratio will create an increase of 0.5 to 1.0% in VMA.	An increase of FA _c Ratio will increase compactability.
FA _r Ratio: Fine Aggregate Fine Ratio	A decrease of 0.05 in the FA _r Ratio will create an increase of 0.5 to 1.0% in VMA.	An increase of FA _r Ratio will increase compactability.

Studies have investigated the feasibility of using the Bailey method (Vavrik et al., 2002), including its application to dense-graded mixtures, SMA, and mixtures contain RAP. Graziani et al. (2012) verified the validity of the Bailey Method for the sieve sizes used in European standards. In their work, the effects of the CUW, CA, FA_c and FA_r on the VMA and compactability were studied.

2.3.6 Effects of Other Aggregate Properties on Compaction

In the experimental study of Leiva and West (2008), aggregate-related properties such as type, shape, and nominal maximum aggregate size (NMAS) were studied. It was found that fine-graded mixtures are more compactable than coarse-graded mixtures, followed by SMA which is the most difficult to compact. In terms of NMAS, it was found that compactability of the mixture decreases with increasing NMAS. The same trend had been also observed by Gudimettla et al. (2004). A nonlocal analytical model was developed by Yan et al. (2022) which provides a theoretical explanation to the effects of NMAS and angularity on compaction process of asphalt mixtures.

In terms of aggregates type, it was found that mixtures containing limestone as the primary aggregate source tended to be difficult to compact. The main differences between limestone and other aggregate types are that they are tougher, more angular and contain more mineral filler. Marble-schist mixtures are more easily compacted, followed by granite mixtures. Marble-schist aggregate is characterized by flat and elongated particles and low strength aggregates. These properties are related to aggregate

degradation and allow denser aggregate packing to be achieved. On the other hand, granite mixtures contain some flat and elongated particles and intermediate aggregate strength, but most of these mixtures are fine graded, which may explain their ability to be easily compacted. In general, the marble-schist and granite mixtures were easier to compact than the limestone mixes.

Gudimettla et al. (2004) studied the shape of aggregates. The authors showed that mixtures prepared with cubical, angular granite were less workable than mixes prepared with semi-angular crushed gravel.

The effect of aggregate shape was also studied using DEM (discrete element method) simulations (Chen, 2011; Gong, 2018a, 2018b; Liu, 2018). The general result is that elongated and flat aggregates are more difficult to compact, compared with round aggregates.

The effect of fine aggregate angularity (FAA) on compaction was studied by Stakston et al. (2002). For laboratory compaction below 92% G_{mm} (that represents the construction compaction), a consistent trend of higher resistance to compaction with higher FAA was observed. For compaction above 92% G_{mm} , the effect of FAA on compaction is inconsistent and is dependent on the source of aggregate and gradation.

Mineral filler is composed of particles passing the No. 200 sieve ($<0.075\text{mm}$). It is so small that it is usually considered as part of binder suspension (mastic) and it is not included in the aggregate gradation. The mineral filler was found to improve the rutting resistance of the mixture (Kallas et al., 1962; Wang et al., 2011), but it increases the compaction efforts as well (Kallas et al., 1962). If the mineral filler and binder are considered together as the mastic, it is shown that the dosage of mineral filler increases the viscosity of mastic (Ebrahim et al., 2012), which is probably the main reason for which mineral filler increases the compaction efforts.

2.4 FIELD COMPACTION

In this section studies addressing field compaction are reviewed and good practices for achieving desired field compaction are summarized.

2.4.1 Randomness in Field Density

It has widely been acknowledged that the field density exhibits considerable randomness. The standard deviation of the field density is typically in the range of 1.0~2.0% G_{mm} (Aschenbrener and Tran, 2020; Yan et al., 2021b; 2022b). Recognizing this uncertainty, reliability concepts have been used for the QC/QA of field density. One example is the Percent Within Limit (PWL) method, which has been applied in many parts of the United States (Aschenbrener and Tran 2020, Burati et al. 2003, AASHTO R9 2005). For the sake of simplicity, the randomness of the field density is often assumed to follow the Normal distribution, which is symmetrical with respect to its the mean value. However, recent investigation (Yan et al., 2021b; 2022b) has shown that field density distribution consistently exhibits left-skewed (skewness < 0) and leptokurtic (kurtosis > 3) features. A probabilistic model for field density distribution has been proposed based on the mechanistic modeling of compaction process and considering the randomness in field compaction effort and material composition (Yan et al., 2022c). The model captures

the left-skewed and leptokurtic features of field density distribution and has a potential to be used for characterizing and predicting field density distribution.

2.4.2 Traffic Compaction

Many studies have been conducted to monitor the densification process of pavements under traffic (Epps et al., 1970; Stroup-Gardiner et al., 1997; Blankenship et al., 1994; Prowell and Brown, 2007). Generally, pavements reach their ultimate density after 2 to 3 years of traffic compaction, with most densification occurring in the first 3 months after construction (Prowell and Brown, 2007).

The design laboratory compaction effort in Superpave (AASHTO R35, 2015) was determined based on traffic compaction. It was assumed that the logarithm of the number of gyrations of SGC is linearly related to the logarithm of the traffic volume. However, even in the studies in which N_{design} table was determined, the quality of linear correlation was shown to be very low (Blankenship et al., 1994; Prowell and Brown, 2007).

Based on this idea, Superpave mixtures are designed to be compacted to about 7% of air voids during construction and further compaction to 4% is done by traffic loading. However, this idea has been criticized, because the as-constructed air voids are too high and can lead to durability-related premature distresses.

By contrast, in the LCPC mix design in France, mixtures are compacted to ultimate density during construction. It was shown that there is little or no increase in density under traffic loading (Huber et al., 2016).

Clearly, the role of traffic in compaction is still under debate. The relationship between density and traffic compaction is not as simple as a linear relation between density and logarithm of traffic volume. The relationship is more complex and affected by many other factors. Among these factors, the as-constructed density is a very important factor. If the as-constructed density is high, then, it seems plausible to have little or no further densification by traffic.

2.4.3 Lift Thickness

Though lift thickness has long been known as significantly influencing compaction, the optimal lift thickness is still under debate. Brown et al. (2004) conducted a field compaction study, in which the t/NMAS ratio (the ratio of lift thickness over NMAS) was changed from 2 to 5. It was found that the in-place density increased with an increase in t/NMAS ratio. The effect of t/NMAS ratio is more evident for coarse graded mixtures than fine graded mixtures. This study recommended a minimum t/NMAS of 3 for fine graded mixtures, and 4 for coarse graded mixtures. It was found, however, that an excessively high t/NMAS ratio (>5) would cause difficulty in the compaction of the material at the bottom of the lift, and was not recommended.

In another study in Mississippi, Cox (2015) collected data from 12 projects. Statistical analysis showed that t/NMAS ratio had a greater effect on air voids than aggregate properties such as fine aggregate

angularity, moisture content, methylene blue value, surface area of the fines, and others. An optimal t/NMAS range of 4 to 6 was suggested.

Another statistical analysis was conducted by Williams et al. (2015). The final regression models related air voids to t/NMAS, initial surface temperature, distance between percent passing the No. 8 sieve and the maximum density line, accumulated compaction pressure, aggregate surface areas, and total asphalt binder content. The results also suggested an optimal t/NMAS ratio of 4 to 6.

Bahia and Paye (2001), studied the effect of lift thickness using laboratory gyratory compactor. It was found that density increased with increase in the mass of the sample compacted in the gyratory compactor. This laboratory compaction study also suggested a t/NMAS ratio of 4 to 6.

Recently, McDaniel (2019) conducted a study on the effect of lift thickness on pavement quality. The study includes a comprehensive literature review, and surveyed state highway agencies, paving contractors, and paving associations to determine the state of their practices, experiences, and polices related to lift thickness.

2.4.4 Field Compaction Equipment

The traditional compaction equipment includes paver screed, steel wheel roller, and pneumatic tire roller. The Paver screed can compact the mixture to approximately 75% to 85% of the maximum density of the mixture (US Army Corps of Engineers, 2000).

Steel wheel rollers can apply both static and vibratory loads. The vibratory roller offers greater compaction effort over the static roller, but if the force amplitude is too high it may result in coarse aggregate breakdown (Choubane et al., 2006; Brown, 1982). The vibration force also allows aggregate particles to move and reorient to produce greater friction and interlock than what could be achieved without vibration. However, the frequency of vibration should match the speed of the roller (Nittinger, 1997). If the roller is moving too fast, it will result in ripples on the surface. On the other hand, a slowly moving roller can achieve better density, but it also reduces the productivity and cause difficulty in keeping up with the paver. The amplitude should also match the lift thickness. Usually, coarse graded mixture with thicker lift thickness will need higher amplitude of vibration and larger number of roller passes.

Pneumatic tire roller provides a slightly different type of compaction than steel wheel rollers. Pneumatic tire rollers also provide a kneading action between the tires and mixture that tends to reduce permeability by “sealing” the surface (Retzer, 2008).

New technologies are evolving in the compaction of asphalt mixtures. Recently, a German company developed a paver that can compact the HMA to a higher density, and under ideal conditions, even the final density (VÖGELE, 2018). Three compacting systems are combined in the paver screed, including tamper, vibrators, and one or two pressure bars, to ensure the mixture reaches its maximum density.

Another technology is the Intelligent Compaction (IC) roller. An IC roller is “a vibratory roller equipped with accelerometers mounted on the axle of drums, global positioning systems (GPS), infrared

temperature sensors, and onboard computers that can display IC measurements as color-coded maps in real time” (Chang et al, 2014). The IC roller measures a great deal of data in real time, including IC measurement values (ICMV), roller passes, asphalt surface temperatures, roller vibration frequencies/amplitudes, and speeds. Based on these data, the roller can automatically adjust the setting of the roller to achieve optimum compaction. It is a combination of technologies from different disciplines that is still rapidly developing.

2.5 IMPLEMENTATION OF SUPERPAVE 5 IN MINNESOTA

In order to implement Superpave 5 mix design in Minnesota, possible changes to the current MnDOT Standard specification 2360 (plant mixed asphalt pavement) and 3139 (graded aggregate for bituminous mixtures) need to be identified. First, the current MnDOT standards are presented, followed by the Superpave 5 standard recently released by InDOT. Based on a preliminary comparison, a number of possible changes are proposed.

2.5.1 Current MnDOT Standards

As shown in Figure 2.5, Table 2360-7 shows the mixture requirements of the current MnDOT standard. For Superpave 5, the design air voids should be increased to 5%, and the N_{design} should be decreased. Most likely, further investigation of Minnesota local materials and field compaction efforts is needed in order to determine the exact number for N_{design} .

Traffic Level	2	3	4	5
20 year design ESALs	< 1 million	1 – 3 million	3 – 10 million	10 – 30 million
Gyratory mixture requirements:				
Gyrations for N_{design}	40	60	90	100
% Air voids at N_{design} , wear	4.0	4.0	4.0	4.0
% Air voids at N_{design} , Non-wear and all shoulder	3.0	3.0	3.0	3.0
Adjusted Asphalt Film Thickness, minimum μ	8.5	8.5	8.5	8.5
TSR*, <i>minimum %</i>	75	75	80†	80†
Fines/effective asphalt	0.6 – 1.2	0.6 – 1.2	0.6 – 1.2	0.6 – 1.2
* Use 6 in specimens in accordance with 2360.2.I, "Field Tensile Strength Ratio (TSR)." MnDOT minimum = 65 † MnDOT minimum = 70				

Figure 2.5 Table 2360-7 of the MnDOT construction standard 2360.

As shown in Figure 2.6, Table 2360-19 shows the requirements of the as-constructed density of the current MnDOT standard. For Superpave 5, the values should be replaced with 95% G_{mm} mixtures, corresponding to 5% final air void compaction in the field (as-constructed density).

Table 2360-19 Required Minimum Lot Density (Mat)				
	4% Design Voids*	3% Design Voids*	One Percent Reduced Density*	
			3% Design Voids	4% Design Voids
% Gmm	92	93	92	91
* Reduce density required on the first lift constructed over PCC pavements. Reduce density, when maximum density is waived, for the first lift constructed on aggregate base (mainline and shoulder), reclaimed or cold in place recycled base courses and first lift of an overlay on roadway with a spring load restriction no greater than 7 ton, including shoulders.				

Figure 2.6 Table 2360-19 of the MnDOT construction standard 2360.

As shown from Figure 2.7 to Figure 2.10, Table 2360-22 to Table 2360-25 list the payment schedule of the current MnDOT standard, which is corresponding to the as-constructed densities. Since the as-constructed density of Superpave 5 is increased to 95% G_{mm}, the pay factor should be changed accordingly.

Table 2360-22 Payment Schedule for Maximum Mat Density			
Density (4% Design Void), %*	Density (3% Design Void), %*	Mat Density Pay Factor A	
		Traffic Level 2 & 3	Traffic Level 4 & 5
≥ 93.6	≥ 94.6	1.03	1.05
93.1 – 93.5	94.1 – 94.5	1.02	1.04
92.0 – 93.0	93.0 – 94.0	1.00	1.00
91.0 – 91.9	92.0 – 92.9	0.98	0.98
90.5 – 90.9	91.5 – 91.9	0.95	0.95
90.0 – 90.4	91.0 – 91.4	0.91	0.91
89.5 – 89.9	90.5 – 90.9	0.85	0.85
89.0 – 89.4	90.0 – 90.4	0.70	0.70
< 89.0	< 90.0	†	†

Figure 2.7 Table 2360-22 of the MnDOT construction standard 2360.

Table 2360-23* 1 Percent Reduced Table		
Density (4% Design Void), %	Density (3% Design Void), %	Payment, %
≥ 91.0	≥ 92.0	100
90.0 – 90.9	91.0 – 91.9	98
89.7 – 89.9	90.5 – 90.9	95
89.4 – 89.6	90.0 – 90.4	91
89.2 – 89.3	89.5 – 89.9	85
89.0 – 89.1	89.0 – 89.4	70
< 89.0†	< 89.0	†

Figure 2.8 Table 2360-23 of the MnDOT construction standard 2360.

Table 2360-24* Payment Schedule for Longitudinal Joint Density 4% Design Void					
Longitudinal Joint (Confined Edge) Density, % 	Pay Factor B Longitudinal (Confined Edge)		Longitudinal Joint (Unsupported Edge) Density, % 	Pay Factor C (Unsupported Edge)	
	Traffic Level 2 & 3	Traffic Level 4 & 5		Traffic Level 2 & 3	Traffic Level 4 & 5
≥ 92.1	1.02†	1.03†	≥ 91.0	1.02†	1.03†
91.6 – 92.0	1.01†	1.02†	90.1 – 90.9	1.01†	1.02†
89.5 – 91.5	1.00	1.00	88.1 – 90.0	1.00	1.00
88.5 – 89.4	0.98	0.98	87.0 – 88.0	0.98	0.98
87.7 – 88.4	0.95	0.95	86.0 – 86.9	0.95	0.95
87.0 – 87.6	0.91	0.91	85.0 – 85.9	0.91	0.91
< 87.0	0.85	0.85	< 85.0	0.85	0.85

Figure 2.9 Table 2360-24 of the MnDOT construction standard 2360.

Table 2360-25* Payment Schedule for Longitudinal Joint Density 3% Design Void					
Longitudinal Joint (Confined Edge) Density, % 	Pay Factor B Longitudinal (Confined Edge)		Longitudinal Joint (Unsupported Edge) Density, % 	Pay Factor C (Unsupported Edge)	
	Traffic Level 2 & 3	Traffic Level 4 & 5		Traffic Level 2 & 3	Traffic Level 4 & 5
≥ 93.1	1.02†	1.03†	≥ 92.0	1.02†	1.03†
92.6 – 93.0	1.01†	1.02†	91.1 – 91.9	1.01†	1.02†
90.5 – 92.5	1.00	1.00	89.1 – 91.0	1.00	1.00
89.5 – 90.4	0.98	0.98	88.0 – 89.0	0.98	0.98
88.7 – 89.4	0.95	0.95	87.0 – 87.9	0.95	0.95
88.0 – 88.6	0.91	0.91	86.0 – 86.9	0.91	0.91
< 88.0	0.85	0.85	< 86.0	0.70	0.85

Figure 2.10 Table 2360-25 of the MnDOT construction standard 2360.

As shown in Figure 2.11, the Table 3139-2 shows the broad bands of the aggregate gradation of the current MnDOT standard. It is anticipated that for Superpave 5 the aggregate gradation will change to improve compactability. The specific adjustment to the aggregate gradation will be investigated later in this study.

Table 3139-2 Aggregate Gradation Broad Bands (percent passing of total washed gradation)				
Sieve size	A	B	C	D
1 in	—	—	100	—
¾ in	—	100*	85 – 100	—
½ in	100*	85 – 100	45 – 90	—
⅜ in	85 – 100	35 – 90	—	100
No. 4	60 – 90	30 – 80	30 – 75	65 – 95
No. 8	45 – 70	25 – 65	25 – 60	45 – 80
No. 200	2.0 – 7.0	2.0 – 7.0	2.0 – 7.0	3.0 – 8.0

* The Contractor may reduce the gradation broadband for the maximum aggregate size to 97 percent passing for mixtures containing RAP, if the oversize material originates from the RAP source. Ensure the virgin material meets the requirement of 100 percent passing the maximum aggregate sieve size.

Figure 2.11 Table 3139-2 of the MnDOT construction standard 3139.

2.5.2 Superpave 5 Mix Design at Indiana DOT

To date, the Superpave 5 mix design has been successfully implemented at Indiana. In the newly released asphalt mixture standard (Indiana DOT, 2019) the complete transition from the traditional Superpave design for dense graded mixtures to the new Superpave 5 mix design was accomplished. In the following tables, the values shaded in yellow represent the changes that occurred as part of this transition (Indiana DOT, 2019).

As shown in Figure 2.12, the design air voids of all NMAS for dense graded mixtures were changed to 5%. The traditional 4% air voids design has been totally abandoned.

Air Voids at Optimum Binder Content								
Mixture Designation	Dense Graded					Open Graded		
	25.0 mm	19.0 mm	12.5 mm	9.5 mm	4.75 mm	25.0 mm	19.0 mm	9.5 mm
Air Voids	5.0%	5.0%	5.0%	5.0%	5.0%	15.0% - 20.0%		10.0% - 15.0%

Figure 2.12 Design air void ratio in Indiana standard (Indiana DOT, 2019)

Another important change is in the design number of gyrations. As shown in Figure 2.13, the design gyration numbers (N_{ini} , N_{des} , and N_{max}) were decreased for most NMAS of mixtures (except NMAS = 4.75mm) compared to the traditional Superpave mix design (Table 2.1). The reason for keeping 4.75 mm mixtures the same is the tendency to produce tender mixtures for 4.75 mm mixtures.

Gyratory Compaction Effort					
ESAL	N_{ini}^*	N_{des}^*	N_{max}^*	Max. %Gmm @ N_{ini}	Max. %Gmm @ N_{max}
Dense Graded 4.75 mm					
< 3,000,000	7	75	115	90.5	98.0
3,000,000 to < 10,000,000	8	100	160	89.0	98.0
≥ 10,000,000	8	100	160	89.0	98.0
Dense Graded 9.5 mm, 12.5 mm, 19.0 mm, and 25.0 mm					
< 3,000,000	5	30	40	91.5	97.0
3,000,000 to < 10,000,000	6	50	75	91.5	97.0
≥ 10,000,000	6	50	75	91.5	97.0
Open Graded					
All ESAL	n/a	20	n/a	n/a	n/a

* N_{ini} , N_{des} , N_{max} - definitions are included in AASHTO R 35.

Figure 2.13 Gyratory compaction effort in the new Indiana standard (Indiana DOT, 2019)

Since the design air voids of Superpave 5 has increased by 1% compared to traditional Superpave, the minimum requirement of VMA has also increased by 1% to ensure the effective binder content remains unchanged. As shown in Figure 2.14, the minimum VMA for all NMAS sizes, except 4.75mm, was increased by 1%.

VOIDS IN MINERAL AGGREGATE, VMA, CRITERIA @ N _{des}	
Mixture Designation	Minimum VMA, %
4.75 mm	17.0
9.5 mm	16.0
12.5 mm	15.0
19.0 mm	14.0
25.0 mm	13.0
OG	n/a

Figure 2.14 VMA requirements in the new Indiana standard (Indiana DOT, 2019)

Figure 2.15 and Figure 2.16 shows the requirements for the volume of effective binder (Vbe) and voids filled with asphalt (VFA) in the new Indiana standard. Vbe and VFA can be obtained from VMA and air-void ratio, i.e., Vbe is VMA minus air void ratio, and VFA is the Vbe divided by VMA. Since VMA and design air voids have been changed, Vbe and VFA were changed correspondingly.

VOLUME OF EFFECTIVE BINDER, Vbe, CRITERIA @ N _{des}	
Mixture Designation	Minimum Vbe, %
4.75 mm	12.0
9.5 mm	11.0
12.5 mm	10.0
19.0 mm	9.0
25.0 mm	8.0
OG	n/a

Figure 2.15 Requirements of volume of effective binder in the new Indiana standard (Indiana DOT, 2019)

VOIDS FILLED WITH ASPHALT, VFA, CRITERIA @ N _{des}	
ESAL	VFA, %
< 3,000,000	60 – 73
3,000,000 to < 10,000,000	60 – 70
≥ 10,000,000	60 – 70

Notes:

1. For 4.75 mm mixtures, the specified VFA range shall be 67% to 79%.
2. For 9.5 mm mixtures, the specified VFA range shall be 68% to 71% for design traffic levels ≥ 3,000,000 ESALs.
3. For 25.0 mm mixtures, the specified lower limit of the VFA shall be 62% for design traffic levels < 300,000 ESALs.
4. For OG mixtures, VFA is not applicable.

Figure 2.16 Requirements of VFA in the new Indiana standard (Indiana DOT, 2019)

The quality control requirements also changed in accordance with the change in the mixture design. Figure 2.17, Figure 2.18, and Figure 2.19 list how the pay factors are determined for Vbe, air voids, and in-place density, respectively.

Volume of Effective Binder, Vbe	
Dense Graded	Pay Factors
Deviation from Spec Minimum	
> +3.0	Submitted to the Office of Materials Management*
> +2.5 and ≤ +3.0	1.00 - 0.05 for each 0.1% above +2.5%
> +2.0 and < +2.5	1.05 - 0.01 for each 0.1% above +2.0%
> +0.5 and < +2.0	1.05
≥ 0.0 and ≤ +0.5	1.05 - 0.01 for each 0.1% below +0.5%
≥ -0.5 and < 0.0	1.00 - 0.02 for each 0.1% below 0.0%
≥ -2.0 and < -0.5	0.90 - 0.06 for each 0.1% below -0.5%
< -2.0	Submitted to the Office of Materials Management*

* Test results will be considered and adjudicated as a failed material in accordance with normal Department practice as listed in 105.03.

Figure 2.17 Pay factor of Vbe in the new Indiana standard (Indiana DOT, 2019)

Air Voids		
Dense Graded	Open Graded	Pay Factor
Deviation from Spec (±%)	Deviation** (±%)	
≤ 0.5	≤ 3.0	1.05
> 0.5 and ≤ 1.7	> 3.0 and ≤ 4.0	1.00
	4.1	0.98
1.8	4.2	0.96
	4.3	0.94
	4.4	0.92
1.9	4.5	0.90
2.0	4.6	0.84
	4.7	0.78
	4.8	0.72
	4.9	0.66
	5.0	0.60
> 2.0	> 5.0	Submitted to the Office of Materials Management*

* Test results will be considered and adjudicated as a failed material in accordance with normal Department practice as listed in 105.03.

** Deviation shall be from 17.5% for OG25.0 mm and OG19.0 mm mixtures and shall be from 12.5% for OG9.5 mm mixtures.

Figure 2.18 Pay factor of design air voids in the new Indiana standard (Indiana DOT, 2019)

As shown in Figure 2.19, the required in-place density for Superpave 5 is 95%, which is a significant increase compared to the traditional Superpave (92%). In-place densities within the range of 94% to 97% will get a bonus, while density less than 93% or larger than 98% will be penalized.

Density	
Percentages are based on %MSG	Pay Factors, %
Dense Graded	
≥ 98.0	Submitted to the Office of Materials Management*
97.0 - 97.9	1.00
96.6 - 96.9	1.05 - 0.01 for each 0.1% above 96.5
95.0 - 96.5	1.05
94.1 - 94.9	1.00 + 0.005 for each 0.1% above 94.0
93.0 - 94.0	1.00
92.0 - 92.9	1.00 - 0.005 for each 0.1% below 93.0
91.0 - 91.9	0.95 - 0.010 for each 0.1% below 92.0
90.0 - 90.9	0.85 - 0.030 for each 0.1% below 91.0
≤ 89.9	Submitted to the Office of Materials Management*
* Test results will be considered and adjudicated as a failed material in accordance with normal Department practice as listed in 105.03.	

Figure 2.19 Pay factor of in-place density in the new Indiana standard (Indiana DOT, 2019)

InDOT standard also contain recommendations for field compaction operations, as shown in Figure 2.20. Currently, MnDOT standard does not include similar recommendations.

Rollers	Number of Roller Applications						
	Courses						
	≤ 440 lb/sq yd					> 440 lb/sq yd	
	Option 1	Option 2	Option 3	Option 4	Option 5	Option 1	Option 2
Three Wheel	2		4			4	
Pneumatic Tire	2	4				4	
Tandem	2	2	2			4	
Vibratory				6			8
Oscillatory					6	-	-

Figure 2.20 Recommended field compaction operation in the new Indiana standard (Indiana DOT, 2019)

2.5.3 Possible Changes

Based on a preliminary comparison of the two standards, possible changes to the current MnDOT Standard specification 2360 (plant mixed asphalt pavement) and 3139 (graded aggregate for bituminous mixtures) are identified:

- Design air void ratio increases from 4% to 5%.
- Design VMA also increases by 1%. Since MnDOT use asphalt film thickness (AFT), the increase in VMA can be converted to the increase in AFT.
- N_{design} value decreases and is not directly related to traffic.
- Effective binder content remains the same as the traditional Superpave mix design.
- Aggregate gradation can be adjusted to make the mixture more compactable. The specific adjustment needs further study.
- Field required air voids will increase from 7-8% to 5%. (92/93% density to 95% density)

Other significant differences were noted between the InDOT and MnDOT standards:

- In mix design and production, MnDOT uses the concept of asphalt film thickness (AFT), while InDOT uses only VMA.
- For density acceptance, MnDOT pay factors are only determined by field core. MnDOT volumetric acceptance is based on gradation, air voids, G_{mm} , FAA, CAA, and AFT. The InDOT standard has other factors considered, such as V_{be} and air voids at N_{des} . For in-place density, InDOT has an upper limit requirement (98%), while MnDOT does not have one.
- InDOT standard contains recommendations for field compaction operations. MnDOT standard does not include similar recommendations.

CHAPTER 3: DATA ANALYSES OF 2018~2019 PROJECTS

In this chapter, the research team collected mix design and field density data from projects constructed in 2018~2019 in Minnesota. For these mixtures, a comprehensive analysis is performed, which includes analyzing aggregate gradations using parameters calculated as part of Bailey method. In addition, a comprehensive gradation analysis is performed for Superpave 5 asphalt mixtures used in three projects constructed in Indiana in 2018. The materials have already been collected and were available for use at University of Minnesota. A statistical analysis is conducted to identify correlations between mixtures properties and field densities.

3.1 MIX DESIGN INFORMATION

Mix design information from 15 previous MnDOT projects constructed in 2018 and 2019 was collected. Two levels of nominal maximum aggregate size (NMAS), 9.5mm and 12.5mm (3/8in and 1/2in), denoted as A and B respectively by conventional MnDOT designation were used in these projects.

Table 3.1 details the seven mixtures with NMAS = 9.5mm (3/8in); two of them are level 3 (1-3 million ESAL), and five mixtures are level 4 (3-10 million ESAL). Table 3.2 details the eight mixtures with NMAS = 12.5mm (1/2in); three are level 3, three are level 4, and two are level 5 (10-30 million ESAL).

Table 3.1 Summary of MnDOT mixtures with NMAS = 9.5mm (3/8in)

Traffic level		Level 3		Level 4				
MnDOT Mixture Type		A340	A340	A440	A440	A440	A440	A440
Mixture ID		A3-1	A3-2	A4-1	A4-2	A4-3	A4-4	A4-5
RAP Content		20%	30%	20%	19%	17%	22%	15%
Sieve Size	1in, 25mm	100	100	100	100	100	100	100
	3/4in, 19mm	100	100	100	100	100	100	100
	1/2in, 12.5mm	100	100	100	100	100	100	100
	3/8in, 9.5mm	92	86	87	96	96	88	88
	No.4, 4.75mm	67	67	65	65	65	65	65
	No.8, 2.36mm	51	57	50	45	45	53	53
	No.16, 1.18mm	36	45	38	32	32	42	42
	No.30, 0.6mm	24	30	28	20	20	28	28
	No.50, 0.3mm	11	13	15	11	11	14	14
	No.100, 0.15mm	6	6	6	5	5	6	6
No.200, 0.075mm	4.5	3.4	3.8	3.4	3.4	3.2	3.2	
%AC		5.6	4.9	4.8	5.3	5.3	5.6	5.6

Table 3.2 Summary of MnDOT mixtures with NMAS = 12.5 mm (1/2in)

Traffic level		Level 3			Level 4			Level 5	
MnDOT Mixture Type		B340	B340	B340	B440	B440	B440	B540	B540
Mixture ID		B3-1	B3-2	B3-3	B4-1	B4-2	B4-3	B5-1	B5-2
RAP Content		17%	26%	27%	20%	17%	18%	25%	20%
Sieve Size	1in, 25mm	100	100	100	100	100	100	100	100
	3/4in, 19mm	100	100	100	100	100	100	100	100
	1/2in, 12.5mm	95	90	90	94	92	92	91	90
	3/8in, 9.5mm	89	76	78	81	80	83	82	81
	No.4, 4.75mm	70	57	62	63	60	67	66	65
	No.8, 2.36mm	50	45	49	46	40	51	51	50
	No.16, 1.18mm	38	35	38	32	27	37	36	34
	No.30, 0.6mm	26	26	28	22	19	26	24	22
	No.50, 0.3mm	13	13	14	12	11	14	13	12
	No.100, 0.15mm	6	6	5	7	6	6	6	5
No.200, 0.075mm	3.6	4.2	2.8	3.5	3.5	3.4	3.3	2.8	
%AC		5.5	5.6	5.2	5.3	5.3	5.5	5.1	5.3

Table 3.3 Summary of Indiana Superpave 5 mixtures

Location		Seymour	Crawfordsville	Greenfield
Mixture ID		SM	CF	GF
NMAS (mm)		9.5	9.5	19.0
RAP content		19.5% fractionated RAP <9.5mm	26.0% fractionated RAP <9.5mm	9% fine RAP, 12% coarse RAP
Sieve Size	1in, 25mm	100	100	100
	3/4in, 19mm	100	100	96.9
	1/2in, 12.5mm	100	100	88.5
	3/8in, 9.5mm	93.6	93.5	80.7
	No.4, 4.75mm	61.1	61.6	54.1
	No.8, 2.36mm	35.7	41.9	34
	No.16, 1.18mm	23	26.2	21.2
	No.30, 0.6mm	15.4	16.2	13.7
	No.50, 0.3mm	9.2	9.8	8.7
	No.100, 0.15mm	6	6.5	6.1
No.200, 0.075mm	4.8	5	5.1	
Air voids, %		5.0	5.0	5.0
%AC		6.2	6.1	5.4
N _{design}		50	50	50

All mixtures were designed according to the current Superpave method, in which N_{design} is related to traffic levels. The N_{design} of level 3, 4, and 5 are 60, 90, and 100, respectively, according to the MnDOT specification 2360 (MnDOT, 2018). All mixtures have a design air voids of 4.0% and all mixtures contain reclaimed asphalt pavement (RAP), ranging from 17% to 30% by weight.

Visual inspection of the data shows that mixtures A4-2 and A4-3 have the same gradation; the only differences between them is the content of RAP. Similar relationship can be seen between mixtures A4-4 and A4-5. For this reason, the four mixtures will be investigated as two pairs of mixtures in the gradation analysis.

The information for the three Indiana Superpave 5 mixtures, provided by the research group at Purdue University, is shown in Table 3.3. As shown, the design air voids is 5% and the N_{design} is 50.

3.2 AGGREGATE GRADATION AND ANGULARITY

3.2.1 Gradation Curves

The gradation curves for Indiana Superpave 5 and for MnDOT 9.5mm mixtures are plotted in Figure 3.1. Visual inspection does not reveal any clear trends in the change of gradation with traffic level increase from level 3 to level 4, or to N_{design} increase from 60 to 90. However, MnDOT and Indiana Superpave 5 gradation curves show a clear difference. Indiana Superpave 5 mixtures clearly tend to have lower % passing for sieve sizes from 0.3mm to 4.75mm (No.50 to No.4). Note that MDL stands for maximum density line.

The gradation curves of MnDOT 12.5mm (1/2in) mixtures and Indiana Superpave 5 19mm (3/4in) mixture are plotted in Figure 3.2. Similar to Figure 3.1, no clear trends are observed in the change of gradation with the increase in traffic level or N_{design} . However, a clear difference is observed between MnDOT and Indiana Superpave 5 mixtures. Indiana Superpave 5 mixtures tend to have lower % passing for sieve sizes from 0.3mm to 9.5mm (No.50 to 3/8in).

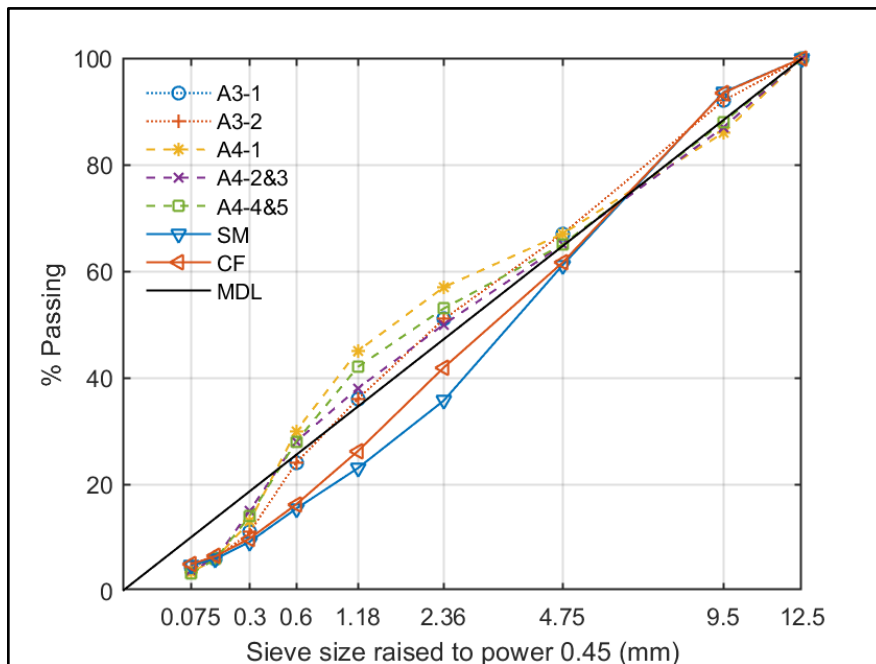


Figure 3.1 Gradation curves of mixtures with NMAS = 9.5 mm (3/8in)

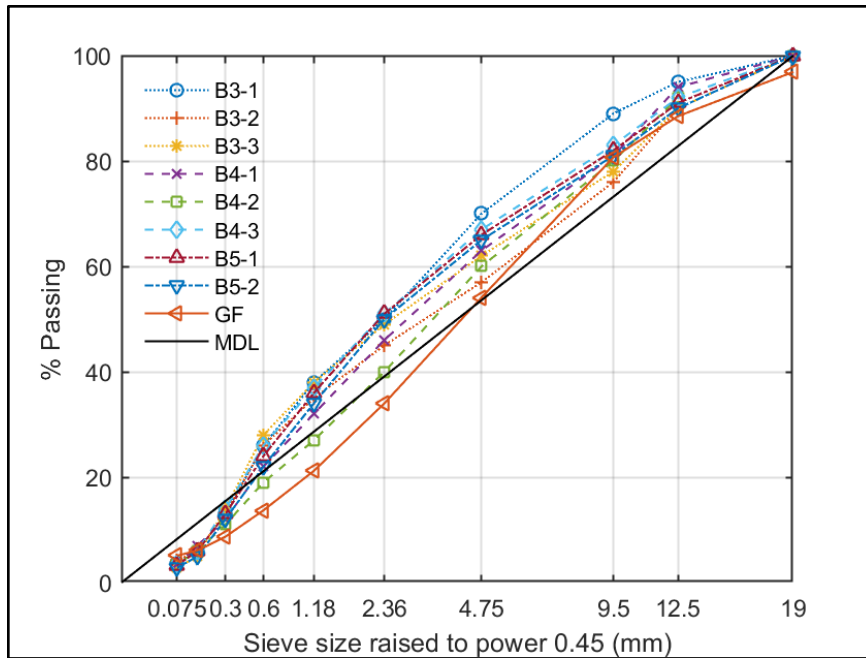


Figure 3.2 Gradation curves of mixtures with NMAS = 12.5 mm (1/2in)

3.2.2 Gradation Characterization

To further characterize the gradations of the investigated mixture, Bailey method parameters are computed and listed in Table 3.4, Table 3.5, and Table 3.6 respectively, for MnDOT 9.5mm (3/8in) mixtures, 12.5mm (1/2in) mixtures, and Indiana Superpave 5 mixtures.

In Bailey method, aggregates are separated into different portions by three critical sieve sizes. They are the Primary Control Sieve (PCS), Secondary Control sieve (SCS), and Tertiary Control Sieve (TCS). The control sieve sizes have the following relationships: PCS = 0.22*NMAS (nominal maximum aggregate size), SCS = 0.22*PCS, and TCS = 0.22*SCS. The gradations are characterized by Primary Control Sieve Index (PCSI), Coarse Aggregate Ratio (CA Ratio), Fine Aggregate Coarse Ratio (FAC Ratio), and Fine Aggregate Fine Ratio (FAf Ratio), which are defined by the following formulae:

$$PCSI = \%Passing\ PCS$$

$$CA\ Ratio = \frac{(\%Passing\ Half\ Sieve - \%Passing\ PCS)}{(100\% - \%Passing\ Half\ Sieve)}$$

$$FAC\ Ratio = \frac{\%Passing\ SCS}{\%Passing\ PCS}$$

$$FAf\ Ratio = \frac{\%Passing\ TCS}{\%Passing\ SCS}$$

Half Sieve is the sieve size equals 0.5*NMAS (maximum aggregate size).

In Bailey method, PCSI characterizes the overall fineness of the aggregates, CA characterizes the fineness of coarse aggregates (aggregates larger than PCS), FAc characterizes the fineness of coarse portion of fine aggregates (aggregates larger than SCS but smaller than PCS), and FAf characterizes the fineness of fine portion of fine aggregates (aggregates smaller than SCS).

In this investigation, we also calculate another parameter called the distance to maximum density line (Dmdl), that is defined as the accumulated difference of the passing rate between the gradation curve and the maximum density line:

$$Dmdl = \sum_{\text{min sieve}}^{\text{max sieve}} |\%Pass \text{ of the sieve} - \%Pass \text{ of the sieve on MDL}|$$

This is based on previous research that showed that mixture compactability is related to how close the gradation curve is to the maximum density line (Hekmatfar et al., 2015; Huber et al., 2016).

The results of Dmdl are also listed in Table 3.4, Table 3.5, and Table 3.6.

Table 3.4 Bailey Method Parameters for MnDOT mixtures with NMAS = 9.5mm (3/8in)

Mixture ID	A3-1	A3-2	A4-1	A4-2&3	A4-4&5
PCSI	51	57	50	45	45
CA	0.48	0.30	0.43	0.57	0.57
FAc	0.47	0.53	0.56	0.44	0.44
FAf	0.19	0.11	0.14	0.17	0.17
Dmdl	27.95	42.71	21.71	34.55	34.55

Table 3.5 Bailey Method Parameters for MnDOT mixtures with NMAS = 12.5mm (1/2in)

Mixture ID	B3-1	B3-2	B3-3	B4-1	B4-2	B4-3	B5-1	B5-2
PCSI	50	45	49	46	40	51	51	50
CA	1.08	0.49	0.55	0.72	0.78	0.75	0.69	0.67
FAc	0.52	0.58	0.57	0.48	0.48	0.51	0.47	0.44
FAf	0.14	0.16	0.10	0.16	0.18	0.13	0.14	0.13
Dmdl	77.29	38.29	54.29	47.29	36.80	64.29	59.29	53.29

Table 3.6 Bailey Method Parameters for Indiana Superpave 5 mixtures

Mixture ID	SP5-1 (SM)	SP5-2 (CF)	SP5-3 (GF)
PCSI	35.7	41.9	34
CA	0.65	0.51	0.76
FAc	0.43	0.39	0.40
FAf	0.31	0.31	0.37
Dmdl	59.15	47.25	65.07

A number of trends are identified. Indiana Superpave 5 mixtures have higher CA, lower FAc, and higher FAf than MnDOT mixtures, which suggests that Indiana Superpave 5 mixtures have a finer coarse

aggregate portion, a coarser coarse portion of fine aggregates and a finer fine portion of fine aggregates than MnDOT mixtures.

3.2.3 Aggregate Angularity

Aggregate angularity is another factor that may have a great effect on field compaction. In MnDOT current specification (2018), the aggregate angularity is quantified by the Coarse Aggregate Angularity (CAA) of one face and two faces (ASTM D5821), and the Fine Aggregate Angularity (FAA) (AASHTO T304 Method A). The aggregate properties requirements of MnDOT specification (2018) are shown in [Figure 3.3](#). It can be seen that angularity increases with the increase in traffic level.

This information is available for the 15 MnDOT projects presented before. The aggregate angularity average values obtained as part of the quality control and quality assurance (QC&QA) process are listed in Table 3.7. For the three Indiana Superpave 5 mixtures, the QC&QA angularity data is not available, however, the angularity data of the mixture design process is available and is listed at the bottom of Table 3.7.

Table 3139-3 Mixture Aggregate Requirements				
Aggregate Blend Property	Traffic Level 2	Traffic Level 3	Traffic Level 4	Traffic Level 5
20 year Design ESAL's	<1 million	1 - 3 million	3 - 10 million	10 - 30 million
Min. Coarse Aggregate Angularity (ASTM D5821) (one face / two face), % (one face / two face), % Non-Wear	30/- 30/-	55 / - 55 / -	85 / 80 60/ -	95 / 90 80 / 75
Min. Fine Aggregate Angularity (FAA) (AASHTO T304, Method A) % %-Non-Wear	40 40	42 40	44 40	45 40
Flat and Elongated Particles, max % by weight, (ASTM D 4791)	-	10 (5:1 ratio)	10 (5:1 ratio)	10 (5:1 ratio)
Min. Sand Equivalent (AASHTO T 176)	-	-	45	45
Max. Total Spall in fraction retained on the #4 sieve – Wear	5.0	2.5	1.0	1.0
Non-Wear	5.0	5.0	2.5	2.5
Maximum Spall Content in Total Sample – Wear	5.0	5.0	1.0	1.0
Non-Wear	5.0	5.0	2.5	2.5
Maximum Percent Lumps in fraction retained on the #4 sieve	0.5	0.5	0.5	0.5
Class B Carbonate Restrictions				
Maximum% -#4 Final Lift/All other Lifts	100/100	100/100	80/80	50/80
Maximum% + #4 Final Lift/All other Lifts	100/100	100/100	50/100	0/100
Max. allowable scrap shingles –MWSS ⁽¹⁾ Wear/Non Wear	5/5	5/5	5/5	5/5
Max. allowable scrap shingles –TOSS ⁽¹⁾ Final Lift/All other Lifts	5/5	5/5	0/5	0/0

(1) MWSS is manufactured waste scrap shingle and TOSS is tear-off scrap shingle.

Figure 3.3 Aggregate properties requirements in MnDOT specification (2018).

Table 3.7 Aggregate angularity

Mixture ID	FAA	CAA One Face	CAA Two Faces	Mixture ID	FAA	CAA One Face	CAA Two Faces
A3-1	42.60	91.40	NA	B3-3	42.00	96.50	NA
A3-2	NA	NA	NA	B4-1	44.10	98.40	97.50
A4-1	44.00	91.04	87.86	B4-2	44.90	98.90	97.80
A4-2	44.63	91.88	91.13	B4-3	NA	NA	NA
A4-3	44.50	92.00	91.40	B5-1	45.69	98.53	98.53
A4-4	43.80	96.10	95.80	B5-2	45.00	97.88	97.88
A4-5	44.04	97.91	97.91	SM	46.00	100.0	100.0
B3-1	42.67	84.33	NA	CF	45.00	100.0	100.0
B3-2	42.00	99.00	99.00	GF	46.00	99.00	98.00

3.3 FIELD DENSITY DATA

Field as-constructed density plays a significant role in quality control and quality assurance (QC&QA) of pavement construction. According to MnDOT current specification (2018), for each compaction lot, four cores should be taken. The first two cores are taken from random locations as directed by the engineer. The third and fourth cores are taken as companion cores, which are within 1ft longitudinally from the first two cores. The density of the first two cores is tested by contractors, and at least one of the two companion cores for verification is tested by MnDOT.

3.3.1 Field Density Data for MnDOT Mixtures

A total of 1354 measurements of field core density were collected for the 15 MnDOT projects investigated. The distribution of field core density data is plotted in Figure 3.4. Basic statistics are listed in Table 3.8.

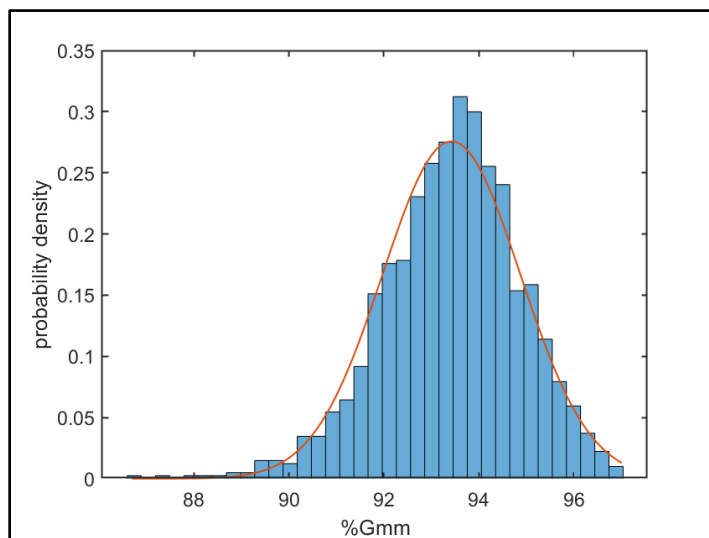


Figure 3.4 Frequency distribution of field cores density data.

Table 3.8 Basic statistics of field cores density data

Statistics	Mean	Median	Std	Skewness	Kurtosis
Value	93.4	93.5	1.45	-0.44	3.68

As shown in Figure 3.4, the data approximately follow normal distribution, with a mean of 93.4 and a standard deviation of 1.45. The red line represents the normal distribution fit of the data. The skewness and kurtosis values, listed in Table 3.8, show that the distribution of the data is a bit left-skewed (skewness<0), which means that the actual probability density function (PDF) of field core density is more concentrated on higher densities. The actual PDF is also a bit leptokurtic (kurtosis>3), which means the peak of the actual PDF is taller compared with the fitted normal distribution.

To further investigate normality of the distribution of the overall data, a q-q (quantile-quantile) plot is drawn in Figure 3.5. As shown, the values are a bit left-skewed, while in the middle range, from 91% to 96% G_{mm} , the normality is good.

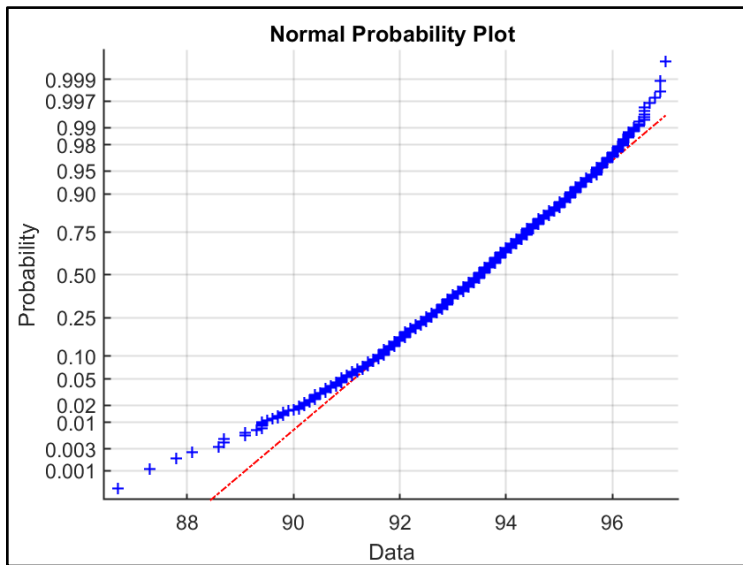


Figure 3.5 Normal distribution q-q plot for cores density data

The cumulative distribution function of the overall density data is plotted in Figure 3.6. There are 16% of the field cores that had lower densities than the density currently required by MnDOT specification (MnDOT, 2018), which is 92% G_{mm} . The vast majority (87%) of field cores have densities less than 95% G_{mm} which is the requirement for a Superpave 5 mixture. To achieve this field density requirement, most of the currently designed mixtures need to be redesigned to improve their field compaction.

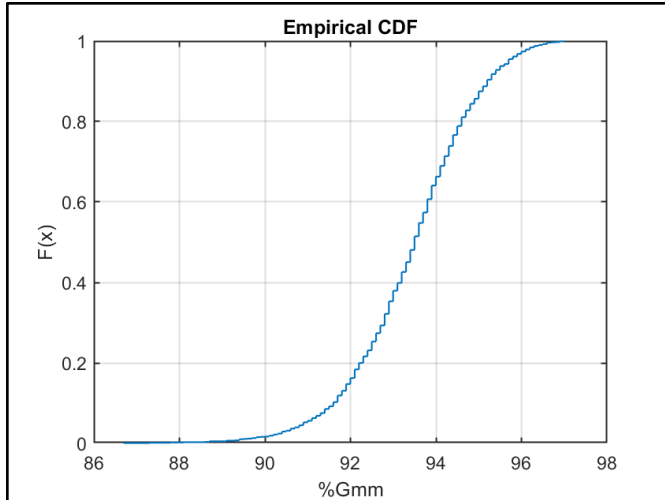


Figure 3.6 Cumulative distribution function of cores density data

The same procedure was performed for the field density data of each project. All projects approximately follow normal distribution, which guarantees the correctness of analysis of variance (ANOVA) that is conducted in the following sections.

Field densities at the longitudinal joints were also measured as part of the QC/QA process. A total of 314 density measurements of longitudinal joint cores were collected for the 15 MnDOT projects investigated. There are two types of longitudinal joints, the confined joints and unconfined joints. The distributions of longitudinal joint densities of the two types are shown in Figure 3.7, and their basic statistics are listed in Table 3.9. As expected, the means of both confined and unconfined joint densities (92.2% G_{mm} and 91.7% G_{mm} respectively) are less than that of the regular field core densities (93.4% G_{mm}), and the mean of confined joint densities are higher than that of the unconfined joints.

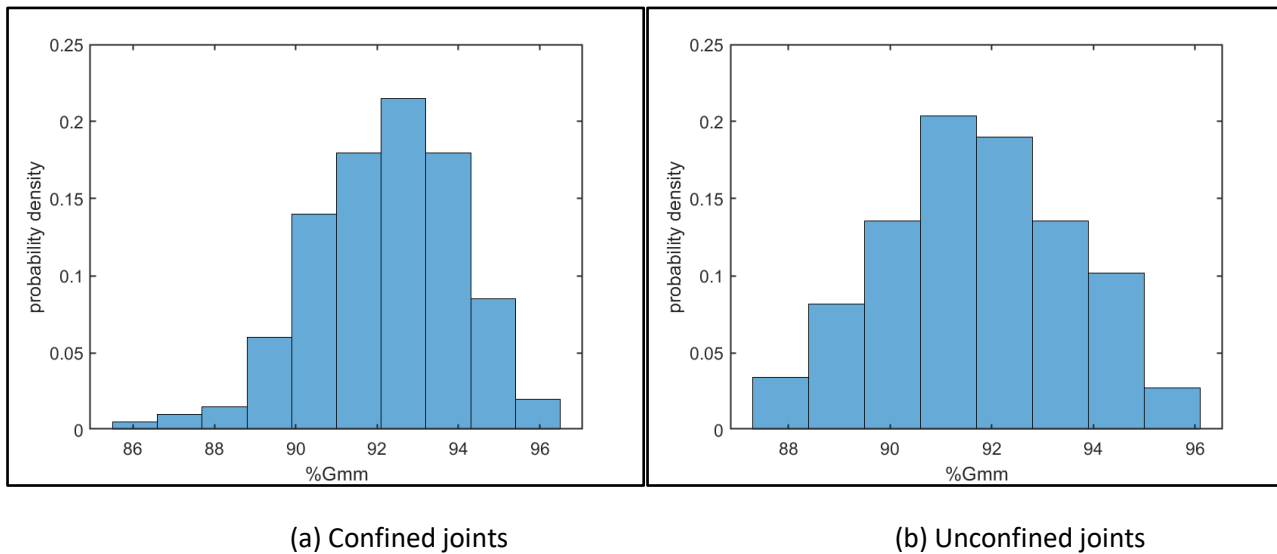


Figure 3.7 Frequency distribution of longitudinal joint densities.

Table 3.9 Basic statistics of longitudinal joint density data

Type of joints	Mean	Median	Std	Skewness	Kurtosis
Confined	92.2	92.5	1.80	-0.43	2.99
Unconfined	91.7	91.7	1.87	-0.06	2.37

3.3.2 Field Density Data for Indiana Superpave 5 Mixtures

In Indiana, after the laboratory testing phase of the new Superpave 5 mixture design method, INDOT constructed 12 trial projects in the six different districts of Indiana. The QC/QA data were analyzed by the research team at Purdue University (Haddock et al., 2020). It was found that the average as-constructed density for the projects is 93.8%, less than the Superpave 5 recommended 95%, and is just 0.4% higher than that of current MnDOT projects (93.4%). It was recommended that agencies should implement some type of additional training for contractor personnel, in order to help them increase their understanding of Superpave 5 concepts and how to best implement the design method in their operation.

3.4 STATISTICAL ANALYSIS OF MNDOT FIELD DENSITY DATA

3.4.1 Analysis of Variance (ANOVA)

In this section, analysis of variance (ANOVA) is conducted. First, a one-way ANOVA is conducted to identify differences between projects. Then, a two-way ANOVA is conducted to study the effect of two factors, namely, NMAAS and traffic levels.

3.4.1.1 One-Way ANOVA

Figure 3.8 shows the box plot of field core density data of all projects. To find out if there is significant difference between projects, a one-way ANOVA is conducted.

In the one-way ANOVA, the null hypothesis H_0 is: the population means of each project are equal, while the alternative hypothesis H_1 is: at least one of the projects has a population mean that is different from others.

The results of the one-way ANOVA is shown in Table 3.10. The P-value, 2.42×10^{-49} , is much smaller than the significant level 0.05, thus we are confident to reject the null hypothesis, and conclude that there are significant difference between the different projects.

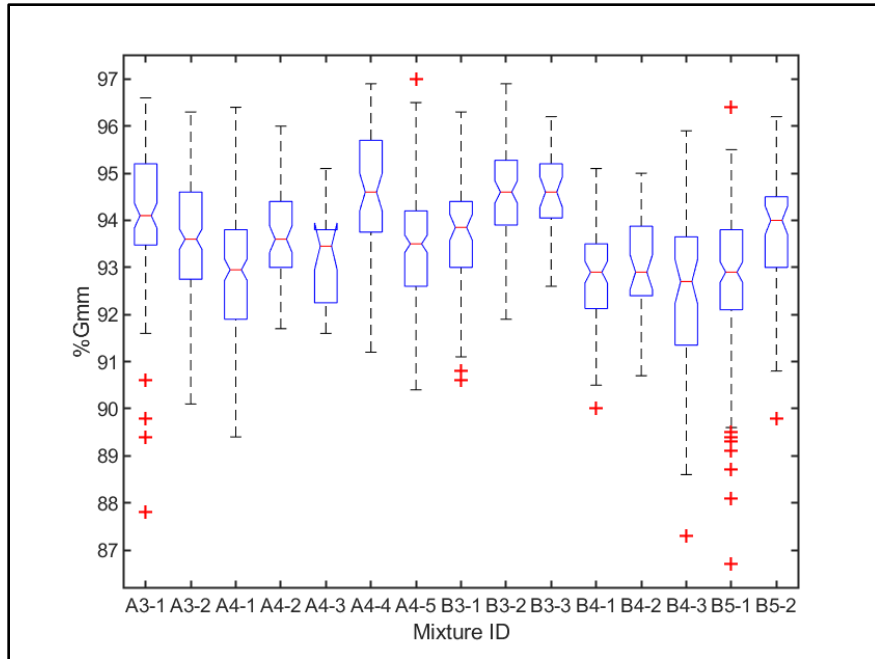


Figure 3.8 Box plot of the core density data for all projects

Table 3.10 One-Way ANOVA of the all projects

Source of Variation	SS	df	MS	F	P-value
Groups	514.38	14.00	36.74	21.24	2.42×10^{-49}
Error	2316.70	1339.00	1.73		
Total	2831.07	1353.00			

Note: SS stands for sum of squares, df stands for degrees of freedom, MS stands for mean square, and F stands for F-ratio.

The one-way ANOVA indicates significant differences between projects, but it does not identify the exact pairs from which the significant differences come from. A Tukey test is conducted, that provide the pairwise comparison between projects.

Figure 3.9 shows the 95% confidence interval for each mixture by Tukey method. Using colored symbols, an example is shown for the comparison between A3-1 (the blue line) and the other mixtures. All mixtures marked by red lines do not have overlap with A3-1 in their confidence intervals, which means they are significantly different from A3-1, while mixtures marked by grey lines overlap with the confidence interval of A3-1, thus the differences between them are not significant. The same procedure can be used to individually compare all other mixtures.

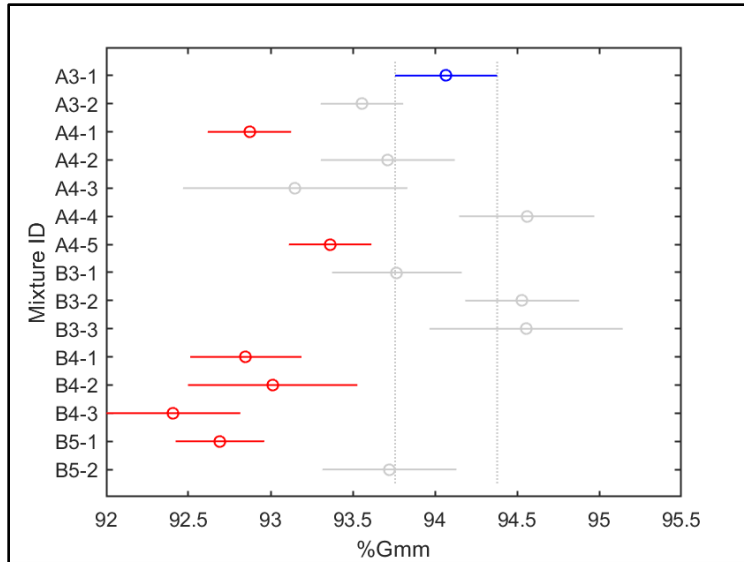


Figure 3.9 95% confidence intervals for all projects

A4-2 and A4-3, and A4-4 and A4-5, respectively, have similar aggregate gradations, but different RAP content. A4-2 and A4-4 have RAP contents higher than A4-3 and A4-5, respectively, as shown in Table 3.1. Any significant differences may indicate the effect of RAP content on field density.

As shown in Figure 3.9, A4-2 and A4-3 densities are not significantly different, although the average field density of A4-2 is higher than that of A4-3. However, A4-4 has a significant higher density than A4-5. The data seems to indicate a trend that RAP content is positively correlated with field density of mixtures. This trend is opposite to common experience that RAP addition adversely impacts field compaction. Other factors, not used in this investigation, could explain this trend.

The estimated mean and standard error of each project by Tukey method are listed in Table 3.11. The mean values are used in the correlation analysis in section 3.5.

Table 3.11 Estimated values of mean and standard error by Tukey method.

Mixture ID	Mean	Standard error	Mixture ID	Mean	Standard error
A3-1	94.07	0.13	B3-1	93.77	0.16
A3-2	93.56	0.10	B3-2	94.53	0.14
A4-1	92.87	0.10	B3-3	94.55	0.24
A4-2	93.71	0.17	B4-1	92.85	0.14
A4-3	93.15	0.27	B4-2	93.01	0.21
A4-4	94.56	0.17	B4-3	92.41	0.17
A4-5	93.36	0.10	B5-1	92.69	0.11
			B5-2	93.72	0.17

3.4.1.2 Two-Way ANOVA

Each project can also be grouped by two factors, NMAAS and traffic level. A two-way ANOVA is conducted to investigate the effect of these two factors and their effect on field density.

The first factor is NMAAS. There are two levels of NMAAS, 9.5 and 12.5 mm (3/8in and 1/2in), which are denoted by A and B respectively, according to the convention of MnDOT designation. The second factor is the traffic level. Traffic levels range from 3 to 5, but there is no level 5 for type A mixtures.

In two-way ANOVA, we need to test the following three pairs of hypotheses:

$$\begin{cases} H_{01}: \text{The population means of the first factor are equal.} \\ H_{11}: \text{The population means of the first factor are not equal} \end{cases}$$

$$\begin{cases} H_{02}: \text{The population means of the second factor are equal.} \\ H_{12}: \text{The population means of the second factor are not equal} \end{cases}$$

$$\begin{cases} H_{03}: \text{There is no interaction between the two factors.} \\ H_{13}: \text{There is interaction between the two factors.} \end{cases}$$

The results of the two-way ANOVA are listed in Table 3.12. The effect of NMAAS is not significant, since P-value = 0.53 > 0.05, while the effect of traffic level and the interaction between NMAAS and traffic level are significant, with P-values close to zero. As shown later, the effect of traffic level on field density is observed through the effect of N_{design} and aggregate angularity, as requirements of N_{design} and aggregate angularity are related to traffic level.

Similar to the procedure of one-way ANOVA, a Tukey method multiple comparison is conducted. Figure 3.10 shows the confidence interval of densities for the two levels of NMAAS. As shown, the difference of field density between different NMAAS levels is not significant, with both means around 93.5% G_{mm} . The estimated means and standard errors of the two NMAAS levels are listed in Table 3.13.

Table 3.12 Two-Way ANOVA for all projects

Source of Variation	SS	df	MS	F	P-value
NMAAS	0.69	1	0.69	0.39	0.53
Traffic Level	218.58	1	218.58	124.32	0.00
NMAAS*Traffic Level	78.65	1	78.65	44.73	0.00
Error	2007.85	1142.00	1.76		
Total	2244.21	1145.00			

Note: SS stands for sum of squares. df stands for degrees of freedom. MS stands for mean square. F stands for F ratio.

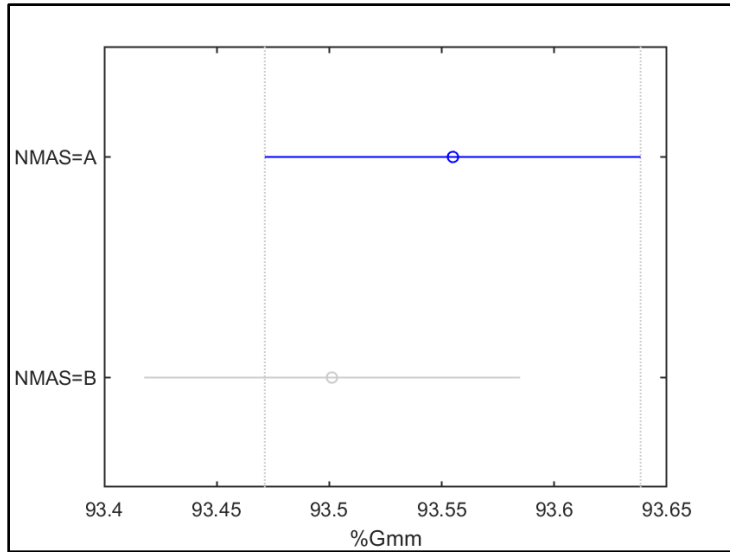


Figure 3.10 Comparison between different NMAS levels. A stands for 9.5mm (3/8in) and B stands for 12.5mm (1/2in).

Table 3.13 Estimated values of mean and standard error of projects grouped by NMAS.

NMAS	Mean	Standard error
A	93.555	0.049
B	93.501	0.070

Figure 3.11 shows the comparison of confidence interval of field densities of different traffic levels. Clearly, the mixtures belonging to traffic level 3 have significantly higher field density (94% G_{mm}) than traffic level 4 (93% G_{mm}). The result of traffic level 5 is not shown in Figure 3.11 **Figure 3.11** because the confidence interval could not be computed due to the lack of data for level 5 type A mixtures. The estimated means and standard errors for the two NMAS levels are listed in Table 3.14.

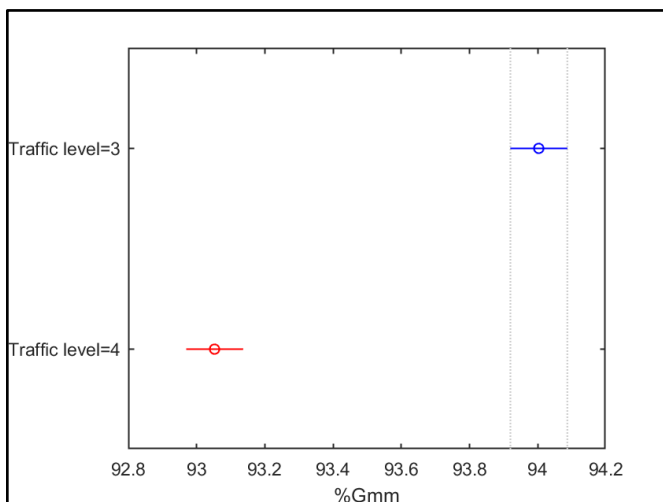


Figure 3.11 Comparison between different traffic levels.

Table 3.14 Estimated value of means and standard errors of projects grouped by traffic levels.

Traffic level	Mean	Standard error
3	94.003	0.063
4	93.053	0.057
5	92.989	0.095

The difference in field density between mixtures of different traffic levels could be related to the difference in the requirements of N_{design} and aggregate angularity for different traffic levels. N_{design} requires as 60, 90, and 100 for level 3, 4, and 5, respectively. The difference of the requirements of aggregate angularity can be seen in Figure 3.3. Given that regardless of traffic level, mixtures are designed to the same air void ratio (4%), the higher the N_{design} , the less compactable the mixture is designed.

The results of the two-way ANOVA show that the interaction between NMAS and traffic level is significant, so we also need to compare the grouping of mixtures by both NMAS and traffic levels. As shown in Figure 3.12, all groups show significant difference, except the pair NMAS = B, traffic level = 4 and NMAS = B, traffic level = 5. The estimated means and standard errors are listed in Table 3.15. To understand the interaction between the two factors, we consider the effect of traffic level at different NMAS levels. It is clear that for both A and B NMAS, field density decreases with the increase in traffic level. However, the decrease in field density at NMAS = A is much smaller than the decrease when NMAS = B.

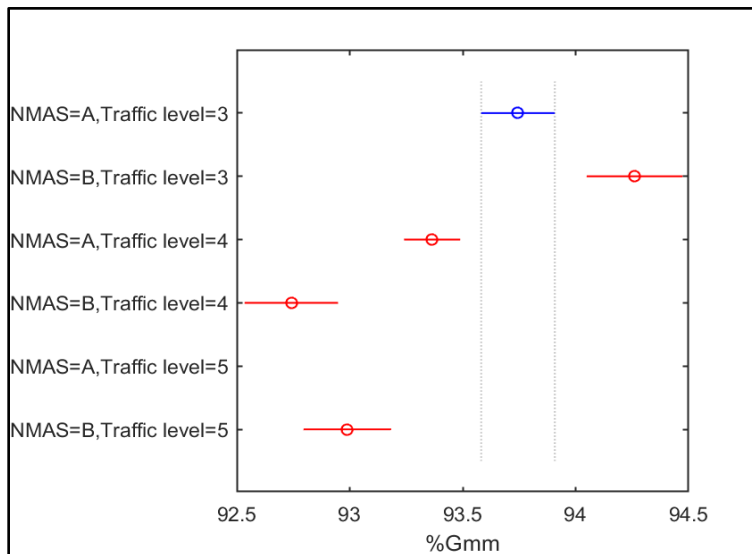


Figure 3.12 Comparison of different NMAS and traffic levels.

Table 3.15 Estimated value of means and standard errors of projects grouped by NMAS and traffic levels.

NMAS	Traffic level	Mean	Standard error
A	3	93.745	0.081
B	3	94.261	0.103
A	4	93.365	0.062
B	4	92.741	0.101
B	5	92.989	0.095

3.5 CORRELATION ANALYSIS BETWEEN MATERIAL PROPERTIES AND FIELD DENSITIES

A correlation analysis is conducted between field cores densities, N_{design} , and material properties, including binder content, RAP content, indices characterizing gradation, and aggregate angularity.

Table 3.16 shows the P-value of the hypothesis test of correlation analysis. In the hypothesis test, the null hypothesis H_0 is that there is no correlation between the two variables. It can be observed that seven pairs have a P-value < 0.05 and passed the hypothesis test, which indicates that the corresponding variables are correlated. The correlation coefficients are listed in Table 3.17. The cells corresponding to significant correlations are shaded in both Table 3.16 and Table 3.17. FD stands for field core density. AC stands for binder content. RAP stands for reclaimed asphalt pavement content. Dmdl stands for distance to maximum density line. CAA1 and CAA2 represents coarse aggregate angularity of one face and two faces respectively.

Table 3.16 P-values for the correlation analysis

	FD	N_{design}	AC	RAP	NMAS	PCSI	CA	FAc	FAf	Dmdl	FA A	CAA1	CAA2
FD	1.000	0.020	0.164	0.154	0.655	0.722	0.248	0.176	0.546	0.563	0.005	0.870	0.595
N_{design}		1.000	0.635	0.089	0.984	0.517	0.843	0.042	0.907	0.642	0.000	0.205	0.715
AC			1.000	0.135	0.716	0.680	0.621	0.904	0.479	0.855	0.164	0.925	0.077
RAP				1.000	0.727	0.200	0.158	0.118	0.170	0.778	0.247	0.216	0.428
NMAS					1.000	0.207	0.003	0.843	0.935	0.001	0.817	0.269	0.019
PCSI						1.000	0.121	0.303	0.003	0.757	0.685	0.591	0.932
CA							1.000	0.267	0.317	0.001	0.777	0.235	0.428
FAc								1.000	0.047	0.882	0.009	0.922	0.966
FAf									1.000	0.350	0.695	0.664	0.722
Dmdl										1.000	0.829	0.535	0.067
FAA											1.000	0.367	0.877
CAA1												1.000	0.000
CAA2													1.000

Table 3.17 Correlation coefficients

	FD	N _{design}	AC	RAP	NMAS	PCSI	CA	FAc	FAf	Dmdl	FAA	CAA1	CAA2
FD	1.00	-0.59	0.38	0.39	-0.13	0.10	-0.32	0.37	-0.17	-0.16	-0.73	-0.05	0.19
N _{design}		1.00	-0.13	-0.45	-0.01	-0.18	0.06	-0.53	0.03	-0.13	0.94	0.38	-0.13
AC			1.00	-0.40	0.10	-0.12	0.14	-0.03	0.20	0.05	-0.41	0.03	0.58
RAP				1.00	0.10	0.35	-0.38	0.42	-0.37	0.08	-0.35	0.37	0.28
NMAS					1.00	-0.35	0.71	0.06	-0.02	0.74	-0.07	0.33	0.72
PCSI						1.00	-0.42	0.29	-0.71	0.09	-0.12	-0.16	0.03
CA							1.00	-0.31	0.28	0.77	0.09	-0.35	0.28
FAc								1.00	-0.52	-0.04	-0.69	0.03	0.02
FAf									1.00	-0.26	0.12	-0.13	-0.13
Dmdl										1.00	-0.07	-0.19	0.60
FAA											1.00	0.27	-0.06
CAA1												1.00	0.98
CAA2													1.00

Field core density has a significant correlation with N_{design}, which is consistent with the results of ANOVA on traffic level. The negative correlation is also illustrated in the scatter plot in [Figure 3.13](#).

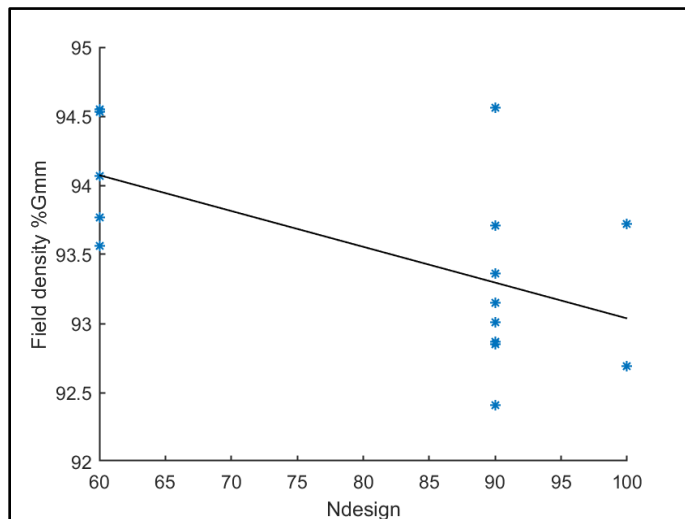


Figure 3.13 Correlation between field density and N_{design}.

To understand the correlation between field density and N_{design}, we need consider what the real meaning of N_{design} is. N_{design} is a mixture design parameter which was originally proposed to represent the traffic level and to control the rutting resistance of mixtures (Blankenship et al., 1994). The logic was that, for higher traffic level pavement, N_{design} should be higher so that the mixture has a higher rutting resistance. However, N_{design} is a parameter of the Superpave gyratory compaction, which is related to compaction but not necessarily related to rutting resistance. Physically, N_{design} represents the laboratory

gyratory compaction effort. For a fixed design air void ratio, it can represent the laboratory compactability of a mixture. The lower the N_{design} , the higher the compactability.

Given that N_{design} is a representation of the laboratory compactability of a mixture, the correlation between field density and N_{design} indicates that the laboratory compactability and field compactability of a mixture are consistent. This finding is important, because it confirms that field compaction can be reasonably predicted by the laboratory gyratory compaction test.

Since both the field compaction and laboratory compaction (N_{design}) are significantly correlated with FAA, it can be concluded that the difference in FAA is the main cause of the difference in compactability. As illustrated in the scatter plots in Figure 3.14, the increase in FAA reduces both laboratory and field compaction.

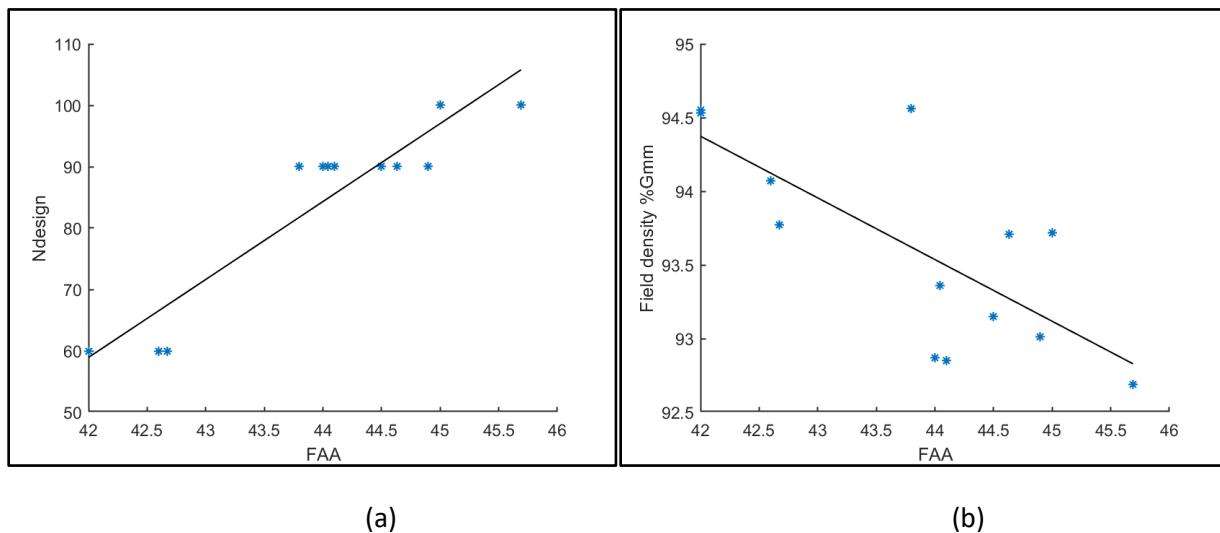


Figure 3.14 Correlations of FAA with N_{design} and field density.

The correlation analysis also reveals the correlations between aggregate angularity and gradation. As illustrated in the scatter plot in Figure 3.15, FAA is significantly correlated with one of the fine aggregate gradation indices, FAC. This correlation is reasonable by examining the test method of FAA (AASHTO, T304, method A), which is actually a test of fine aggregate packing rather than just fine aggregate angularity. Therefore, instead of a representation of fine aggregate angularity, FAA is actually a representation of fine aggregate packing. Though fine aggregate angularity is a main factor affecting fine aggregate packing, gradation of fine aggregates has a significant effect on fine aggregate packing too. This explains why FAA is correlated with the gradation index FAC.

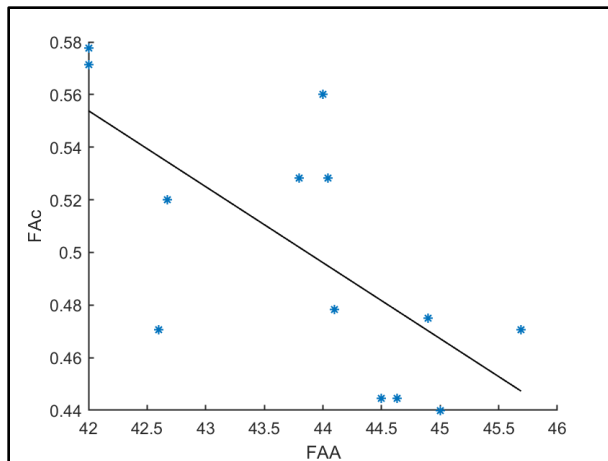


Figure 3.15 Correlations between fine aggregate angularity and gradation.

The identified correlations between compactability and fine aggregate packing suggest a way to design more compactable mixtures, which is using fine aggregates with smaller FAA, or in other words, denser packing. However, in current MnDOT design method, the FAA is restricted mainly to guarantee the rutting resistance (as shown in Figure 3.3). Many other studies have shown the effect of increasing FAA on preventing rutting (Prowell et al., 2005), so reducing FAA may have a potential of reducing the rutting resistance. Therefore, while reducing FAA to improve compactability, other measures must be taken to ensure the rutting resistance is not affected. A possible way of doing that is to concomitantly optimize coarse aggregate packing, like Bailey method. A well designed coarse aggregate packing can achieve a better interlocking of coarse aggregates and therefore increases rutting resistance. By combining the two measures, to design more compactable mixtures, we optimize the fine aggregate packing to increase the compactability of mixtures, while optimizing the coarse aggregate packing to make sure that rutting resistance is not sacrificed.

A number of correlations between aggregate properties are also identified. CAA2 has a positive correlation with NMAAS as shown in Figure 3.16. PCSI and FAC have a negative correlation with FAF, as illustrated in Figure 3.17(b) and (c). NMAAS, CA, and Dmdl are positively correlated with each other, as illustrated in Figure 3.17(d), (e) and (f). Unlike the correlation between FAA and FAC shown in Figure 3.15, which can be explained physically by the fine aggregate packing, the correlations shown in Figure 3.16 and Figure 3.17 cannot be explained by physical reasons, because their physical meanings are clearly independent. For example, Physical meanings of CAA2 and NMAAS are the coarse aggregate angularity and aggregate size, respectively. They are clearly independent because aggregates are free to have any angularity regardless of what size it is. Therefore, the identified correlation between CAA2 and NMAAS cannot be attributed to the dependence between aggregate angularity and size. Rather, the real reason for this correlation is the low representativeness of the data. The identified positive correlation between CAA2 and NMAAS may be significant for the 15 projects we investigated for which the larger size aggregates happen to have higher angularities. However, if a larger and more representative set of projects was studied, the correlation between CAA2 and NMAAS may become not significant. Similarly, the limited set of data can also explain the identified correlations shown in Figure 3.17.

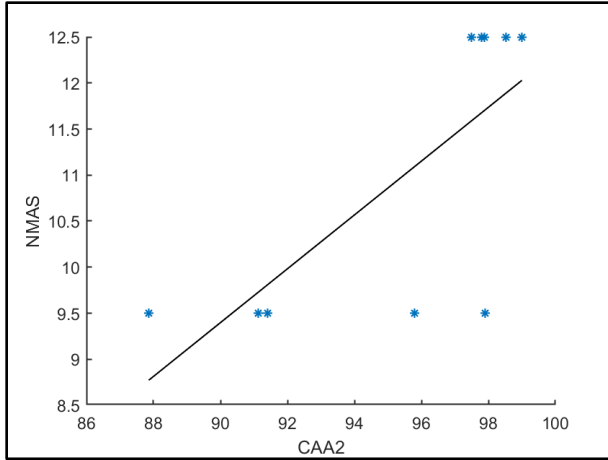
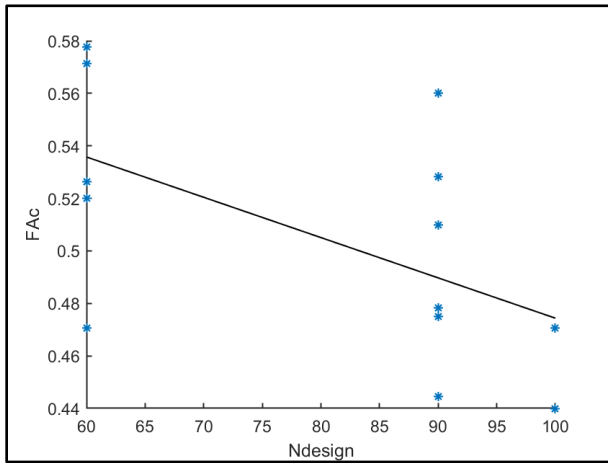
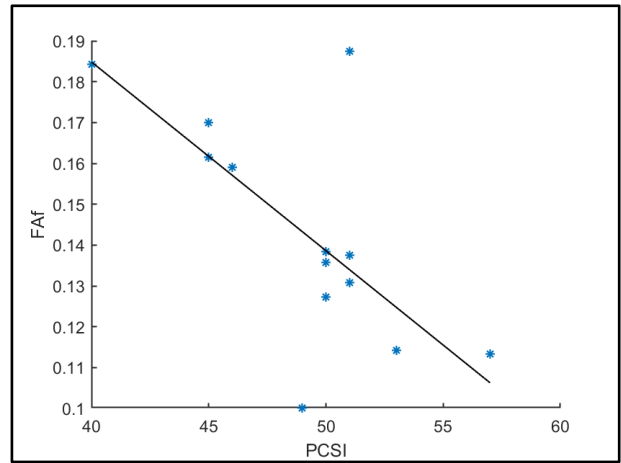


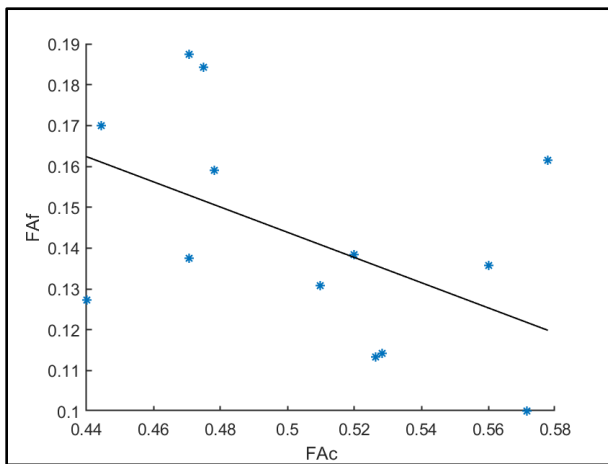
Figure 3.16 Correlation between coarse aggregate angularity and nominal maximum aggregate size



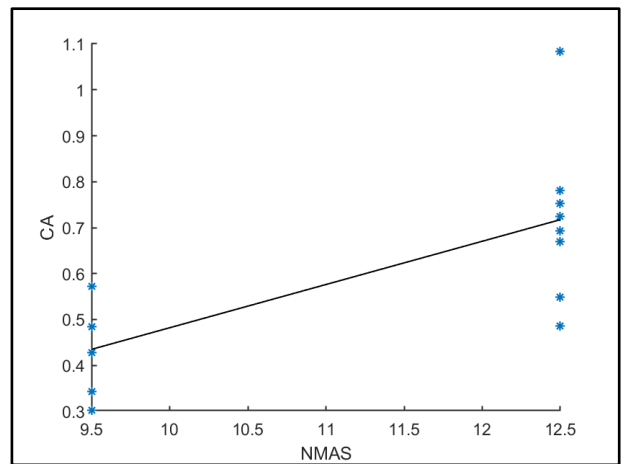
(a)



(b)



(c)



(d)

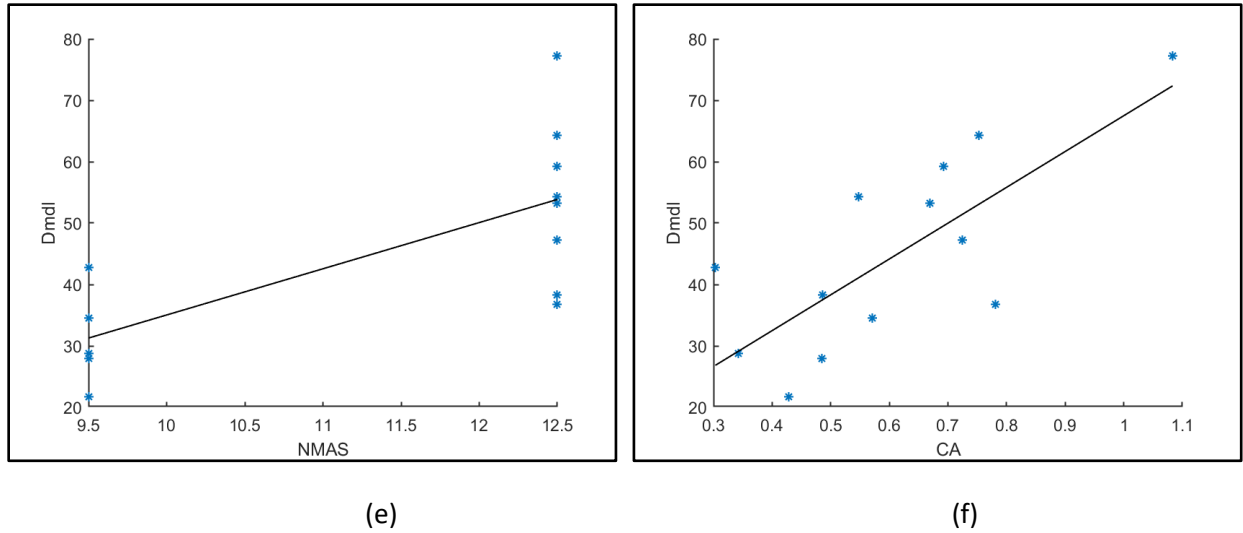


Figure 3.17 Correlations between gradation properties.

3.6 CONCLUSIONS

In this task, the mixture design information and field core densities of 15 past projects were analyzed. The main conclusions are the following:

1. MnDOT mixtures have aggregate gradations that are significantly different compared with the Indiana Superpave 5 mixtures. MnDOT mixtures are fine-graded, while Indiana Superpave 5 mixtures are coarse-graded.
2. Based on Bailey method parameters, Indiana Superpave 5 mixtures have higher CA, lower FAc, and higher FAF than MnDOT mixtures, which suggests that Indiana Superpave 5 mixtures have a finer coarse aggregate portion, a coarser coarse portion of fine aggregates, and a finer fine portion of fine aggregates than MnDOT mixtures.
3. The average field as-constructed density of the 15 MnDOT projects is 93.4 %G_{mm}. The data show that 16% of the field cores have densities less than the lowest requirement 92 %G_{mm}. The vast majority (87%) of the field cores have field as-constructed densities lower than the 95%G_{mm} requirement for Superpave 5. However, it is very important to note that 13% of the cores are denser than 95% G_{mm} without any additional incentive.
4. ANOVA results showed that field densities are significantly affected by traffic level. High traffic level mixtures have lower field density than lower traffic level mixtures, which most likely is related to the different requirements for N_{design} and aggregate angularity for different traffic levels. This result was also confirmed by the correlation analysis. High traffic mixtures have higher aggregate angularity and N_{design} requirements resulting in mixtures which are more difficult to compact.
5. The correlation between N_{design} and field compaction showed that the field compaction and laboratory gyratory compaction results are consistent. Generally, higher field densities are achieved with lower N_{des} (lower traffic) mixtures and lower aggregate angularity.

6. The correlation analysis revealed that mixtures' compactability is significantly correlated with FAA and FAc. Higher field densities are achieved with lower FAA or higher FAc.
7. The identified correlation between FAA and FAc confirmed that FAA values obtained using the standard method (AASHTO T304, method A) are actually a representation of fine aggregate packing, which is affected by not only fine aggregate angularity but also fine aggregate gradation.
8. The correlations between fine aggregate packing (represented by FAA) and compactability suggests a possible way to design more compactable mixture, in which we optimize fine aggregate packing to increase compactability of mixtures, and concomitantly optimize coarse aggregate packing to ensure rutting resistance is not sacrificed.

CHAPTER 4: DATA ANALYSES OF 2020 PROJECTS

In this chapter, mixture design and field density data from ten projects constructed in 2020 were obtained. Comprehensive analyses were performed on mixture properties, field densities, and correlations between them. For three of the ten projects, loose mixtures were also collected, and laboratory compaction was performed to check the original mixture design, and to quantify the field compaction effort of these projects.

4.1 MIXTURE INFORMATION

Ten projects, constructed in 2020, were selected by the technical advisory panel. One of the projects was postponed until 2021, and the data will be analyzed as soon as it becomes available. All mixtures were designed using the Superpave volumetric mixture design method (AASHTO R35, 2019) per MnDOT specification 2360 (2018). Two projects, mix-5 and mix-8, are non-wearing courses which have a design air void ratio of 3%. The other projects are all wearing courses which have a design air void ratio of 4%. Four projects are traffic level 3 (1-3 million ESAL), and the other five projects are traffic level 4 (3-10 million ESAL). Design number of gyrations (N_{design}) for traffic level 3 and 4 are 60 and 90, respectively (MnDOT 2360, 2018). All mixtures contain reclaimed asphalt pavement (RAP), with their RAP content ranging from 18% to 30% by weight. Detailed information about the mixtures used in the selected projects is shown in Table 4.1. RAP content and binder content (%AC) information were from MDR.

Table 4.1 Summary of the mixtures used in the ten 2020 MnDOT projects

Mix ID	mix-1	mix-2	mix-3	mix-4	mix-5	mix-6	mix-7	mix-8	mix-9	mix-10
Traffic level	3	3	4	5	3	3	4	4	4	4
Course type ¹	W	W	W	W	NW	W	W	NW	W	W
NMAS ²	A	B	B	B	B	B	A	B	A	B
Design Air voids	4	4	4	4	3	4	4	3	4	4
Binder PG	58S-28	58S-28	58H-28	58V-34	58S-28	58S-28	58V-34	58S-28	58V-34	58H-34
RAP content	24%	30%	22%	20%	30%	28%	20%	25%	18%	19%
N_{design}	60	60	90	100	60	60	90	90	90	90
%AC	4.8	5.6	5	5.4	5.3	5.3	5.1	5.1	5.3	5

Note: 1, W stands for wearing course; NW stands for non-wearing course. 2, A stands for NMAS=9.5mm (3/8in); B stands for NMAS=12.5mm (1/2in).

4.2 AGGREGATE GRADATION AND ANGULARITY

4.2.1 Gradation Curves

The nine mixtures include two levels of nominal maximum aggregate size (NMAS), 9.5mm (3/8in) and 12.5mm (1/2in). For simplicity, they are denoted by A and B respectively according to MnDOT designation (MnDOT 2360, 2018). As listed in Table 4.1, three mixtures are type A and six mixtures are type B. The aggregate gradation data were obtained from MDR.

Table 4.2 Summary of the aggregate gradations

Mix ID	mix-1	mix-2	mix-3	mix-4	mix-5	mix-6	mix-7	mix-8	mix-9	mix-10
NMAS	A	B	B	B	B	B	A	B	A	B
Sieve Size	1in, 25mm	100	100	100	100	100	100	100	100	100
	3/4in, 19mm	100	100	100	100	100	100	100	100	100
	1/2in, 12.5mm	100	94	86	93	92	91	100	91	100
	3/8in, 9.5mm	88	89	77	85	85	85	97	82	89
	No.4, 4.75mm	65	75	57	68	67	68	67	64	65
	No.8, 2.36mm	55	61	45	53	52	50	47	52	55
	No.16, 1.18mm	42	42	33	38	42	39	31	42	40
	No.30, 0.6mm	26	28	21	26	30	26	20	29	25
	No.50, 0.3mm	11	15	11	15	15	13	10	14	13
	No.100, 0.15mm	5	8	5	7	6	6	6	6	6
	No.200, 0.075mm	3.7	5.7	3.4	4.4	3.3	3.3	3.5	3.2	4

The gradation curves for type A and B mixtures are plotted in Figure 4.1 and Figure 4.2, respectively. Note that MDL stands for maximum density line.

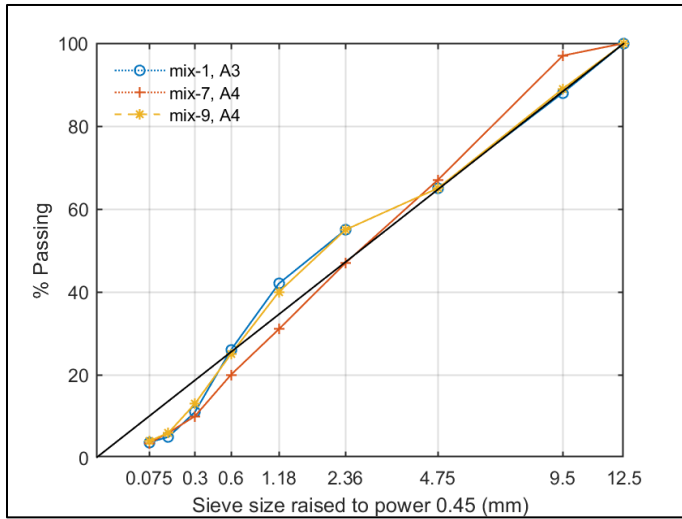


Figure 4.1 Gradation curves of type A mixtures with NMAS = 9.5 mm (3/8in)

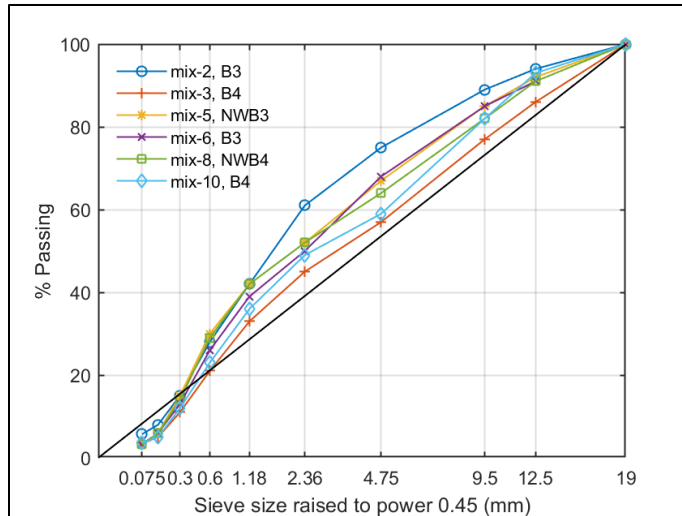


Figure 4.2 Gradation curves of type B mixtures with NMAS = 12.5 mm (1/2in)

4.2.2 Gradation Characterization

Aggregate gradations were further characterized using the Bailey method. Aggregates are separated into different portions using three critical sieve sizes: the Primary Control Sieve (PCS), the Secondary Control sieve (SCS), and the Tertiary Control Sieve (TCS). The control sieve sizes have the following relationships:

$$PCS = 0.22 * NMAS \text{ (nominal maximum aggregate size),}$$

$$SCS = 0.22 * PCS, \text{ and}$$

$$TCS = 0.22 * SCS.$$

The gradations are characterized by Primary Control Sieve Index (PCSI), Coarse Aggregate Ratio (CA Ratio), Fine Aggregate Coarse Ratio (FAc Ratio), and Fine Aggregate Fine Ratio (FAf Ratio), which are defined by the following formulae:

$$PCSI = \%Passing \text{ PCS}$$

$$CA \text{ Ratio} = \frac{(\% \text{ Passing Half Sieve} - \% \text{ Passing PCS})}{(100\% - \% \text{ Passing Half Sieve})}$$

$$FAc \text{ Ratio} = \frac{\% \text{ Passing SCS}}{\% \text{ Passing PCS}}$$

$$FAf \text{ Ratio} = \frac{\% \text{ Passing TCS}}{\% \text{ Passing SCS}}$$

Half Sieve is the sieve size equal to $0.5 * NMAS$ (maximum aggregate size).

PCSI characterizes the overall fineness of the aggregates, CA characterizes the fineness of coarse aggregates (aggregates larger than PCS), FAc characterizes the fineness of coarse portion of fine aggregates (aggregates larger than SCS but smaller than PCS), and FAf characterizes the fineness of fine portion of fine aggregates (aggregates smaller than SCS).

In this investigation, we also calculate another parameter called the distance to maximum density line (Dmdl), that is defined as the accumulated difference of the passing rate between the gradation curve and the maximum density line:

$$Dmdl = \sum_{\text{min sieve}}^{\text{max sieve}} |\%Pass \text{ of the sieve} - \%Pass \text{ of the sieve on MDL}|$$

This is based on previous research that showed that mixture compactability is related to how close the gradation curve is to the maximum density line (Hekmatfar et al., 2015; Huber et al., 2016).

The calculated Bailey method parameters and the Dmdl values are listed in Table 4.2.

Table 4.2 Bailey Method Parameters for 2020 MnDOT mixtures.

Mix ID	NMAS (mm)	PCSI (%)	CA	FAc	FAf	Dmdl (mm)	Mix ID	NMAS (mm)	PCSI (%)	CA	FAc	FAf	Dmdl (mm)
mix-1	9.5	55	0.65	0.47	0.14	39.02	mix-6	12.5	50	0.56	0.52	0.23	73.27
mix-2	12.5	61	1.03	0.46	0.29	96.87	mix-7	9.5	47	0.61	0.43	0.18	43.06
mix-3	12.5	45	0.65	0.47	0.24	36.42	mix-8	12.5	52	0.33	0.56	0.21	73.37
mix-4	12.5	68	0.87	0.46	0.24	45.33	mix-9	9.5	55	0.29	0.45	0.16	33.96
mix-5	12.5	52	0.45	0.58	0.20	80.27	mix-10	12.5	49	0.24	0.47	0.22	57.97

4.2.3 Aggregate Angularity

Aggregate angularity is another factor that affects compaction. In MnDOT 2360 specification (2018), the aggregate angularity is quantified by the Coarse Aggregate Angularity (CAA) of one face and two faces (ASTM D5821), and the Fine Aggregate Angularity (FAA) (AASHTO T304 Method A). The aggregate angularities were obtained as part of the quality control and quality assurance (QC&QA) process. The averaged values for each project are listed in Table 4.3. The required aggregate angularity increases with traffic level of projects. As listed in the Table 3 of MnDOT specification 3139 (2018), the required minimum FAA for traffic level 3, 4 and 5 are 42%, 44% and 45%, respectively. The corresponding values for CAA1 are 55%, 85% and 95% respectively. There is no minimum requirement of CAA2 for traffic level 3, while for traffic level 4 and 5, the required minimum CAA2 values are as 80% and 90%, respectively.

Table 4.3 Aggregate angularity

Mix ID	FAA, %	CAA One Face, %	CAA Two Faces, %	Mix ID	FAA, %	CAA One Face, %	CAA Two Faces, %
mix-1	42.00	90.20	NA	mix-6	42.4	82.0	NA
mix-2	42.00	99.00	93.00	mix-7	45.74	93.26	92.16
mix-3	44.73	95.36	94.73	mix-8	41.50	85.00	NA
mix-4	46.00	97.00	96.00	mix-9	44.33	87.43	84.14
mix-5	41.00	79.00	NA	mix-10	44.33	94.33	93.67

4.3 FIELD DENSITY DATA

Field density plays a significant role in quality control and quality assurance (QC&QA) of pavement construction. According to MnDOT 2360 specification (2018) for determining mat density, two cores should be taken from random locations, for each compaction lot, as directed by the engineer. The average density of the two cores are determined by the contractor, which determines the pay factor of each lot. The minimum required field density in Minnesota for mat density cores is 92% G_{mm} . An average density of the two cores less than 92% G_{mm} will be penalized, while bonus will be given if the field density is greater than 93% G_{mm} . MnDOT requires two additional cores to be taken within 1ft longitudinally from the first two cores. At least one of the additional cores per lot are tested by MnDOT for verification purposes.

4.3.1 Field Density Data for MnDOT Mixtures

A total of 480 field core densities were collected from seven out of the ten projects investigated. Field density data were not available for mix-4, mix-5 and mix-6. The distribution of field core density data is plotted in Figure 4.3. Basic statistics are listed in Table 4.4.

Table 4.4 Basic statistics of field cores density data

Statistics	Mean	Median	Std	Skewness	Kurtosis
Value	93.73	93.80	1.59	-0.39	3.35

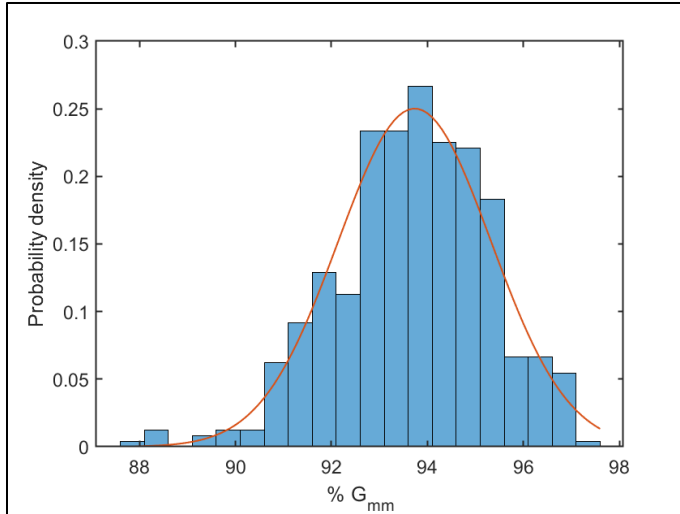


Figure 4.3 Frequency distribution of field cores density data.

As shown in Figure 4.3, the data approximately follows normal distribution, with a mean of 93.73 and a standard deviation of 1.59. The red line represents the normal distribution fit of the data. The skewness and kurtosis values, listed in Table 4.4, show that the distribution of the data is a bit left-skewed (skewness<0), which means that the actual probability density function (PDF) of field core density is more concentrated on higher densities. The actual PDF is also a bit leptokurtic (kurtosis>3), which means the peak of the actual PDF is taller compared with the fitted normal distribution.

To further investigate normality of the distribution of the overall data, a q-q (quantile-quantile) plot is drawn in Figure 4.4. As shown, the values are a bit left-skewed, while in the middle range, from 91% to 96% G_{mm} , the normality is good.

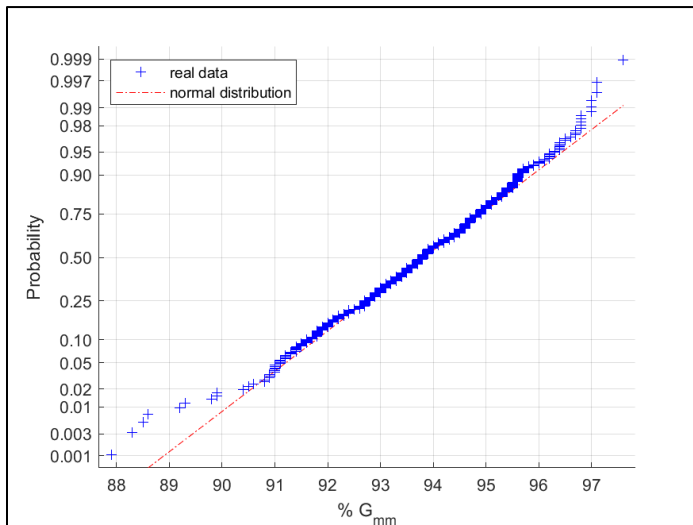


Figure 4.4 Normal distribution q-q plot for cores density data

The cumulative distribution function of the overall density data is plotted in Figure 4.5. Similar to the results in Task 3. There are 16% of the field cores that had lower densities than the density currently required by MnDOT specification (MnDOT 2360, 2018), which is 92% G_{mm} . The vast majority (80%) of field cores have densities less than 95% G_{mm} which is the requirement for a Superpave 5 mixture. To achieve this field density requirement, most of the currently designed mixtures need to be redesigned to improve their field compaction.

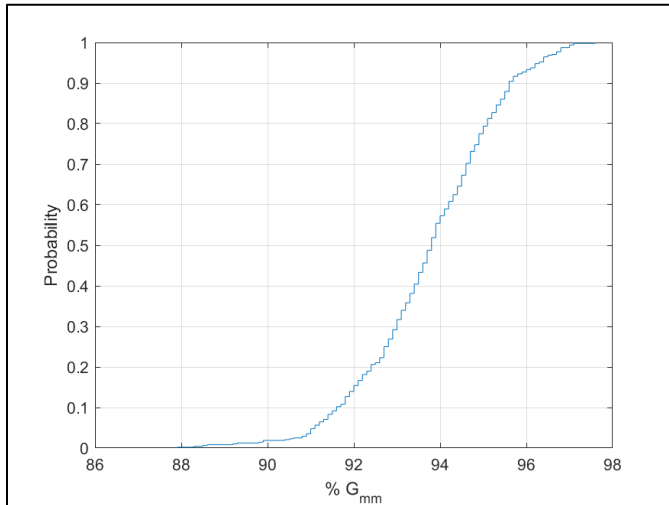


Figure 4.5 Cumulative distribution function of cores density data

The same procedure was performed for the field density data of each project. All projects approximately follow normal distribution, which guarantees the correctness of analysis of variance (ANOVA) that is conducted in the following sections. The boxplots of field densities of each mixture are shown in Figure 4.6. Their means and standard deviations are summarized in Table 4.5, which will be used later in the correlation analysis. Note that mix-10 has a small sample size of only 9 field core data, and the statistical results may not be representative.

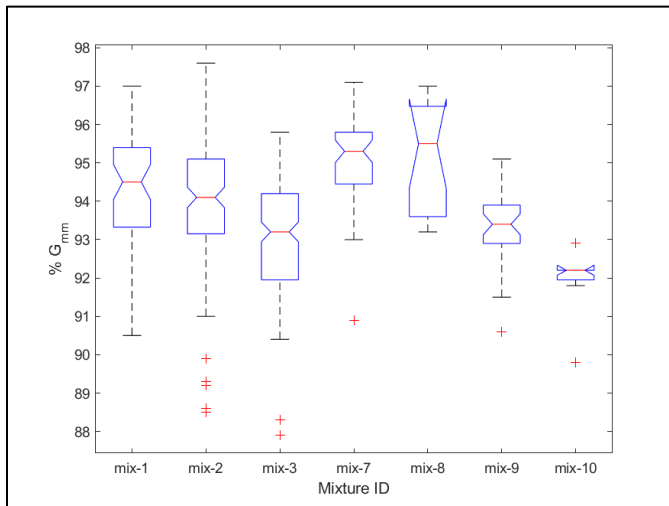


Figure 4.6 Boxplot of field density data of each mixture.

Table 4.5 Mean and standard deviation (std.) of field density data for each mixture

Mix ID	Mean	Std.	Mix ID	Mean	Std.
mix-1	94.29	1.32	mix-6	NA	NA
mix-2	93.98	1.72	mix-7	94.95	1.30
mix-3	93.10	1.38	mix-8	95.23	1.42
mix-4	NA	NA	mix-9	93.37	0.91
mix-5	NA	NA	mix-10	91.92	0.85

Field densities at the longitudinal joints were also measured, as part of the QC/QA process. A total of 117 density measurements at longitudinal joints were collected from the projects investigated. The two sides of longitudinal joints may have different densities, because during construction of longitudinal joints typically one side is confined while the other side is unconfined. The distribution of longitudinal joint densities is shown in Figure 4.7 (including data of both confined and unconfined sides), and their basic statistics are listed in Table 4.6. As expected, the means of both confined and unconfined side joint densities (92.0% G_{mm} and 90.29 % G_{mm} respectively) are less than that of the regular field core densities (93.73% G_{mm}), and the mean of confined side densities are higher than that of the unconfined side.

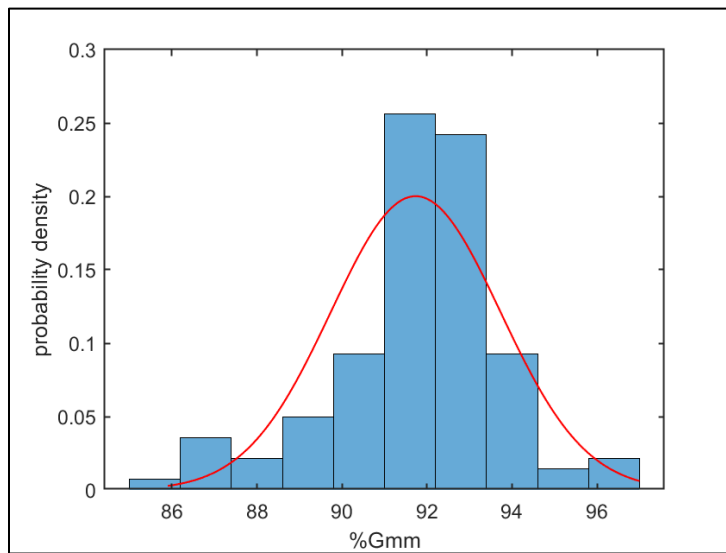


Figure 4.7 Frequency distribution of longitudinal joint densities (including both confined and unconfined sides).

Table 4.6 Basic statistics of longitudinal joint density data

Type of joints	Mean	Median	Std	Skewness	Kurtosis
Confined	92.00	92.0	1.81	-0.24	3.99
Unconfined	90.29	91.0	2.37	-0.81	2.20

Compared with the 2018 and 2019 projects studied in Task 3, the mean field density for 2020 projects (93.73 % G_{mm}) is slightly higher than that of 2018 and 2019 projects (93.40 % G_{mm}). However, the means

of confined and unconfined joint density of 2020 projects (92.00 % G_{mm} and 90.29 % G_{mm} respectively) are lower than those of 2018 and 2019 projects (92.2 % G_{mm} and 91.7 % G_{mm}).

4.4 STATISTICAL ANALYSIS OF MNDOT FIELD DENSITY DATA

The field density data from the ten new projects are added to the statistical analysis that we conducted in the Chapter 3. The results are shown in this section, which is similar to what we found in Chapter 3.

4.4.1 Analysis of Variance (ANOVA)

Projects are grouped by their NMAS and traffic level. A two-way ANOVA is conducted to investigate if these two factors have any significant effect on the variation of field densities.

The two-way ANOVA is conducted by testing the following three pairs of hypotheses:

$$\begin{cases} H_{01}: \text{The mean densities of mixtures separated by NMAS are equal.} \\ H_{11}: \text{The mean densities of mixtures separated by NMAS are not equal.} \end{cases} \quad (3)$$

$$\begin{cases} H_{02}: \text{The mean densities of mixtures separated by traffic level are equal.} \\ H_{12}: \text{The mean densities of mixtures separated by traffic level are not equal.} \end{cases} \quad (4)$$

$$\begin{cases} H_{03}: \text{There is no interaction effect between NMAS and traffic level.} \\ H_{13}: \text{There is interaction effect between NMAS and traffic level.} \end{cases} \quad (5)$$

Results of the two-way ANOVA are shown in Table 4.7. It can be seen that the main effects of NMAS and traffic level on field density are significant since their p-values are less than the significance level 0.05, while the interaction effect between NMAS and traffic level is not significant, since its p-value 0.055 is larger than the significance level 0.05.

Table 4.7 Anova results

Source of Variation	SS	df	MS	F ratio	p-value
NMAS	81.84	1	81.8442	38.02	<0.001
Traffic Level	47.9	1	47.8965	22.25	<0.001
NMAS*Traffic Level	7.97	1	7.9651	3.7	0.055
Error	3443.85	1600	2.1524		
Total	3569.93	1603			

To further explore where exactly the significant difference comes from, a Tukey method multiple pairwise comparison is conducted. The results of the multiple comparison are shown in Figure 4.8 and Figure 4.9, for the effect of NMAS and effect of traffic level respectively. It is clear that mixtures with larger aggregate size tend to have lower densities in the field; mixtures with higher traffic level also tend to have lower densities in the field.

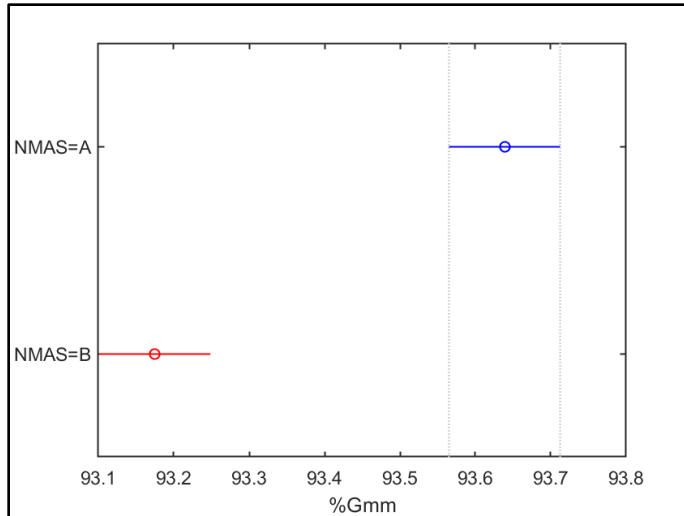


Figure 4.8 Effect of NMAAS on field density.

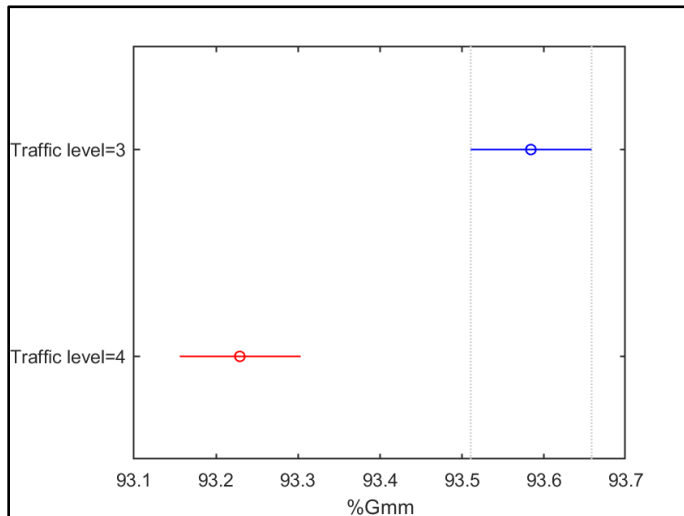


Figure 4.9 Effect of traffic level on field density.

Similar to the ANOVA result from Task 3, traffic level has a significant effect on field density. Although aggregate size (NMAAS) was not identified as a significant factor in Task 3, it becomes significant after the new projects data was added in the analysis.

4.4.2 Correlation Analysis between Material Properties and Field Densities

A correlation analysis is conducted to identify the significant correlations between mixtures' compaction properties (represented by field densities (FD) and N_{design}) and material properties. The material properties include the asphalt binder content (AC), reclaimed asphalt pavement content (RAPC), aggregate gradation (characterized by NMAAS, CA, FA_c , FA_f , and D_{mdl}), and aggregate angularity (characterized by FAA, CAA1, and CAA2).

In this investigation, we interpret FD as an indicator of field compactability since, physically, FD means how dense the mixture can be compacted under a relative consistent field compaction effort. Field compactability of mixtures increases with the increase in FD. Similarly, N_{design} can be interpreted as an indicator of laboratory compactability, since, physically, N_{design} is the laboratory compaction effort (number of gyration) needed to reach the design air voids (4%). A higher N_{design} indicates a less compactable asphalt mixture in laboratory conditions.

Table 4.8 shows the p-value of the correlation analysis. If the p-value of a pair is less than the significance level of 0.05, then we can conclude the correlation of that pair is statistically significant. Eleven pairs are shown having significant correlations, and they are shaded in Table 4.8. The correlation coefficients are listed in Table 4.9, and the pairs having significant correlations are again shaded.

Table 4.8 p-values for the correlation analysis

	FD	N_{design}	AC	RAPC	NMAS	PCSI	CA	FA _c	FA _f	D _{mdl}	FAA	CAA1	CAA2
FD	1.00	0.01	0.20	0.09	0.24	0.41	0.85	0.33	0.45	0.75	0.01	0.89	0.71
N_{design}		1.00	0.59	0.06	0.99	0.10	0.95	0.07	0.82	0.25	0.00	0.38	0.88
AC			1.00	0.09	0.51	0.86	0.12	0.66	0.78	0.26	0.21	0.41	0.19
RAP				1.00	0.77	0.34	0.20	0.08	0.30	0.96	0.15	0.21	0.23
NMAS					1.00	0.29	0.03	0.64	0.26	0.00	0.71	0.05	0.02
PCSI						1.00	0.15	0.79	0.92	0.13	0.08	0.57	0.34
CA							1.00	0.81	0.67	0.01	0.79	0.83	0.15
FA _c								1.00	0.03	0.84	0.02	0.62	0.40
FA _f									1.00	0.26	0.94	0.61	0.58
D _{mdl}										1.00	0.27	0.59	0.37
FAA											1.00	0.62	0.88
CAA1												1.00	0.00
CAA2													1.00

Table 4.9 Coefficients of correlation

	FD	N_{design}	AC	RAPC	NMAS	PCSI	CA	FA _c	FA _f	D _{mdl}	FAA	CAA1	CAA2
FD	1.00	-0.58	0.29	0.38	-0.27	0.19	-0.04	0.23	-0.17	-0.07	-0.56	-0.03	0.10
N_{design}		1.00	-0.13	-0.45	0.00	-0.37	0.01	-0.41	-0.05	-0.26	0.93	0.21	-0.04
AC			1.00	-0.38	0.15	0.04	0.35	0.10	0.06	0.26	-0.30	0.20	0.36
RAP				1.00	0.07	0.22	-0.29	0.39	-0.24	0.01	-0.35	0.30	0.33
NMAS					1.00	-0.24	0.47	0.11	0.26	0.65	-0.09	0.46	0.60
PCSI						1.00	-0.32	0.06	-0.02	0.34	-0.41	-0.14	-0.27
CA							1.00	-0.06	-0.10	0.54	0.06	-0.05	0.39
FA _c								1.00	-0.49	-0.05	-0.53	0.12	0.24
FA _f									1.00	0.26	-0.02	0.12	-0.16
D _{mdl}										1.00	-0.26	0.13	0.25
FAA											1.00	0.12	-0.04
CAA1												1.00	0.93
CAA2													1.00

The significant correlations identified are illustrated in Figure 4.10. The variables are grouped according to their physical meanings into two categories: compactability and material properties. Material properties are further separated into two categories: aggregate angularity and gradation. The significantly correlated pairs are connected by arrows, and the coefficients of correlation are listed along the arrows. The same significant correlated pairs found in Task 3, are identified for the new projects, although the correlation coefficients have changed slightly.

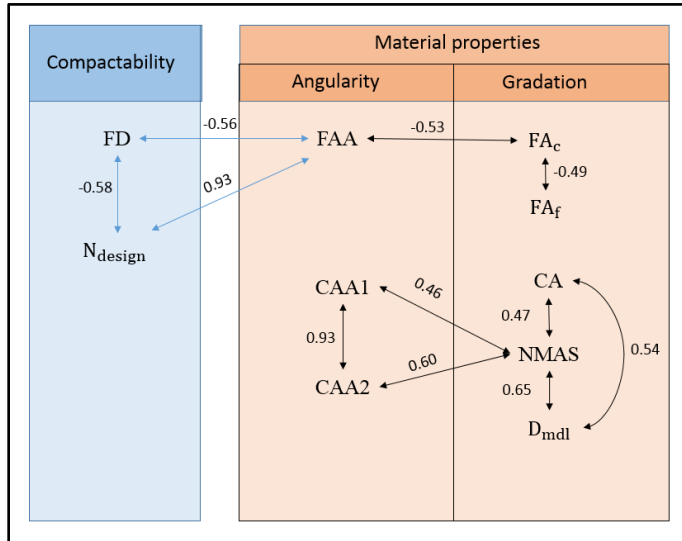


Figure 4.10 Diagram of the identified significant correlations.

It can be seen from Figure 4.10 that within the category of compactability, FD and N_{design} are significantly correlated, with a negative coefficient of correlation of -0.58. Given that FD and N_{design} represent field and laboratory compactability of mixtures, respectively, their correlation indicates that the laboratory gyratory compaction and field compaction are consistent. In other words, mixtures that compact better in the laboratory also compact better in the field.

The main focus is the correlations between compactability variables and material properties. It can be seen that both field compaction (FD) and laboratory compaction (N_{design}) are significantly correlated to FAA. More specifically, better field and laboratory compaction are achieved with lower FAA. Also, FAA is significantly correlated to FA_c that characterizes the gradation of the coarse portion of fine aggregate. More specifically, better laboratory compaction is achieved with higher FA_c .

The correlation analysis reveals significant effects of fine aggregate angularity (FAA) and fine aggregate gradation (FA_c) on mixtures' compactability. Both fine aggregate angularity and fine aggregate gradation point to the packing properties of fine aggregates. Mesoscopically, the compactability depends on the packing of aggregate which further depends on aggregate angularity and gradation. Therefore, the identified effects of fine aggregate gradation and angularity on compaction indicate an overall strong effect of fine aggregate packing on compactability. This is not entirely surprising given the fact that in the current test method (AASHTO, T304, method A), FAA actually represents a measure of fine aggregate packing.

In Figure 4.10, a number of correlations within the material properties are also identified, and are shown the pairs connected by black arrows, in contrast to blue arrows used for pairs in different categories. However, material properties should be independent of each other. For example, CAA2 and NMA5 are the coarse aggregate angularity and aggregate size, respectively. They are clearly independent because physically aggregates can have any angularity regardless of the particle size. These correlations are artificial and are a result of the low representativeness of the sampling. For example, the positive correlation between CAA2 and NMA5 shows that the mixtures investigated happen to have more angular coarse aggregates as their NMA5 increases. Also, the mixtures investigated used similar aggregate sources and similar gradations, which could be another reason for these significant correlations between material properties.

4.5 LABORATORY GYRATORY COMPACTION OF LOOSE MIXTURES

Loose mixtures were obtained from the first three projects of the ten projects investigated. Laboratory gyratory compactions were conducted on these loose mixtures, to check the original mixture design, and to quantify the field compaction effort of these projects. The compaction curves are shown in Figure 4.11, Figure 4.12, and Figure 4.13, respectively.

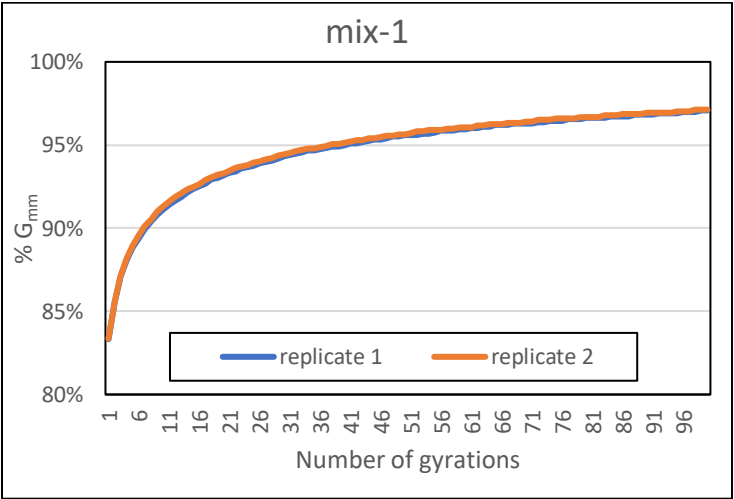


Figure 4.11 Gyratory compaction curves of mix-1 loose mixture.

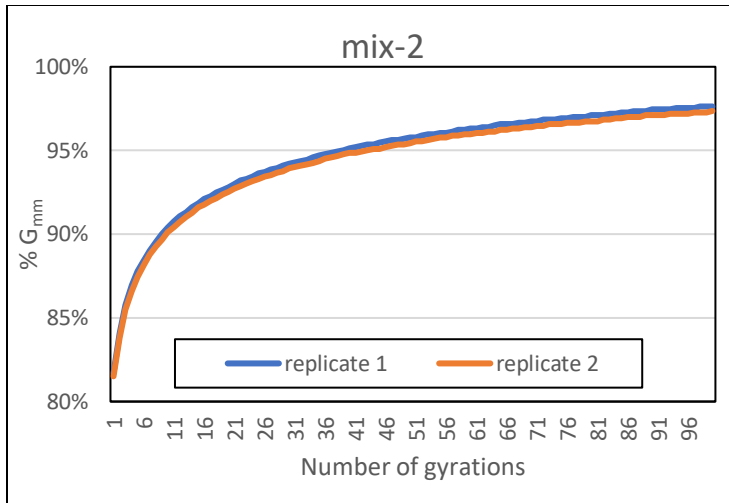


Figure 4.12 Gyrotary compaction curves of mix-1 loose mixture.

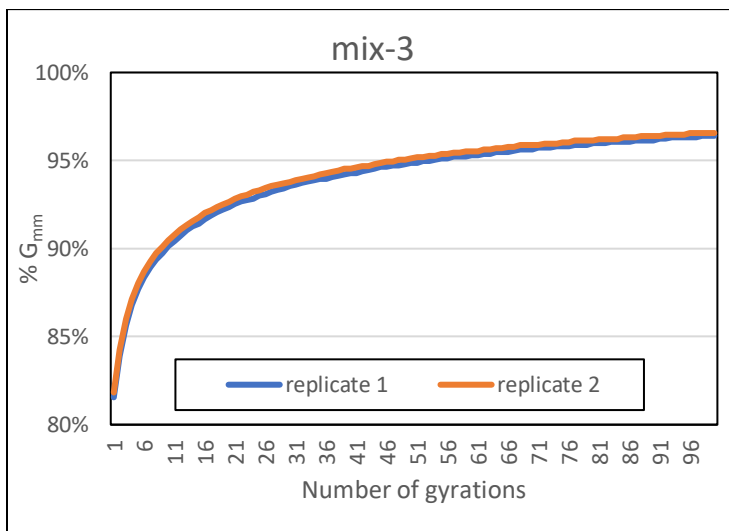


Figure 4.13 Gyrotary compaction curves of mix-1 loose mixture.

From the gyrotary compaction results, we first check the air voids at the N_{design} . The air voids at N_{design} are listed in Table 4.10, and it can be observed that the values are very close to the design value of 4 %, which verifies the original mixture design of these projects.

Table 4.10 Air voids at N_{design} and N_{equ} values

	NMAS(mm)	N_{design}	Air voids @ N_{design}	Ave. field density(% G_{mm})	N_{equ}
mix-1	9.5	60	3.99	94.29	29
mix-2	12.5	60	3.86	93.89	29
mix-3	12.5	90	3.73	93.1	26

To quantify the field compaction effort, we propose a new parameter: the equivalent number of gyrations to field compaction (N_{equ}). The field compaction effort is represented by the mean field density of the project. N_{equ} is computed as the number of gyrations at which the laboratory compacted

specimen reaches the mean field density. A schematic diagram of computing N_{equ} is shown in Figure 4.14.

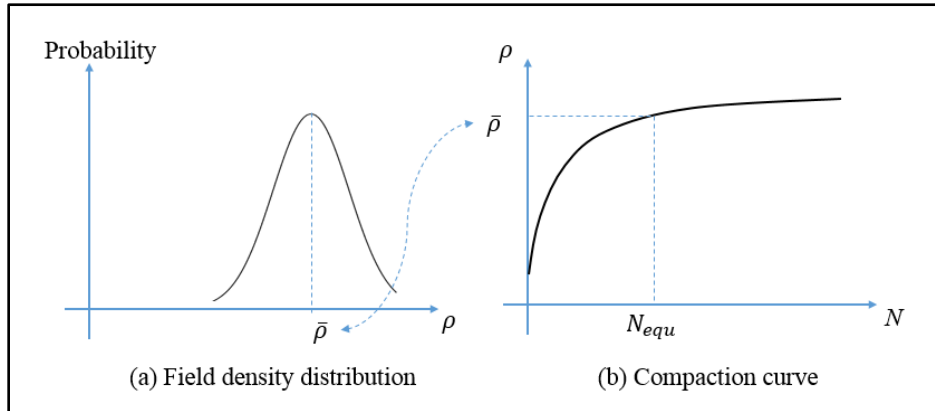


Figure 4.14 Schematic diagram of computing N_{equ} (ρ represents field density).

Two replicates were compacted for each project. Then, the N_{equ} value is computed using the approach demonstrated in Figure 4.14. One example of mix-1 is demonstrated in Figure 4.15. The averaged compaction curve is used to determine the N_{equ} . The computed N_{equ} values for the three projects are also listed in Table 4.10.

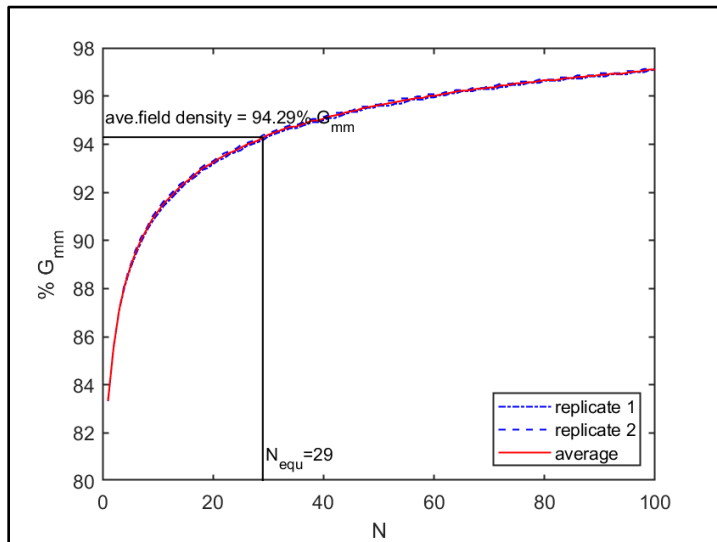


Figure 4.15 Compaction curves and N_{equ} for mix-1

As shown in Table 4.10, the N_{equ} for the three projects are 29, 29 and 26 for mix-1, mix-2 and mix-3 respectively, which represent the field compaction effort of these projects. From the results we cannot see any tendency of the increase in field compaction effort (N_{equ}) with N_{design} . On the contrary, the field compaction effort is similar for traffic level 3 and 4, with both their N_{equ} range very narrowly from 26 to 29. This level may represent the maximum field compaction effort that are currently available. It is

notable that the computed N_{equ} is very close to the $N_{\text{design}} = 30$ used in Superpave 5 for traffic level 3. However, Superpave 5 used $N_{\text{design}} = 50$ for traffic level 4 and 5 which is more than 20 gyrations higher than the N_{equ} computed in this study.

4.6 CONCLUSIONS

In task 4, field density data and the material information of ten more projects constructed in 2020 were investigated. First, the field density distribution was analyzed. Then, the correlations between field density and material properties were studied. Gyratory compactions were conducted on the loose mixtures from three of the ten projects to check the original mixture design and quantify the field compaction effort of these projects. The following conclusions were drawn.

1. Similarly to the 2018 and 2019 projects studied in Task 3, the field density data of the 2020 projects also approximately follows a normal distribution. The mean field density and standard deviation of 2020 projects are 93.73 % G_{mm} and 1.59 % G_{mm} respectively, which are slightly higher than that of 2018 and 2019 projects (93.40 % G_{mm} and 1.45 % G_{mm} respectively).
2. Similarly to Task 3 results, traffic level had a significant effect on field density after the 2020 projects data was added in the ANOVA. As shown in Task 3, mixtures with higher traffic level tend to have lower field density. However, unlike Task 3 results, the aggregate size (NMAAS) was identified to have a significant influence on field density after the data from the new projects data was added in the analysis. Mixtures with larger aggregate size (NMAAS) tend to have lower field density.
3. The correlation analysis shows that field density is significantly correlated with laboratory compaction (N_{design}) and fine aggregate angularity (FAA), similarly to the results in Task 3.
4. Gyratory compaction of loose mixtures verified the original mixture design of the three projects. At N_{design} all of them reached the 4% design air voids.
5. A new parameter, called the equivalent number of gyrations to field compaction (N_{equ}), is proposed to quantify the field compaction effort. N_{equ} values for different projects of different traffic levels are similar, with $N_{\text{equ}} = 29$, 29 and 26 for mix-1, mix-2 and mix-3 respectively, which may indicate that this number of gyration level represents the current field compaction effort in Minnesota.

CHAPTER 5: DATA ANALYSES OF SUPERPAVE 5 PROJECTS

In this chapter, mix design and field density data from four Superpave 5 projects constructed in 2020 and 2021 in Minnesota are analyzed and compared with traditional Superpave projects. Laboratory tests (SCB, E^* , and flow number test) are conducted on the Superpave 5 mixtures to obtain relevant mechanical properties related to pavement performance.

5.1 MIXTURE INFORMATION

Four Superpave 5 (SP5) projects, constructed in 2020 and 2021, were selected by the technical advisory panel for Task 4B. They were designed to 5% air voids in the lab and were designed to be compacted to also 5% air voids in the field. The main difference between Superpave 5 and the traditional Superpave mixtures designed according to MnDOT standard 2360 (2018) is the design number of gyrations (N_{design}). N_{design} is reduced from 60, 90 and 100 to 30, 50 and 50, respectively, for traffic level 3 (1-3 million ESAL), 4 (3-10 million ESAL) and 5 (>10 million ESAL), respectively, from traditional Superpave to Superpave 5.

The basic information of three of the four mixtures is listed in Table 5.1. Information for the last project SP54 has not been collected and will be added when data becomes available. The first two mixtures, SP5-1 and SP5-2, are traffic level 3, and the third mixture SP5-3 is traffic level 4. All mixtures are wearing course type. All mixtures contain reclaimed asphalt pavement (RAP), with their RAP content ranging from 10% to 20% by weight. The RAP content and binder content (%AC) information shown in the table are from MDR.

Table 5.1 Summary of the Superpave 5 mixtures

Mix ID	SP5-1	SP5-2	SP5-3
Traffic level	3	3	4
NMAS	12.5	12.5	9.5
Design Air voids	5	5	5
Binder PG	58S-28	58H-34	58H-34
RAP content	10%	17%	20%
N_{design}	30	30	50
AC, %	5.5	5.2	5.5
P_{be} , %	4.7	5.0	5.1
G_{mm}	2.478	2.484	2.498

5.2 AGGREGATE GRADATION AND ANGULARITY

5.2.1 Gradation Curves

The three SP5 mixtures include two levels of nominal maximum aggregate size (NMAS), 9.5mm (3/8in) and 12.5mm (1/2in). For simplicity, they are denoted by A and B, respectively, according to MnDOT designation (MnDOT 2360, 2018). Two mixtures are type A and one mixture is type B. The aggregate gradation data were obtained from MDR.

Table 5.2 Summary of the aggregate gradations of the Superpave 5 mixtures

Mix ID	SP5-1	SP5-2	SP5-3	
NMAS	B	B	A	
Sieve Size	1in, 25mm	100	100	100
	3/4in, 19mm	100	100	100
	1/2in, 12.5mm	90	97	100
	3/8in, 9.5mm	84	82	94
	No.4, 4.75mm	68	61	71
	No.8, 2.36mm	51	46	51
	No.16, 1.18mm	33	33	37
	No.30, 0.6mm	24	23	26
	No.50, 0.3mm	13	12	16
	No.100, 0.15mm	7	7	8
	No.200, 0.075mm	5.4	4.7	4.9

The gradation curves for type A and B mixtures are plotted in Figure 5.1 and Figure 5.2, respectively. Note that MDL stands for maximum density line.

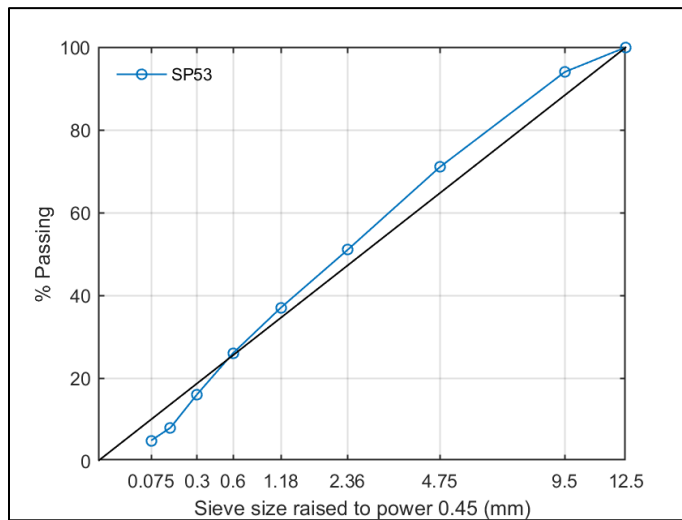


Figure 5.1 Gradation curves of type A mixtures with NMAS = 9.5 mm (3/8in)

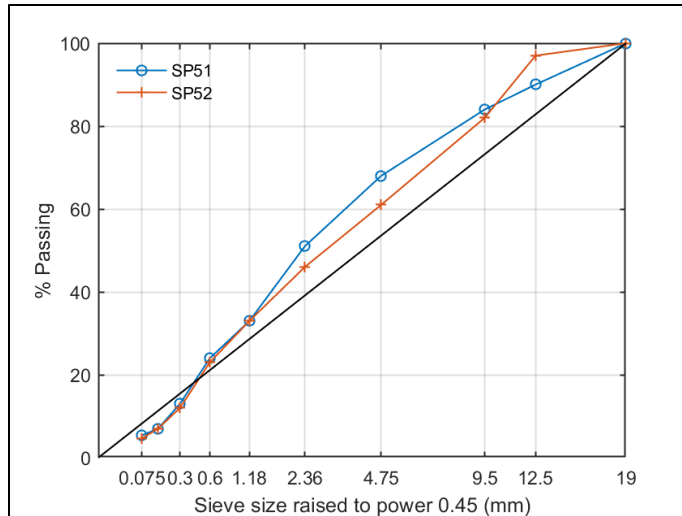


Figure 5.2 Gradation curves of type B mixtures with NMAS = 12.5 mm (1/2in)

5.2.2 Gradation Characterization

Aggregate gradations were further characterized using the Bailey method. Aggregates are separated into different portions using three critical sieve sizes: the Primary Control Sieve (PCS), the Secondary Control sieve (SCS), and the Tertiary Control Sieve (TCS). The control sieve sizes are defined by the following equations:

$$PCS = 0.22 * NMAS \text{ (nominal maximum aggregate size),}$$

$$SCS = 0.22 * PCS, \text{ and}$$

$$TCS = 0.22 * SCS.$$

Mixtures' gradation are characterized by Primary Control Sieve Index (PCSI), Coarse Aggregate Ratio (CA Ratio), Fine Aggregate Coarse Ratio (FAc Ratio), and Fine Aggregate Fine Ratio (FAf Ratio):

$$PCSI = \% \text{ Passing PCS}$$

$$CA \text{ Ratio} = \frac{(\% \text{ Passing Half Sieve} - \% \text{ Passing PCS})}{(100\% - \% \text{ Passing Half Sieve})}$$

$$FAc \text{ Ratio} = \frac{\% \text{ Passing SCS}}{\% \text{ Passing PCS}}$$

$$FAf \text{ Ratio} = \frac{\% \text{ Passing TCS}}{\% \text{ Passing SCS}}$$

Half Sieve is the sieve size equal to $0.5 * NMAS$ (maximum aggregate size).

PCSI characterizes the overall fineness of the aggregates, CA characterizes the fineness of coarse aggregates (aggregates larger than PCS), FAc characterizes the fineness of coarse portion of fine

aggregates (aggregates larger than SCS but smaller than PCS), and Faf characterizes the fineness of fine portion of fine aggregates (aggregates smaller than SCS).

In this investigation, we also calculate another parameter called the distance to maximum density line (Dmdl), that is defined as the accumulated difference of the passing rate between the gradation curve and the maximum density line:

$$Dmdl = \sum_{\text{min sieve}}^{\text{max sieve}} |\%Pass \text{ of the sieve} - \%Pass \text{ of the sieve on MDL}|$$

This is based on previous research that showed that mixture compactability is related to how close the gradation curve is to the maximum density line (Hekmatfar et al., 2015; Huber et al., 2016).

The calculated Bailey method parameters and the Dmdl values are listed in Table 5.3.

Table 5.3 Bailey Method Parameters for Superpave 5 mixtures.

Mix ID	NMAS (mm)	PCSI (%)	CA	FAc	Faf	Dmdl (mm)
SP5-1	12.5	51	0.53	0.47	0.29	61.17
SP5-2	12.5	46	0.38	0.50	0.30	54.87
SP5-3	9.5	51	0.69	0.51	0.19	32.05

5.2.3 Aggregate Angularity

Aggregate angularity is another factor that affects compaction. In MnDOT 2360 specification (2018), the aggregate angularity is quantified by the Coarse Aggregate Angularity (CAA) of one face and two faces (ASTM D5821), and the Fine Aggregate Angularity (FAA) (AASHTO T304 Method A). The aggregate angularities were obtained from the TSS. The averaged values for each project are listed in Table 5.4. The required aggregate angularity increases with traffic level of projects. As listed in the Table 3 of MnDOT specification 3139 (2018), the required minimum FAA for traffic level 3, 4 and 5 are 42%, 44% and 45%, respectively. The corresponding values for CAA1 are 55%, 85% and 95% respectively. There is no minimum requirement of CAA2 for traffic level 3, while for traffic level 4 and 5, the required minimum CAA2 values are as 80% and 90%, respectively

Table 5.4 Aggregate angularity

Mix ID	FAA, %	CAA One Face, %	CAA Two Faces, %
SP5-1	43.1	97.5	94.9
SP5-2	45.8	95.2	95.2
SP5-3	44.2	91.8	86.2
SP5-4	NA	NA	NA

5.3 FIELD DENSITY

Field density plays a significant role in quality control and quality assurance (QC&QA) of pavement construction. According to MnDOT 2360 specification (2018) for determining mat density, two cores should be taken from random locations, for each compaction lot, as directed by the engineer. The agency determines the pay factor based on the average density measurements provided by the contractor. The minimum required field density in Minnesota for mat density cores is 92% G_{mm} . An average density of the two cores less than 92% G_{mm} will be penalized, while bonus will be given if the field density is greater than 93% G_{mm} . MnDOT requires two additional cores to be taken within 1ft longitudinally from the first two cores. At least one of the additional cores per lot are tested by MnDOT for verification purposes.

5.3.1 Field Density Distribution

A total of 482 field core densities were collected from the first three Superpave 5 projects. The distribution of field core density data is plotted in Figure 5.3. Basic statistics are listed in Table 5.5.

Table 5.5 Basic statistics of field cores density data

Statistics	Mean, %	Median, %	Std, %	Skewness	Kurtosis
Value	94.22	94.4	1.92	-0.71	4.2

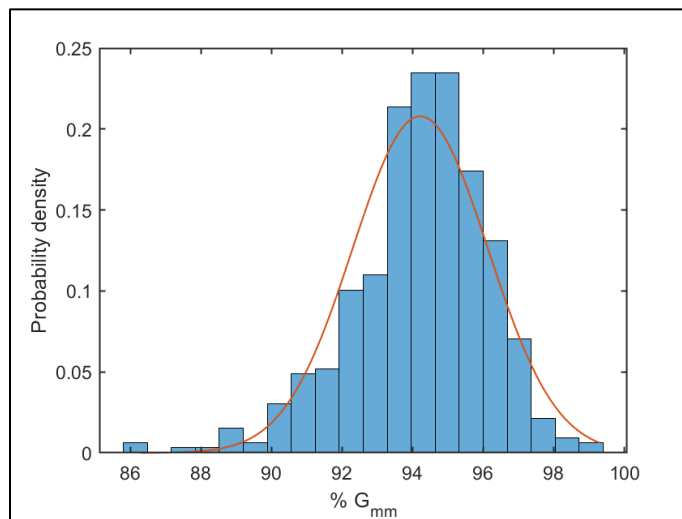


Figure 5.3 Frequency distribution of field cores density data.

As shown in Figure 5.3, the data approximately follows normal distribution, with a mean of 94.22 and a standard deviation of 1.92. The red line represents the normal distribution fit of the data. The skewness and kurtosis values, listed in Table 5.5, show that the distribution of the data is a bit left-skewed (skewness<0), which means that the actual probability density function (PDF) of field core density is more concentrated on higher densities. The actual PDF is also a bit leptokurtic (kurtosis>3), which means the peak of the actual PDF is taller compared with the fitted normal distribution.

To further investigate normality of the distribution of the overall data, a q-q (quantile-quantile) plot is drawn in Figure 5.4. As shown, the values are a bit left-skewed, while in the middle range, from 92% to 97% G_{mm} , the normality is good.

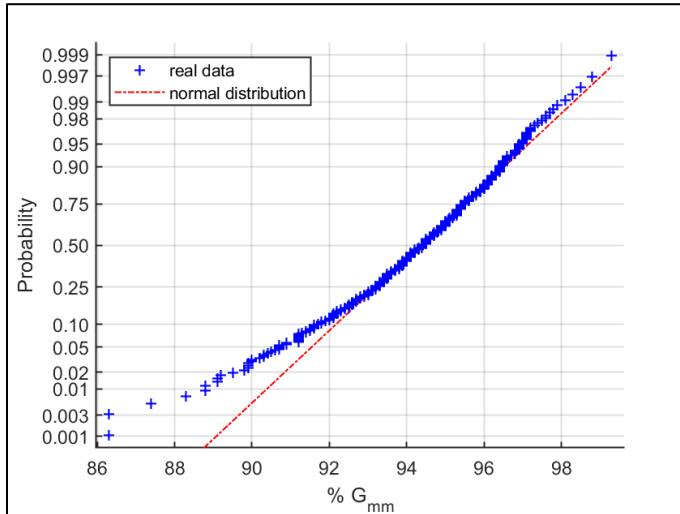


Figure 5.4 Normal distribution q-q plot for cores density data

The cumulative distribution function of the overall density data is plotted in Figure 5.5. It is seen that 37.8% of field cores exceed 95% G_{mm} and thus satisfy the requirement of Superpave 5. The vast majority (88.8%) of the field cores exceed 92% G_{mm} the current required minimum by MnDOT specification (MnDOT 2360, 2018).

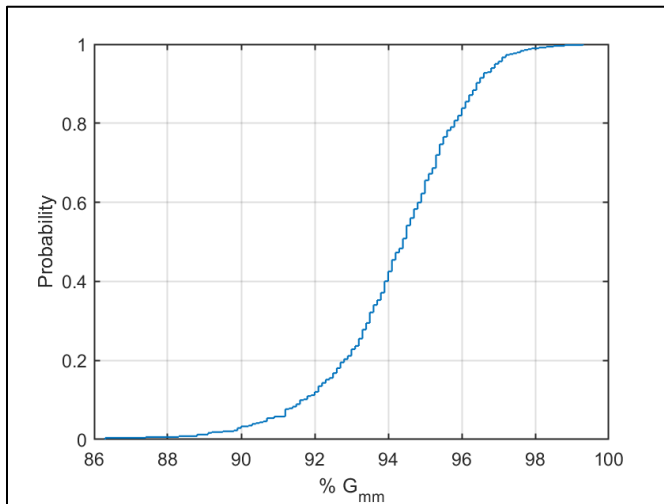


Figure 5.5 Cumulative distribution function of cores density data

5.3.2 Comparison between Superpave 5 Projects

It is found that field densities of all projects approximately follow the normal distribution. They are demonstrated by boxplots and are compared in Figure 5.6. Their means and standard deviations are summarized in Table 5.6.

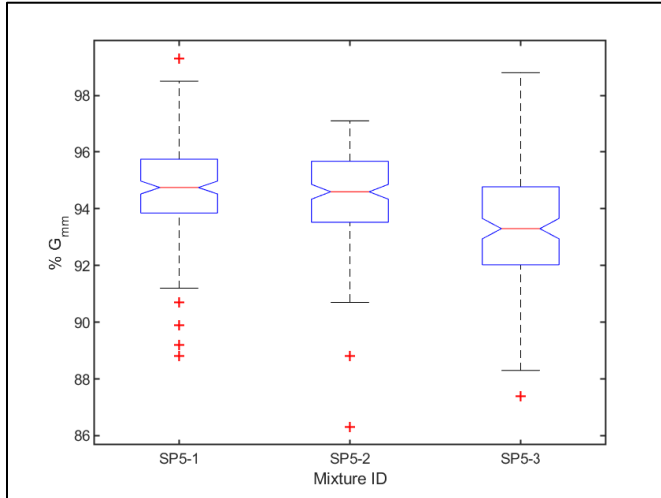


Figure 5.6 Boxplot of field density data of each mixture.

Table 5.6 Mean and standard deviation (std.) of field density data for each mixture

Mix ID	Mean, %	Std. Dev., %	Mode, %	Median, %
SP5-1	94.72	1.77	94.1	94.75
SP5-2	94.51	1.68	94.50	94.60
SP5-3	93.28	2.02	95.00	93.30
SP5-4	NA	NA	NA	NA

It is seen from Figure 5.6 that SP5-1 and SP5-2 have higher field densities than SP5-3. An analysis of variance (ANOVA) is conducted to check if there are significant differences between these projects. The ANOVA Table is shown in Table 5.7. The p-values is less than 0.001, which indicates that there are significant differences between the projects.

Table 5.7 ANOVA table of the comparison between different Superpave 5 projects

Source of Variation	SS	df	MS	F ratio	p-value
Groups	182.62	2	91.31	27.54	<0.001
Error	1588.12	479	3.32		
Total	1770.74	481			

A Tukey method multiple pairwise comparison is conducted to further explore where the significant difference comes from. Result of the multiple comparison is shown in Figure 5.7. It is clear there is no

significant difference between SP5-1 and SP5-2. However, SP5-3 has a significant lower field density level than SP5-1 and SP5-2.

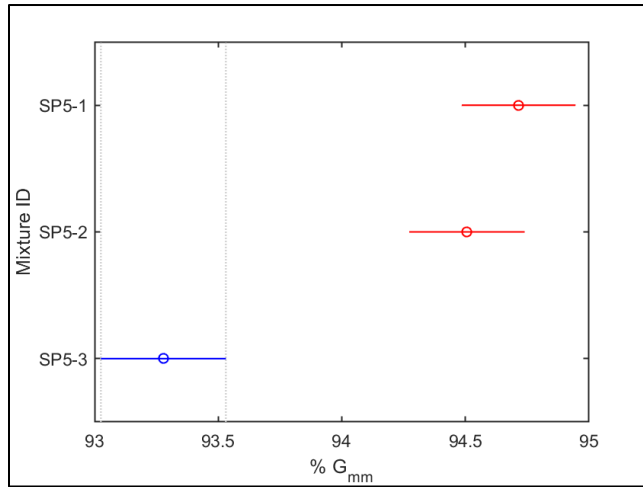


Figure 5.7 Tukey method multiple comparison of different Superpave 5 projects.

A possible reason for the observed difference in field density is the difference in the N_{design} or traffic level of the projects. The N_{design} of SP5-3 is 50 (traffic level 4), whereas the N_{design} 's of SP5-1 and SP5-2 are 30 (traffic level 3). A higher N_{design} implies a lower compactability of the mixture, and thus may lead to the lower field density as observed. More data are needed to further confirm this observed trend. It is possible that a value of N_{design} lower than 50 could be recommended for traffic level 4 and 5.

5.4 COMPARISON BETWEEN SUPERPAVE 5 AND TRADITIONAL SUPERPAVE PROJECTS

5.4.1 Comparison of Field Densities

A visual comparison of field density distributions for Superpave 5 (SP5) and for Superpave (SP4) projects is shown in Figure 5.8. It is seen that Superpave 5 project have a higher mean field density and a higher standard deviation than that of Superpave 4 projects. Basic statistics results are shown and compared in Table 5.8.

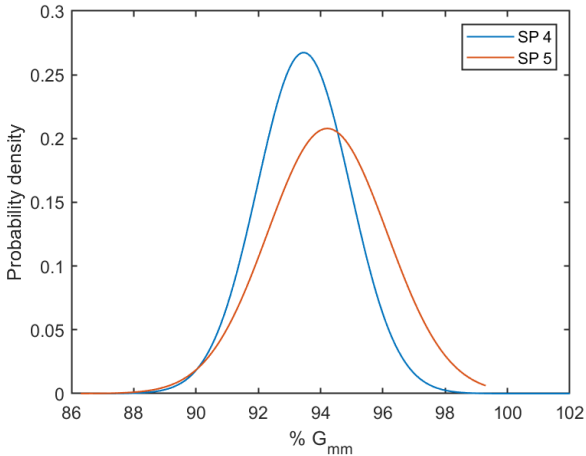


Figure 5.8 Comparison of the field density distribution between SP5 and traditional SP4 projects.

Table 5.8 Comparison of the basic statistics of field densities between SP5 and traditional SP4 projects.

Projects	Mean, %	Median, %	Std, %	Skewness	Kurtosis
SP4	93.46	93.5	1.49	-0.26	4.05
SP5	94.22	94.4	1.92	-0.71	4.20

Figure 5.9 compares the cumulative probability distribution of field densities of Superpave 4 and Superpave 5 projects. A clear increase in field density from SP4 to SP5 projects is observed. Specifically, the percentage of cores with less than 95% G_{mm} decreased from 84.6% for SP4 to 65.6% for SP5.

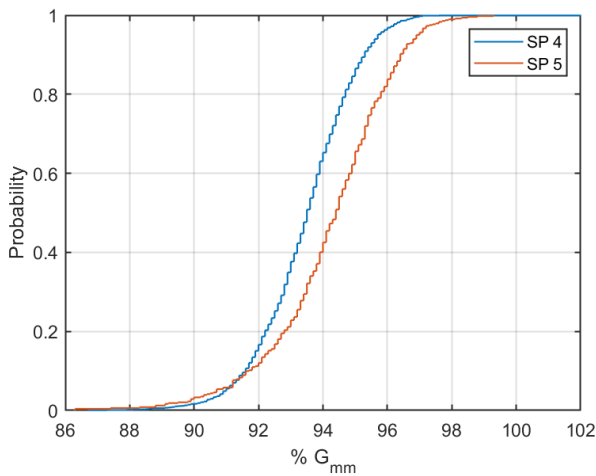


Figure 5.9 Comparison of between the cumulative probability distributions of field densities of SP4 and SP5 projects.

An ANOVA is conducted to check the difference between the field densities of SP5 and SP4 projects. As shown in Table 5.9, the p-value is less than 0.001 which confirms the significant difference in their field densities.

Table 5.9 ANOVA table of the comparison between field densities of SP5 and SP4 projects.

Source of Variation	SS	df	MS	F ratio	p-value
Groups	217.19	1	217.19	85.39	<0.001
Error	5583.09	2195	2.544		
Total	5800.29	2196			

We further compare the field densities of SP4 and SP5 projects that share the same traffic level and NMAS. SP5-1 and SP5-2 belong to traffic level 3 and have a B level (12.5mm) NMAS, so they can be classified as “B3”, and are compared with all SP4 projects in B3 category. Similarly, SP5-3 belongs category “A4”, and are compared with all SP4 projects categorized as A4.

Figure 5.10 shows the field density distribution of the SP4 and SP5 projects in the B3 category. It is seen that for B3 projects, SP5 mixtures have higher mean field density level and higher standard deviation than that of SP4 mixtures. The detailed statistics data are listed in Table 5.10. **Table 5.10** Also, an ANOVA is performed to check the difference between SP4 B3 projects and SP5 B3 projects. The results are listed in Table 5.11, which shows that there exists significant difference between the mean field densities of SP4 B3 projects and SP5 B3 projects.

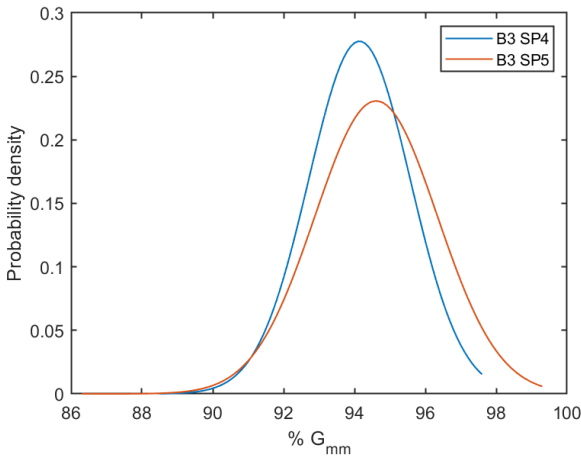


Figure 5.10 Comparison of field density distribution between SP5 B3 projects and SP4 B3 projects.

Table 5.10 Comparison of basic statistics of field densities between SP5 and SP4 projects in B3 category.

Projects	Mean, %	Median, %	Std, %	Skewness	Kurtosis
B3 SP4	94.14	94.3	1.44	-0.77	4.60
B3 SP5	94.61	94.7	1.73	-1.00	6.03

Table 5.11 ANOVA table of the comparison between field densities of SP5 and SP4 projects in the B3 category.

Source of Variation	SS	df	MS	F ratio	p-value
Groups	35.84	1	35.84	14.06	0.0004
Error	1648.91	647	2.55		
Total	1684.76	648			

Figure 5.11 shows the field density distribution of the SP4 and SP5 projects in the A4 category. It is seen that for A4 projects, SP4 and SP5 mixtures have similar mean field density levels, while field density distribution of SP5 mixtures has a higher variation than that of SP4 mixtures. The detailed statistics data are listed in Table 5.12. Also an ANOVA is performed to check the difference between SP4 A4 projects and SP5 A4 projects. The results are listed in Table 5.13, which shows that there is no significant difference between the mean field densities of SP4 A4 projects and SP5 A4 projects.

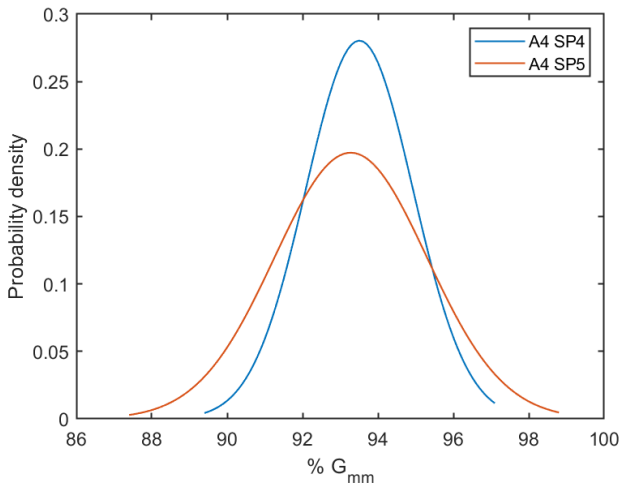


Figure 5.11 Comparison of the field density distribution between SP5 A3 projects and SP4 A3 projects.

Table 5.12 Comparison of the basic statistics of field densities between SP5 and traditional SP4 projects in the A4 category.

Projects	Mean, %	Median, %	Std, %	Skewness	Kurtosis
A4 SP4	93.51	93.5	1.42	-0.04	2.76
A4 SP5	93.28	93.3	2.02	-0.13	3.06

Table 5.13 ANOVA table of the comparison between field densities of SP5 and SP4 projects in the A4 category.

Source of Variation	SS	df	MS	F ratio	p-value
Groups	6.01	1	6.01	2.47	0.1164
Error	1757.12	723	2.43		
Total	1763.13	724			

5.4.2 Comparison of Material Properties

The significant difference in field densities between SP5 and SP4 projects must be a result of the difference in their material composition and properties. In this section, the material properties are compared between SP4 and SP5 projects, with the aim of identifying what changes in material properties lead to the improvement of field density of SP5 projects.

We compare the SP4 and SP5 projects that share the same traffic level and NMA. SP5-1 and SP5-2 belong to traffic level 3 and have a B level (12.5mm) NMA, so they can be classified as “B3”, and are

compared with all SP4 projects in B3 category. Similarly, SP5-3 belongs category “A4”, and are compared with all SP4 projects categorized as A4.

The gradation curves are first compared, as shown in Figure 5.12 and Figure 5.13 respectively for B3 and A3 projects. While there are significant differences in the amount passing the No. 8 (4.75mm) and No. 4 (2.36) sieves between SP4 and SP5 mixtures, the differences are quite random, and do not follow a consistent trend for all mixtures.

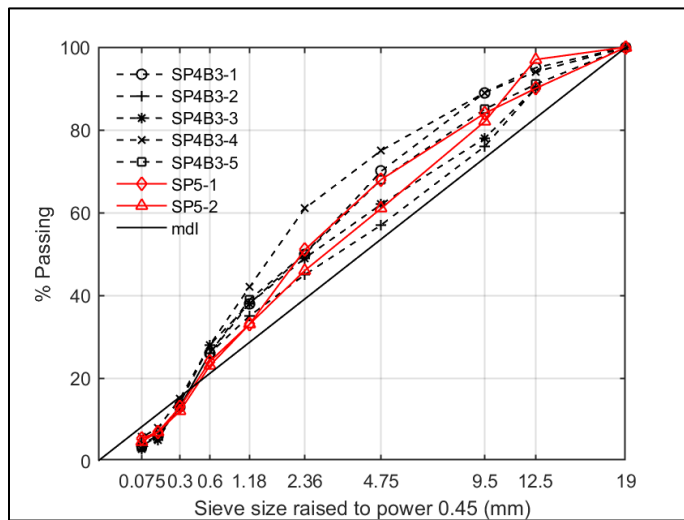


Figure 5.12 Comparison of gradation curves of B3 projects between SP4 and SP5.

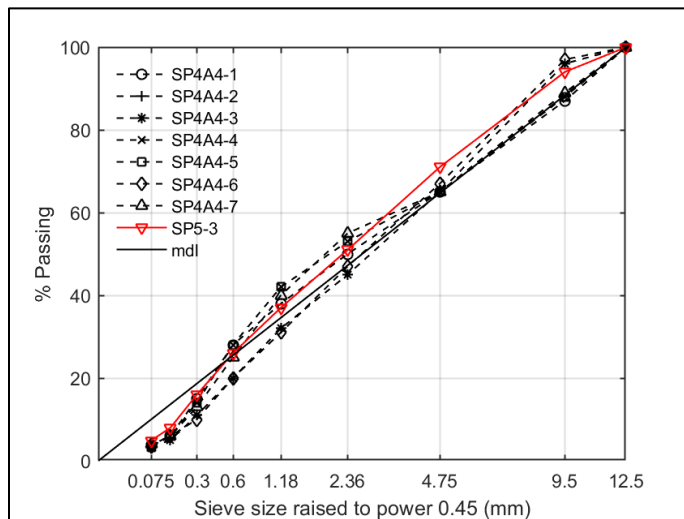


Figure 5.13 Comparison of gradation curves of A4 projects between SP4 and SP5.

The values of material properties, including G_{mm} , binder content, gradation parameters, and aggregate angularities, are listed in Table 5.14 and Table 5.15, for B3 and A4 projects, respectively.

Table 5.14 Material properties of B3 projects.

Mixture ID	SP4B3-1	SP4B3-2	SP4B3-3	SP4B3-4	SP4B3-5	SP5-1	SP5-2
G_{mm}	2.425	2.468	2.495	2.481	2.471	2.478	2.484
P_{be}, %	4.9	5.2	4.5	5.1	5.0	4.7	5.0
AC, %	5.5	5.6	5.2	5.6	5.3	5.5	5.2
PCSI (%)	50	45	49	61	50	51	46
CA	1.08	0.49	0.55	0.56	0.56	0.53	0.38
FA_c	0.52	0.58	0.57	0.46	0.52	0.47	0.5
FA_f	0.14	0.16	0.1	0.29	0.23	0.29	0.3
D_{mdl}	81.97	42.37	59.77	96.87	73.27	61.17	54.87
FAA, %	42.67	42	42	42	42.4	43.1	45.8
CAA1, %	84.33	99	96.5	99	82	97.5	95.2
CAA2, %	NA	99	NA	93	NA	94.9	95.2

Note: the shaded columns are SP5 projects

Table 5.15 Material properties of A4 projects.

Mixture ID	SP4A4-1	SP4A4-2	SP4A4-3	SP4A4-4	SP4A4-5	SP4A4-6	SP4A4-7	SP53
G_{mm}	2.496	2.479	2.479	2.432	2.432	2.470	2.430	2.498
P_{be}, %	4.5	4.7	4.7	5.1	5.1	4.9	4.7	5.1
AC, %	4.8	5.3	5.3	5.6	5.6	5.1	5.3	5.5
PCSI (%)	50	45	45	53	53	47	55	51
CA	0.43	0.57	0.57	0.34	0.34	0.61	0.29	0.69
FA_c	0.56	0.44	0.44	0.53	0.53	0.43	0.45	0.51
FA_f	0.14	0.17	0.17	0.11	0.11	0.18	0.16	0.19
D_{mdl}	27.92	41.16	41.16	35.52	35.52	43.06	33.96	32.05
FAA	44	44.63	44.5	43.8	44.04	45.74	44.33	44.2
CAA1, %	91.04	91.88	92	96.1	97.91	93.26	87.43	91.8
CAA2, %	87.86	91.13	91.4	95.8	97.91	92.16	84.14	86.2

Note: the shaded columns are SP5 projects

Parameters characterizing aggregate gradation are further compared by using bar plots, as shown in Figure 5.14. It is seen that SP5 projects tend to have higher FA_f values than SP4 projects. For other gradation parameters SP4 and SP5 projects are not significantly different. Specifically, variation of a parameter in SP5 projects is within its variation in SP4 projects. The correlation between FA_f and field density was not identified as significant in previous correlation analyses, so more validation is needed on whether the increase in FA_f is a factor that caused the increase in field densities of SP5 projects.

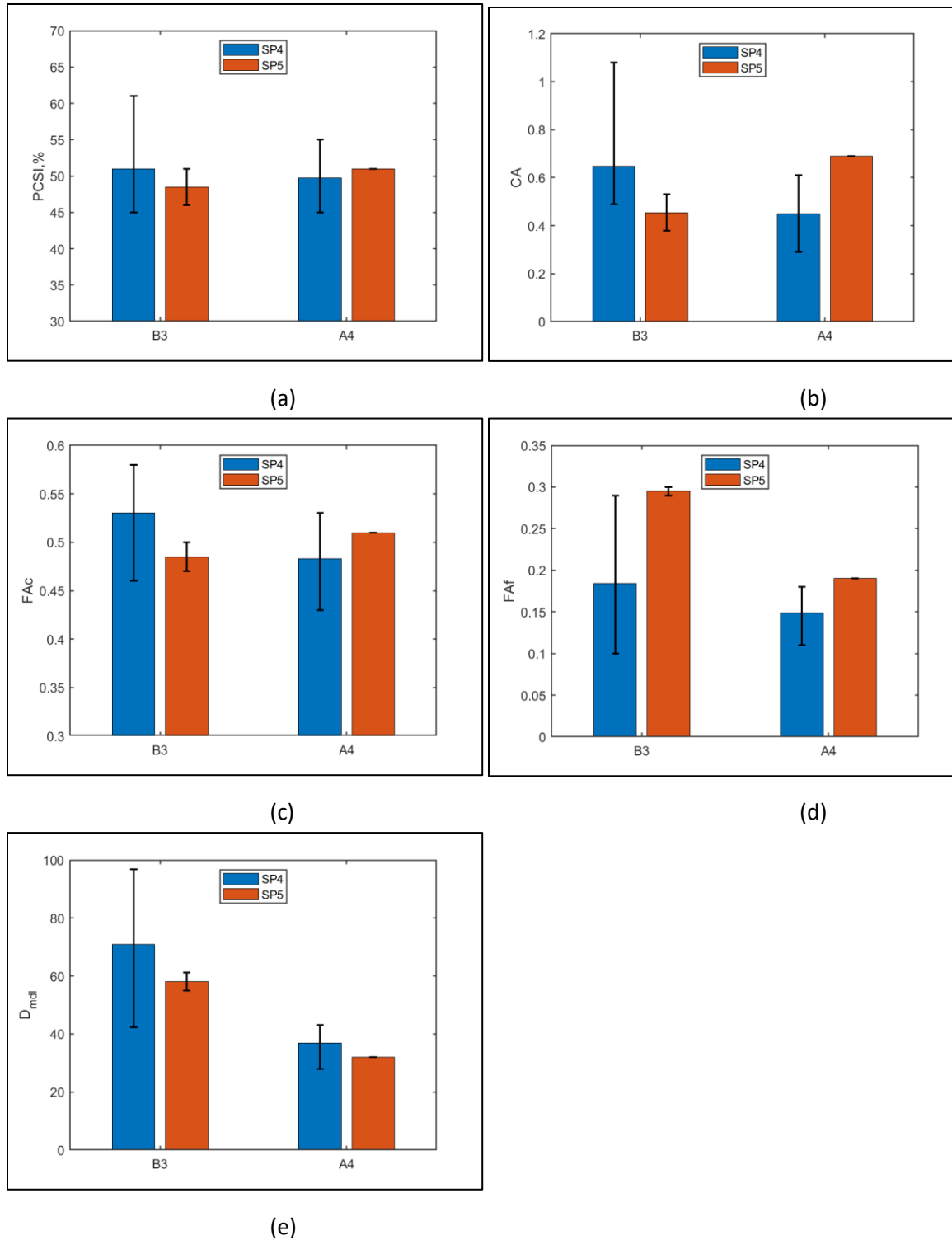


Figure 5.14 Comparison of gradation parameters (the error bar indicates the range of the corresponding values).

The binder content (AC) and effective binder content (P_{be}) of SP4 and SP5 projects are compared by the bar plot in Figure 5.15. It is seen that there is no significant difference in AC or P_{be} between SP4 and SP5 projects.

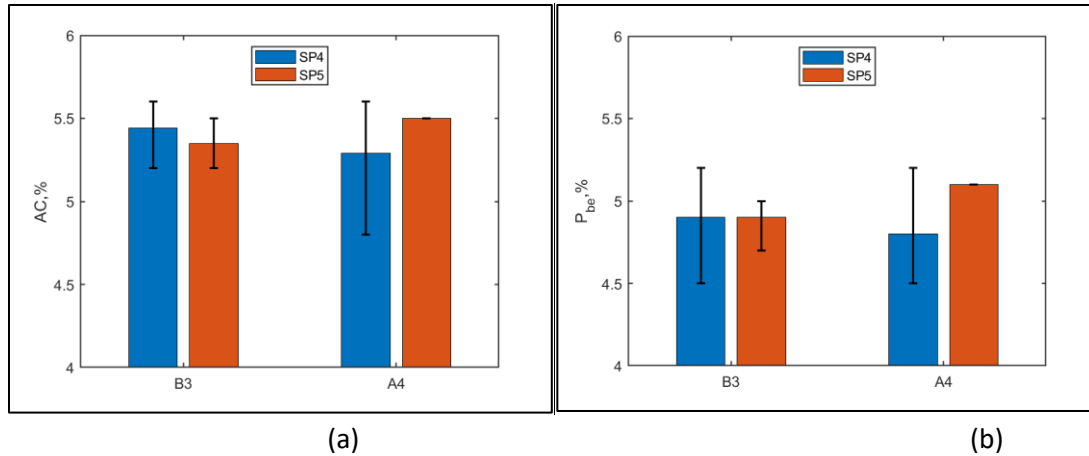


Figure 5.15 Comparison of asphalt binder content (error bar indicates the range of the corresponding values).

The aggregate angularity parameters are visually compared in Figure 5.16. It is seen that for B3 category, SP5 projects tend to have higher FAA values than SP4 projects. Other aggregate angularity parameters do not show any significant difference between SP4 and SP5 projects. However, the increase in FAA is unlikely to be the cause of the increase in field density of SP5 projects, since it is generally accepted that the increase in FAA would lead to a lower compactability of mixture and lower field density.

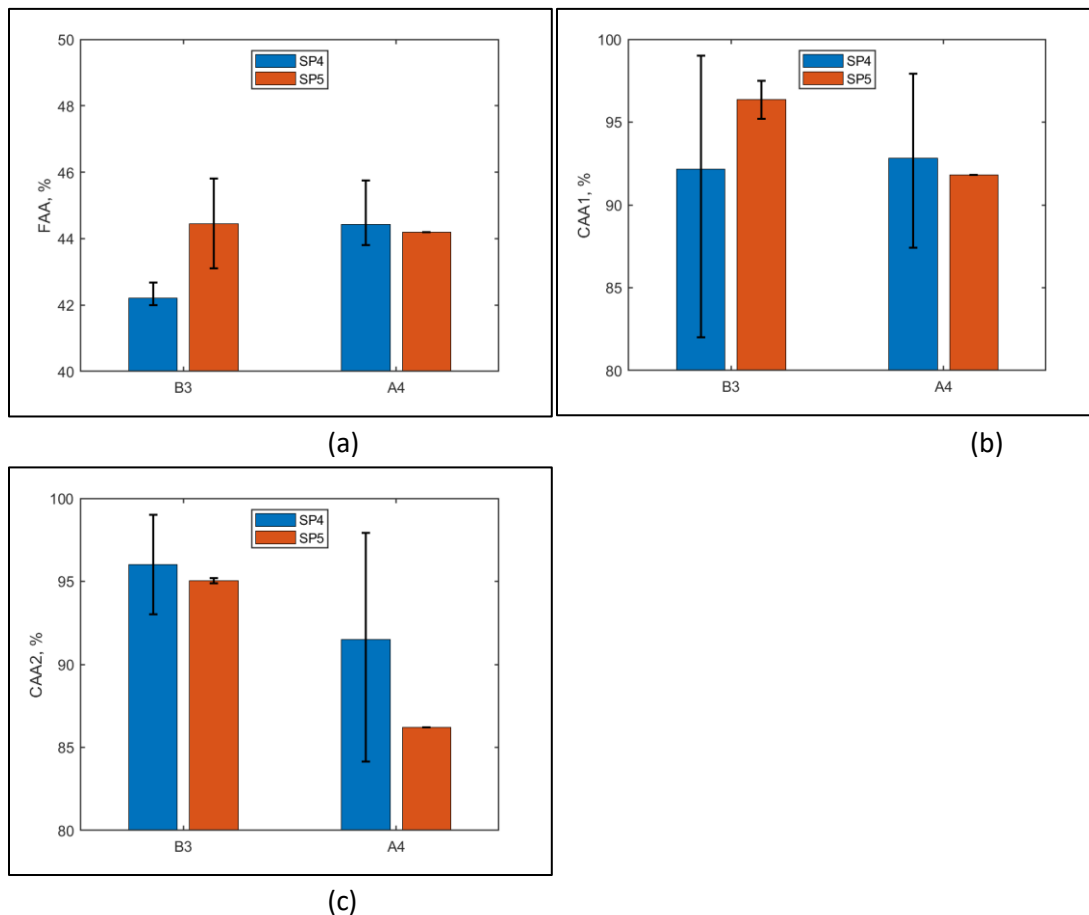


Figure 5.16 Comparison of aggregate angularity (the error bar indicates the range of the corresponding values).

G_{mm} values are visually compared in Figure 5.17. It is seen that there is no significant difference in G_{mm} between SP4 and SP5 mixtures.

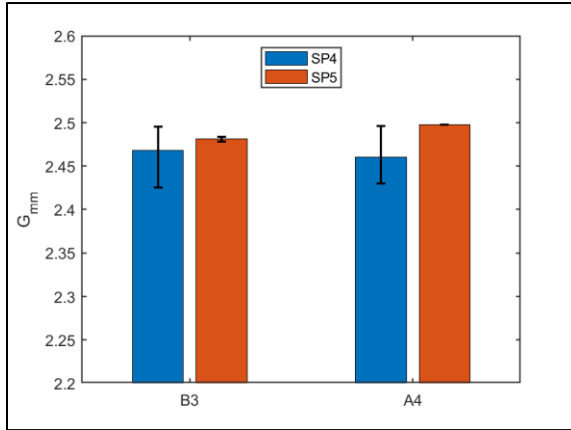


Figure 5.17 Comparison of G_{mm} (the error bar indicates the range of the corresponding values).

5.4.3 Comparison of VMA

Voids in mineral aggregate (VMA) is an important mix design parameter. The VMA of B3 and A4 mixtures are listed in Table 5.16 and Table 5.17, respectively, and are plotted in Figure 5.18. Each value represents the average value of all quality control data of the project.

Table 5.16 VMA of B3 mixtures

Mixture ID	SP4B3-1	SP4B3-2	SP4B3-3	SP4B3-4	SP4B3-5	SP5-1	SP5-2
VMA @ N_{design} , %	15.4	15.0	13.8	14.5	14.9	15.6	15.7

Table 5.17 VMA of A4 mixtures

Mixture ID	SP4A4-1	SP4A4-2	SP4A4-3	SP4A4-4	SP4A4-5	SP4A4-6	SP4A4-7	SP53
VMA @ N_{design} , %	14.9	15.3	15.3	15.6	15.6	15.8	15.1	16.8

Note: the shaded columns are SP5 projects

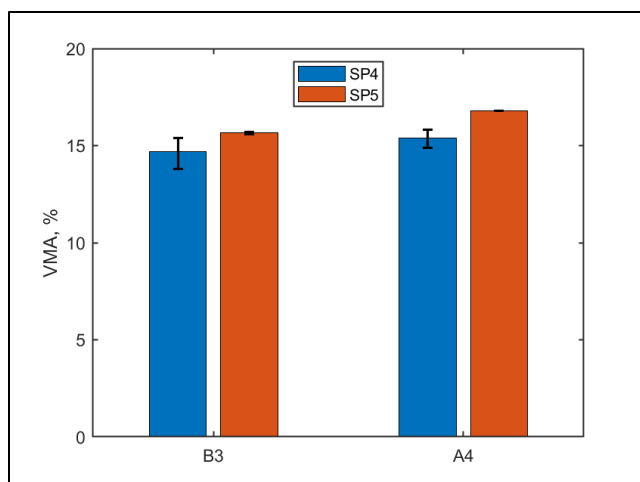


Figure 5.18 Comparison of VMA (the error bar indicates the range of the corresponding values).

It is clear that, as expected, the VMA of SP5 mixtures is about 1% higher than that of SP4 mixtures, for both B3 and A4 mixtures. This is reasonable given that, compared to SP4, SP5 increases the design air voids by 1%, while keeping the binder content level almost unchanged.

5.5 PERFORMANCE TESTS

Diametral Dynamic Modulus (E^*), Semi-Circular Bending (SCB), and Flow Number (FN) tests were conducted in the laboratory to obtain SP5 mixtures mechanical properties related to pavement performance, such as structural capacity, low-temperature cracking, and rutting.

Laboratory test specimens were prepared using loose mix taken during construction. The loose mixtures were compacted using the gyratory compaction method to the target air voids of 5% (AASHTO T 312, 2017). For each mixture, 6 gyratory compacted specimens were prepared, and the air-void ratio and number of gyrations are listed in Table 5.18. The compacted specimens were then sawed and cored to the required shapes and dimensions corresponding to each type of tests (AASHTO R83, 2017).

Table 5.18 Air voids and number of gyrations for the gyratory compacted samples.

	Sample #	1	2	3	4	5	6	Ave.
SP5-1	AV, %	5.15	4.99	5.43	5.25	5.03	5.07	5.15
	N	31	35	30	34	32	33	32.5
SP5-2	AV, %	4.85	4.80	4.92	4.72	5.11	4.93	4.89
	N	58	49	43	55	46	53	50.7
SP5-3	AV, %	5.19	4.95	5.36	5.15	5.28	5.03	5.16
	N	38	40	40	36	38	43	39.2

Note: AV = air-void ratio; N = number of gyrations.

It can be seen that the air voids values of the compacted specimens are close to the 5% target air voids. For SP5-1 and SP5-3, the average number of gyrations for reaching 5% air voids are 32.5 and 39.2,

respectively. They are either close to or less than the N_{design} 's of the corresponding mixtures, 30 and 50 respectively, which confirms the Superpave 5 mix design of these mixtures. However, for SP5-2, the average number of gyrations needed to reach 5% air voids is 50.7, which is comparatively higher than its N_{design} , 30. Therefore, SP5-2 does not satisfy the requirement of Superpave 5 mix design. Table 5.19 shows the test temperatures and the number of replicates for each test.

Table 5.19 Test temperature and replicates.

Tests	Temperature, °C	Replicates
SCB	Actual lowest temperature*	3
	-12	3
E*	-12	3
	12	3
	36	3
FN	49	3

Note: * The actual lowest temperature of the location of the projects. They are, -19.2, -21.1, -23.9 °C for the projects SP5-1, SP5-2, and SP5-3 respectively.

5.5.1 Semi-Circular Bending (SCB) Test

The Semi-Circular Bending (SCB) fracture tests were performed according to AASHTO TP105 (2020) to characterize the low temperature cracking performance of these mixtures. All three mixtures were tested at two temperatures: the actual lowest temperature of the projects and -12 °C. The results for fracture energy and fracture toughness are listed in Table 5.20 and Table 5.21, and are plotted in Figure 5.19 and Figure 5.20, respectively. Each value represents an average of three replicates.

Table 5.20 SCB fracture energy.

Mix ID	Gf @ actual lowest temp., kJ/m ²		Gf @ -12 °C, kJ/m ²	
	Ave.	Std.	Ave.	Std.
SP51	0.231	0.022	0.392	0.096
SP52	0.445	0.098	0.684	0.129
SP53	0.444	0.048	0.596	0.067

Table 5.21 SCB fracture toughness.

Mix ID	K _{Ic} @ actual lowest temp., MPa*m ^{0.5}		K _{Ic} @ -12 °C, MPa*m ^{0.5}	
	Ave.	Std.	Ave.	Std.
SP51	0.660	0.004	0.661	0.005
SP52	0.859	0.077	0.685	0.030
SP53	0.895	0.055	0.764	0.027

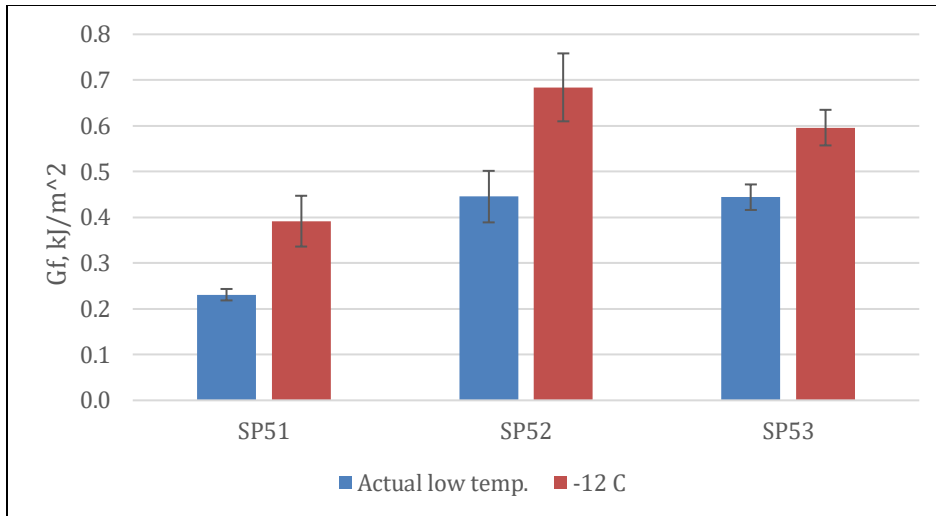


Figure 5.19 Comparison of fracture energy of different mixtures at different temperatures (the error bar indicates the standard error of the mean computed based on three replicates).

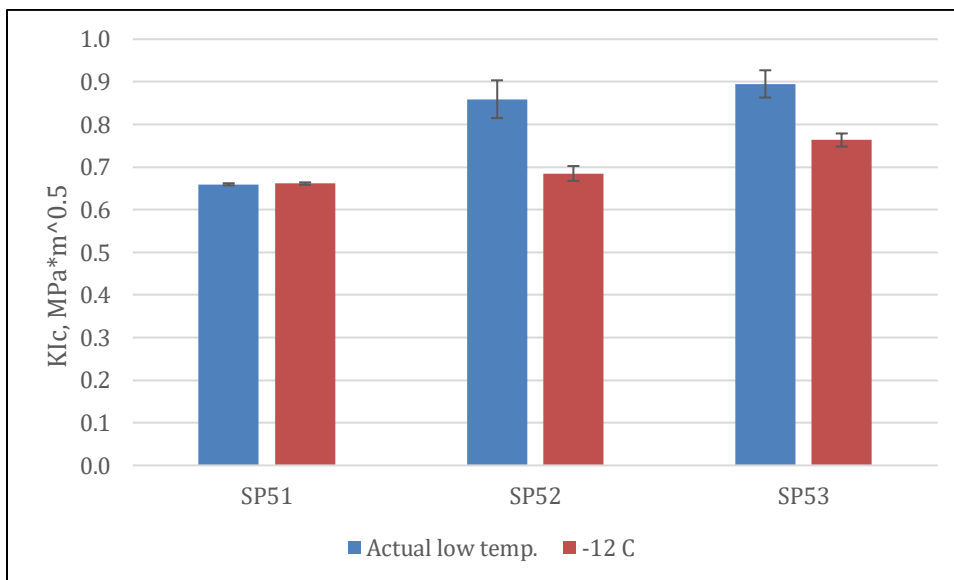


Figure 5.20 Comparison of fracture toughness of different mixtures at different temperatures (the error bar indicates the standard error of the mean computed based on three replicates).

For all mixtures, the fracture energy increases with temperature, while the fracture toughness decreases with temperature. Regardless of test temperature, the comparative trends between the three mixtures are the same. SP52 has the highest fracture energy, while SP53 has the highest fracture toughness.

The criteria for fracture energy and fracture toughness were recommended as 0.4 kJ/m² and 0.8 MPa*m^{0.5} at the temperature PGLT+10 °C (the low temperature of binder performance grade plus 10 °C) (Marasteanu et al., 2012). Given that, for the three projects, PGLT+10 °C are quite close to the actual lowest temperatures of these projects, we conclude that SP52 and SP53 satisfy these recommended criteria, while SP51 does not.

5.5.2 Flow Number

Flow Number (FN) tests (AASHTO T 378, 2017) were conducted to characterize the resistance of the asphalt mixture to permanent deformation. All mixtures were tested at 49 °C. Flow numbers for the SP5 mixture is listed in Table 5.22. Each value in the table represents an average of three replicates.

Table 5.22 Flow number.

Mix ID	Flow number @ 49 °C	
	Ave.	Std.
SP51	152.7	17.5
SP52	535.7	70.9
SP53	859.7	152.6

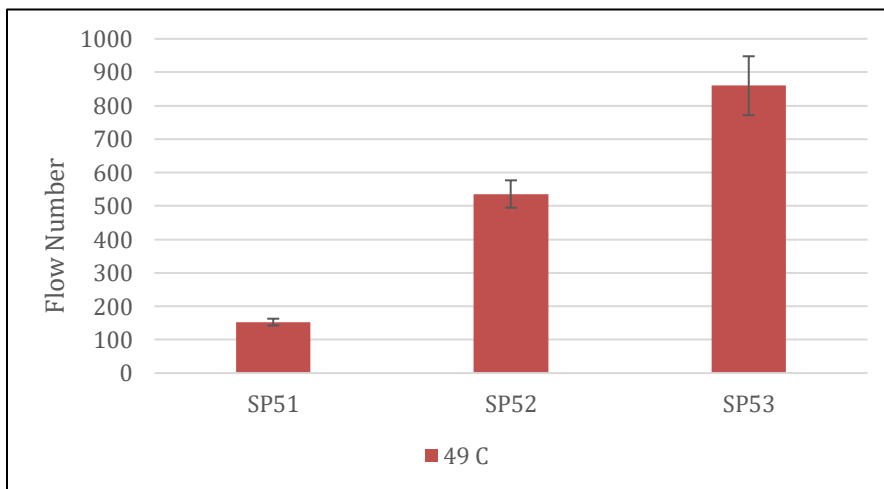


Figure 5.21 Comparison of the flow numbers of different mixtures (the error bar indicates the standard error of the mean computed based on three replicates).

Figure 5.21 compares the flow numbers of different mixtures. It is seen that the mixture SP53 has the highest flow number, followed by SP52 and SP51 is lowest. The results are reasonable since SP53 belongs to traffic level 4, while SP51 and SP52 are traffic level 3. All mixtures passed the minimum FN requirement in AASHTO T 378 (2017), i.e., FN>50 for traffic level 4.

5.5.3 Diametral Dynamic Modulus |E*|

Diametral Dynamic modulus (E*) tests (Kim et al., 2004) were conducted to characterize the stiffness of the mixtures. Frequency sweeps ranging from 0.01 Hz to 25 Hz were performed at 3 temperatures: -12°C, 12°C, and 36°C. Three replicates were tested for each mixture. Table 5.23 lists the test results. Each value in the table represents the average of three replicates.

Table 5.23 |E*| test results.

Mix ID	Temperature, °C	AVG of E* , (GPa)							
		25 Hz	10 Hz	5 Hz	1 Hz	0.5 Hz	0.1 Hz	0.05 Hz	0.01 Hz
SP51	-12	29.49	27.97	27.02	24.78	23.67	20.99	19.87	16.95
	12	14.61	12.34	11.14	8.19	7.01	4.56	3.74	2.15
	36	3.17	2.28	1.73	0.92	0.72	0.44	0.37	0.26
SP52	-12	30.83	29.31	28.07	25.17	23.85	20.85	19.15	15.75
	12	14.24	12.16	10.74	7.43	6.20	3.87	3.08	1.76
	36	2.82	1.96	1.52	0.89	0.73	0.50	0.44	0.34
SP53	-12	27.15	25.45	24.29	21.79	20.69	18.11	16.91	14.20
	12	11.82	10.18	9.07	6.56	5.63	3.79	3.11	1.92
	36	2.79	2.11	1.68	1.01	0.84	0.55	0.47	0.35

|E*| values were then used to construct master curves according to AASHTO R62 (2013). The reference temperature is chosen as 12°C. Figure 5.22 summarizes the master curves of the 3 SP5 mixtures. As shown, in general, the differences between the three mixtures are minor. SP53 has the most desired stiffness among the three mixtures, since its |E*| value is the lowest at high frequency (corresponding to low temperature) and the highest at low frequency (corresponding to high temperature).

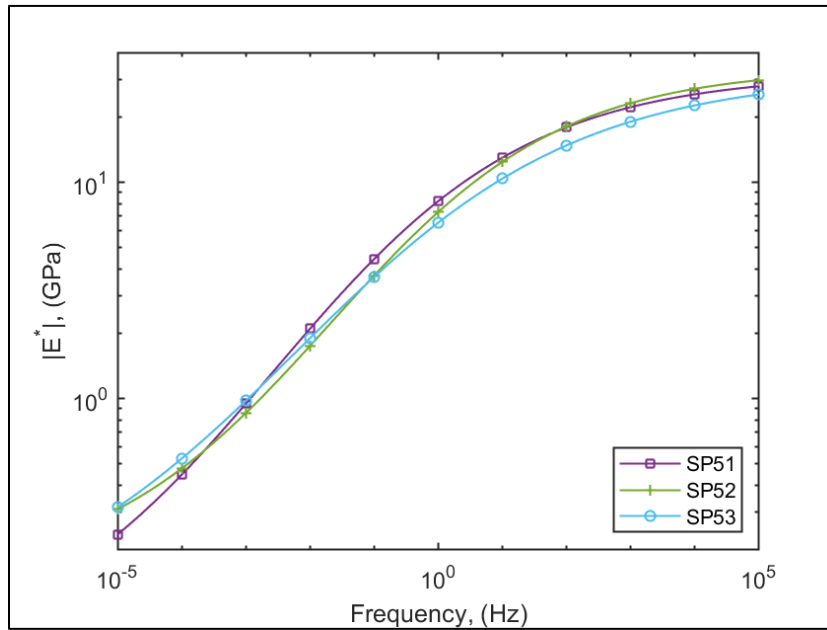


Figure 5.22 |E*| master curves.

Based on the limited experimental results, it appears that SP53 performs the best among the three mixtures, followed by SP52, and SP51. In the next task, the same set of performance tests will be conducted on four SP4 mixtures, and four laboratory-designed SP5 mixtures, and the experimental results of all mixtures will be compared.

5.6 CONCLUSIONS

In this task, field density distribution and material properties of three SP5 projects were studied, and performance tests were conducted. The following conclusions were drawn.

1. The mean field density of SP5 projects, 94.22% G_{mm} , is significantly higher than that of the traditional SP4 projects, 93.46% G_{mm} .
2. For SP5 projects, the field density level of the mixture designed for $N_{design} = 50$ is significantly lower than the two mixtures designed for $N_{design} = 30$. The field density level of the mix designed for $N_{design} = 50$ is closer to the levels observed for traditional Superpave projects. This may suggest that a lower value would be more reasonable for this traffic level of SP5 mix design.
3. The comparison of material properties for SP4 and SP5 mixtures, failed to identify what changes were responsible for the increase in field densities of SP5 projects compared to the traditional SP4 projects.
4. The VMA of SP5 mixtures is about 1% higher than that of SP4 mixtures at their corresponding N_{design} 's, which is expected since SP5 increases the design air voids by 1%, while keeping the binder content level almost unchanged.
5. From the results of the SCB, Flow number, and E^* tests, it was observed that mixture SP53 performed the best, which is reasonable since it is a traffic level 4 project.

CHAPTER 6: DEVELOPMENT OF SUPERPAVE 5 MIX DESIGNS

In this chapter, Superpave 5 mix designs are developed using the same raw materials as four traditional Superpave projects. Laboratory tests are performed at the laboratories of both the University of Minnesota (UMN) and MnDOT Office of Materials and Road Research (OMRR) to further check the mechanical properties of the designed mixtures.

6.1 MIXTURE INFORMATION

As described in Chapter 4, four traditional Superpave (denoted as SP4) projects constructed in 2020 were selected to be modified as Superpave 5 mix designs (denoted as SP5). The four selected SP4 projects cover three traffic levels (3, 4, and 5) and two NMAS (9.5 and 12.5mm). Basic information for the projects is listed in Table 6.1. All mixtures were used as wearing courses. The reclaimed asphalt pavement (RAP) content ranges from 20% to 30%, and the percent asphalt content (AC) by weight ranges from 4.8% to 5.6%. The gradation curves of the four mixtures are shown in Figure 6.1.

Table 6.1 Basic information for the selected SP4 projects

Mix ID	SP4-1	SP4-2	SP4-3	SP4-4
Traffic level	3	3	4	5
Course Type ¹	WE	WE	WE	WE
NMAS ²	A	B	B	B
Binder PG	58S-28	58S-28	58H-28	58V-34
Design Air Voids	4.0	4.0	4.0	4.0
N _{design}	60	60	90	100
% RAP	24	30	22	20
% AC	4.8	5.6	5.0	5.4
% Virgin AC	4.4	4.2	3.6	4.8
% Reclaimed AC	0.4	1.4	1.4	0.6

In the table above, WE represents wearing course; A represents NMAS = 9.5mm (3/8in); B represents NMAS = 12.5mm (1/2in). SP4 stands for the traditional Superpave design at 4% air voids. The corresponding modified mixtures will be denoted as MSP4 hereafter, which represents “Modified Superpave 4”. These new mixtures are designed to meet Superpave 5 mixture requirements.

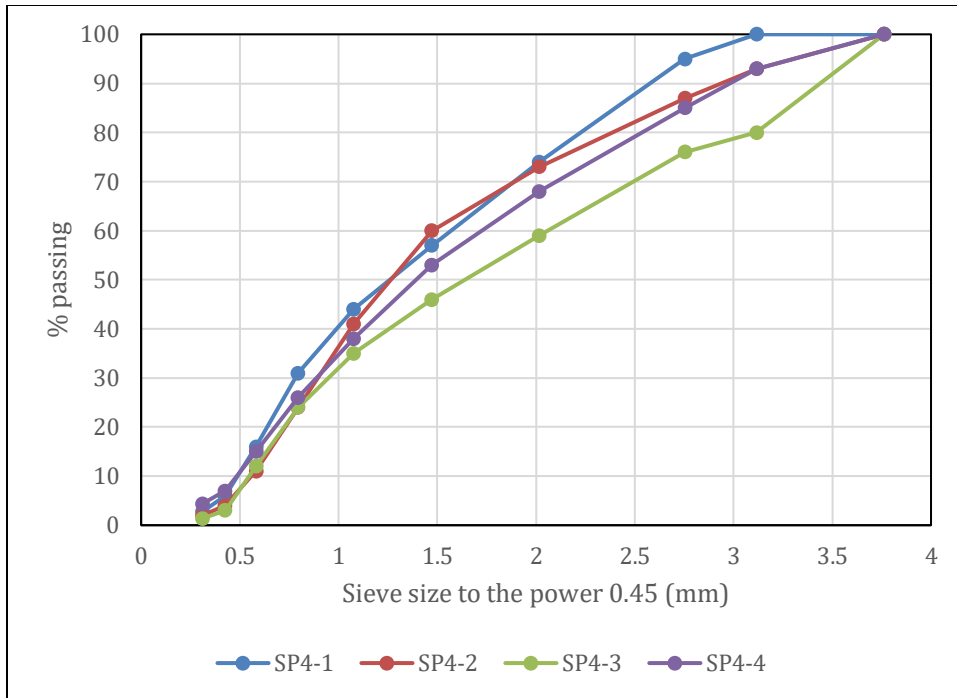


Figure 6.1 Gradation curves of the SP4 mixtures.

The aggregate angularity values for the selected mixtures are summarized in Table 6.2. Two parameters are calculated: Coarse Aggregate Angularity (CAA) of one and two faces (ASTM D5821), and Fine Aggregate Angularity (FAA) (AASHTO T304 Method A). As the traffic level increases, the required aggregate angularity increases. According to MnDOT specification 3139 (2018), minimum FAA values for traffic levels 3, 4, and 5 are 42%, 44%, and 45%, respectively. The minimum CAA1 values that are required for the same traffic levels are 55%, 85%, and 95%, respectively. CAA2 has no minimum requirement for traffic level 3, but for levels 4 and 5, the minimum required CAA2 values are 80% and 90%, respectively. As shown in Table 6.2, the four mixtures satisfy the aforementioned angularity requirements.

Table 6.2 Summary of aggregate angularity values for the selected SP4-4 projects

Mix ID	FAA, %	CAA One Face, %	CAA Two Faces, %
SP4-1	42	90	N A
SP4-2	42	99	93
SP4-3	45	96	95
SP4-4	46	97	96

6.2 DEVELOPMENT OF SUPERPAVE 5 MIX DESIGNS

When developing the SP5 mix designs, the same raw materials (aggregates, binders, and RAPs) used in the original SP4 projects were used. The SP5 mix designs are developed by changing aggregate gradation while keeping the binder content unchanged. In this study, the N_{design} for Superpave 5 is chosen as 30 for

all traffic levels, because it was shown in Chapter 4.5 that the field compaction effort for projects of different traffic levels in Minnesota is equivalent to about 30 gyrations (Yan et al. 2022b).

The procedure for developing SP5 mix designs is described in Figure 6.2. First, the gradations of stockpiles are measured. Then, a few trial blends are designed by changing the weight percentages of aggregates sources. For each trial blend, gyratory compaction of two replicates are performed to the N_{design} of SP5 mix design (30 gyration), and the volumetric properties of compacted samples are evaluated. If there are trials that have 5% or less air voids at N_{design} , the blend that has the lowest air voids (most compactable) is selected. Otherwise, more trials are needed. If the air voids at N_{design} is too low, the binder content can be reduced to increase the air voids. After the candidate trial is selected, performance tests (rutting, cracking and stiffness) are performed to validate the mix design. If the candidate fails the performance tests, more trial blends are needed.

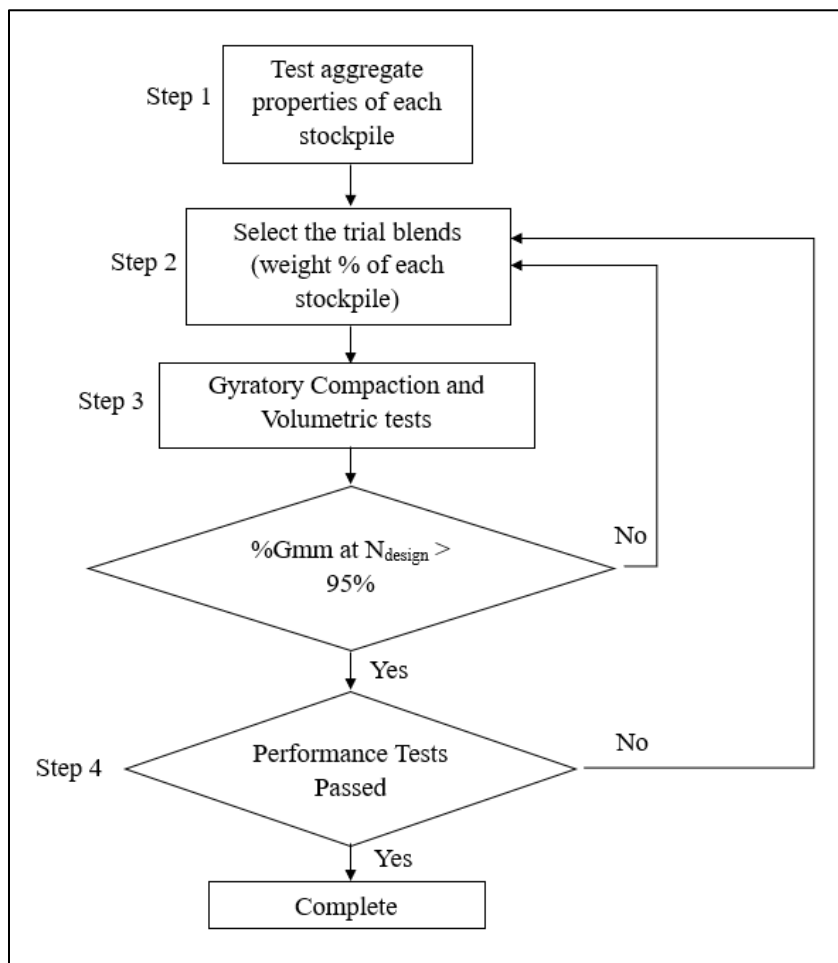


Figure 6.2 Procedure for developing SP5 mix designs.

6.2.1 Project 1 (MSP4-1)

The Superpave 5 mix design for project 1 is denoted as MSP4-1. Six trial blends were designed for MSP4-1. The weight percentages of aggregate sources and virgin binder for the trials are shown in Table 6.3. Trial 1 is the original SP4-1 mix design. The aggregate gradations for the trials are listed in Table 6.4. Figure 6.3 shows the gradations of the trials.

Table 6.3 Weight percentage of aggregate sources and virgin binder content for MSP4-1 trial blends

Trial #	Aggregate 1	Sand	Aggregate 2	RAP	Virgin AC
1	22%	40%	14%	24%	4.4%
2	12%	50%	14%	24%	4.4%
3	32%	30%	14%	24%	4.4%
4	37%	25%	14%	24%	4.4% *
5	42%	20%	14%	24%	4.4%
6	47%	15%	14%	24%	4.4%

Note: * Since 4.4% led to excessively low air void ratio, the virgin binder content of trial 4 was later reduced to 4.0%.

Table 6.4 Gradations for MSP4-1 trial blends

Trial #		1	2	3	4	5	6
% Passing of Each Sieve Size	1 in, 25 mm	100	100	100	100	100	100
	¾ in, 19mm	100	100	100	100	100	100
	½ in, 12.5mm	100	100	100	100	100	100
	3/8 in, 9.5mm	95	96	95	95	94	94
	No.4, 4.75mm	74	79	68	65	63	60
	No.8, 2.36 mm	57	64	50	46	43	40
	No.16, 1.18mm	44	50	38	35	32	29
	No.30, 0.6mm	31	35	27	25	23	20
	No.50, 0.3mm	16	17	14	13	13	12
	No.100, 0.15mm	6	6	6	6	5	5
No.200, 0.075mm	2.8	2.8	2.8	2.8	2.8	2.8	

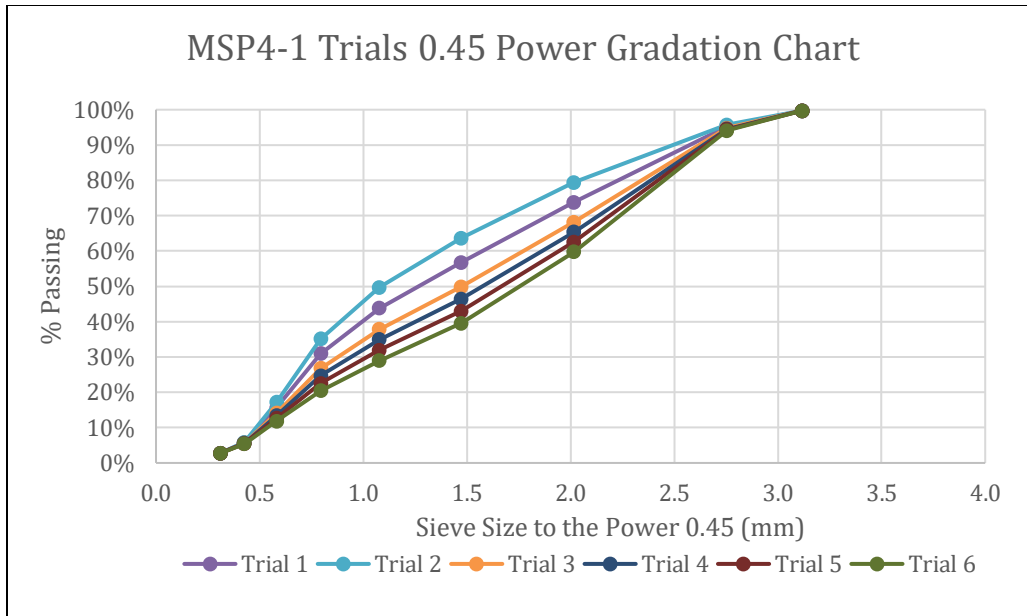


Figure 6.3 The 0.45 gradation chart for the trial blends of MSP4-1.

Two gyratory specimens were compacted for each trial blend. The compacted density, %G_{mm}, at N_{design} are listed in Table 6.5. The compaction curves for the trials are shown in Figure 6.4. It is seen that the gradation closer to the maximum density line had the lower air voids (higher density).

Table 6.5 Compaction data for MSP4-1 trials

Trial #	1		2		3		4		5		6	
Specimen #	1	2	1	2	1	2	1	2	1	2	1	2
% G _{mm}	95.0	95.2	92.8	92.8	98.1	97.5	97.7	97.1	98.1	97.8	96.5	96.1

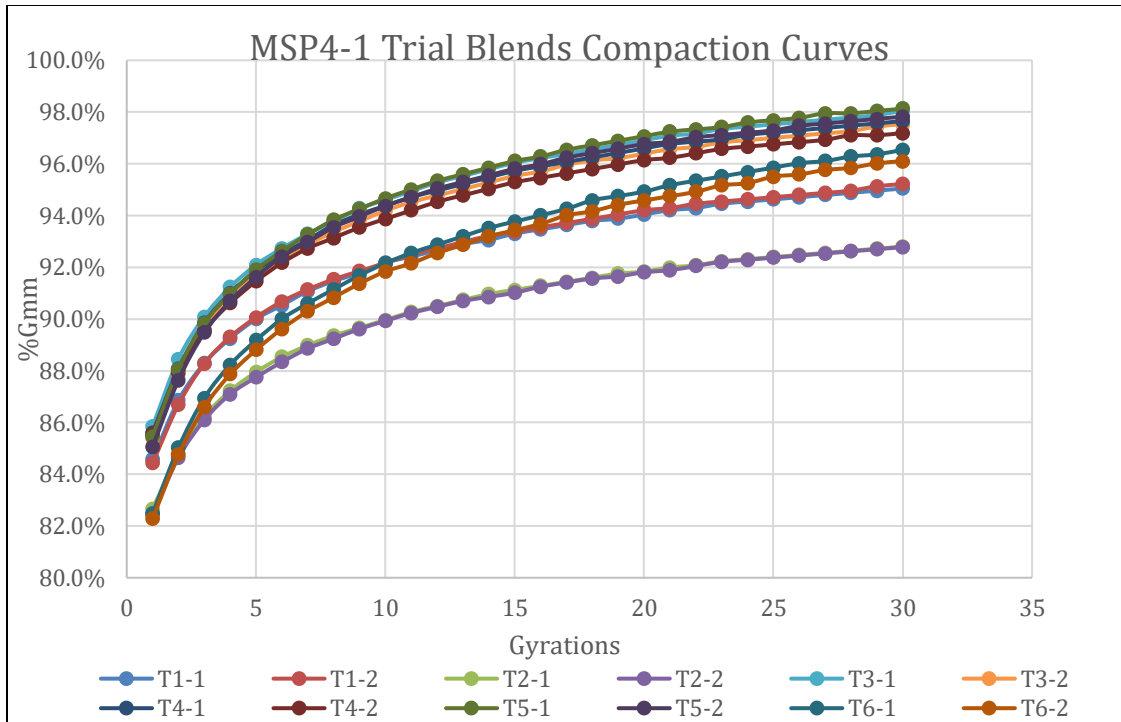


Figure 6.4 Compaction curves for MSP4-1 trial blend specimens.

It is seen from Figure 6.4 that the compaction curves of trial 3, 4, and 5 are close to each other and they are clearly more compactable than the other trials. The trial 4 is selected as the candidate of the final mix design. However, it is seen that the air voids at N_{design} is about 2.5% which is much lower than the 5% design air voids. Therefore, the virgin binder content of trial 4 was reduced to 4.0%, which led to an air-void ratio of 4.7% at N_{design} . Trial 4 with 4.0% virgin binder content is selected the candidate of the modified mix design, MSP4-1, which is later validated by performance tests, as discussed in Chapter 6.3 and 6.4.

6.2.2 Project 2 (MSP4-2)

The Superpave 5 mix design for project 2 is denoted as MSP4-2. Three trial blends were designed for MSP4-2. The same procedure used in the Project 1 was implemented for this project. The first trial blend is the original SP4-2 mix design. The weight percentages of aggregate sources and virgin binder for the trials are shown in Table 6.6. The aggregate gradations of the trial blends are shown in Table 6.7. Figure 6.5 shows the gradations of trials.

Table 6.6 Weight percentage of aggregate sources and virgin binder content for MSP4-2 trial blends

Trial #	Aggregate 1	Aggregate 2	Sand 1	Sand 2	Sand 3	RAP	Millings	Virgin AC
1	13%	7%	10%	14%	26%	20%	10%	4.2%
2	20%	11%	8%	11%	21%	20%	10%	4.2%
3	26%	14%	6%	8%	16%	20%	10%	4.2%

Table 6.7 Gradations for MSP4-2 trial blends

Trial #		1	2	3
% Passing of Each Sieve Size	1in, 25 mm	100	100	100
	¾ in, 19mm	100	100	100
	½ in, 12.5mm	93	91	88
	3/8 in, 9.5mm	87	83	78
	No.4, 4.75mm	73	66	58
	No.8, 2.36 mm	60	52	45
	No.16, 1.18mm	41	36	31
	No.30, 0.6mm	24	22	19
	No.50, 0.3mm	11	10	10
	No.100, 0.15mm	4	4	4
	No.200, 0.075mm	2.0	2.0	2.0

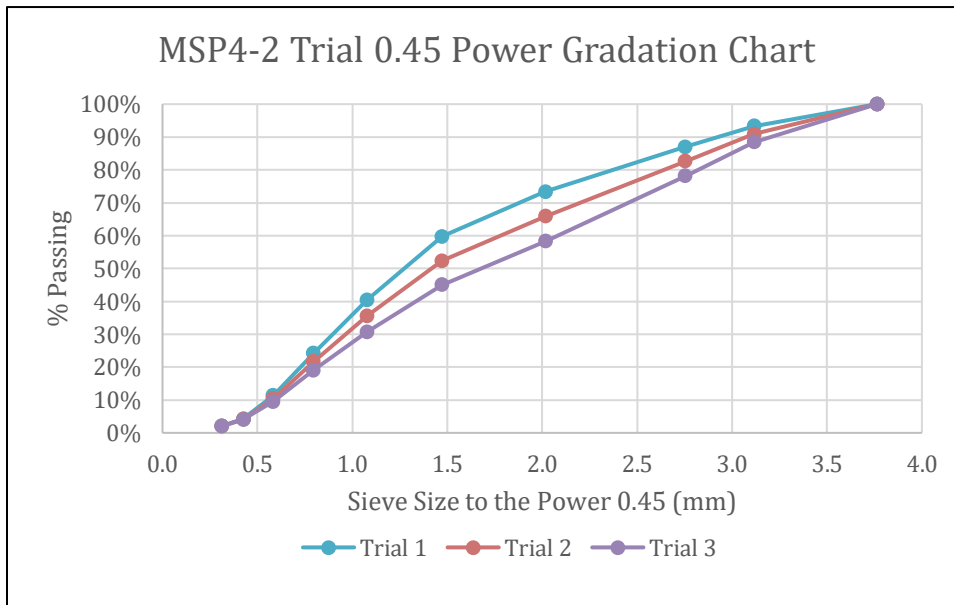


Figure 6.5 The 0.45 gradation chart for the trial blends of MSP4-2.

Two gyratory specimens were compacted to the N_{design} 30 gyrations, for each trial blend. The density, $\%G_{mm}$, for each compacted specimen were recorded in Table 6.8. The compaction curves for the six trials are shown in Figure 6.6.

Table 6.8 Compaction data for MSP4-2 trials

Trial #	1		2		3	
Specimen #	1	2	1	2	1	2
% G_{mm}	92.8	92.4	95.2	94.7	95.7	95.5

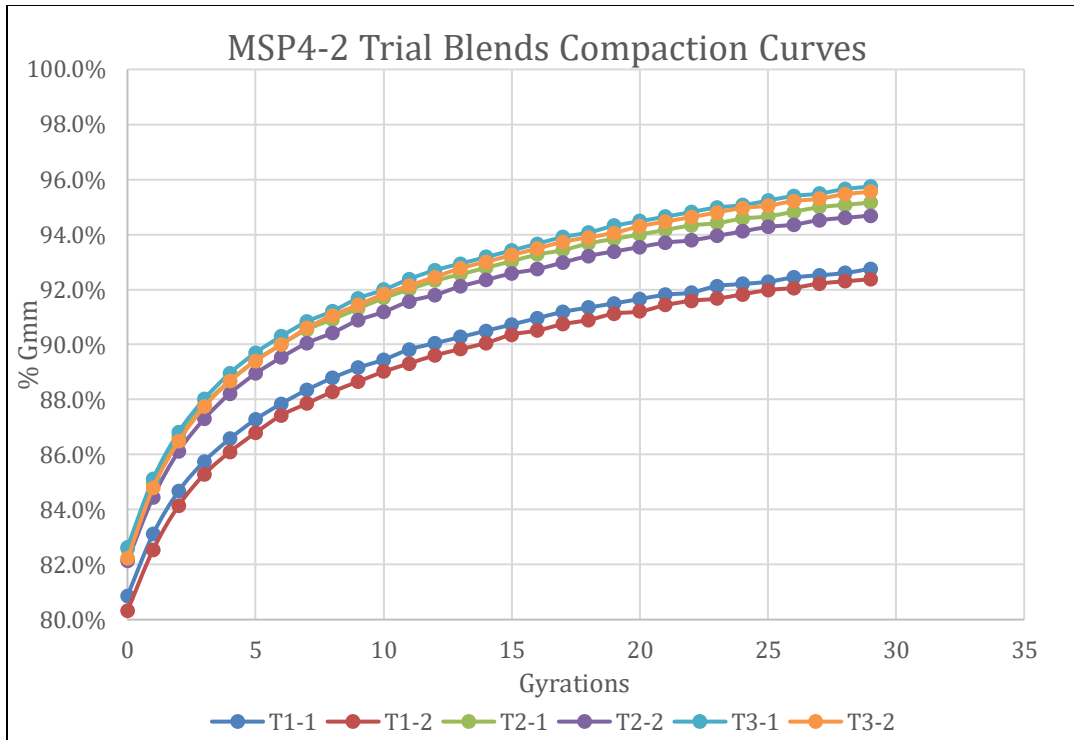


Figure 6.6 Compaction curves for MSP4-2 trial blend specimens.

It is seen that trial 3 is the most compactable blend. It reached about 4.4% air voids at N_{design} , which satisfies the SP5 mix design criterion. Other trials did not reach 5% air voids at N_{design} . Therefore Trial 3 was selected as the candidate for the modified mix design, MSP4-2. It is later validated by performance tests, as discussed in Chapter 6.3 and 6.4. It is important to note that, once again, the results show that the gradation closest to the maximum density line had the lowest air voids (highest density).

6.2.3 Project 3 (MSP4-3)

The Superpave 5 mix design for project 1 is denoted as MSP4-3. Four trial blends were designed for MSP4-3. The first trial blend was the original SP4-3 mix design. The weight percentages of aggregate sources and virgin binder for the trials are shown in Table 6.9. The aggregate gradations and packing fractions of the trial blends are shown in Table 6.10. Figure 6.7 shows the gradations of trials.

Table 6.9 Weight percentage of aggregate sources and virgin binder content for MSP4-3 trial blends

Trial #	Sand 1	Aggregate 1	Aggregate 2	Sand 2	Millings	Virgin AC
1	13%	15%	22%	28%	22%	3.6%
2	11%	19%	25%	22%	22%	3.6%
3	7%	24%	32%	15%	22%	3.6%
4	17%	12%	16%	33%	22%	3.6%

Table 6.10 Gradations for MSP4-3 trial blends

Trial #		1	2	3	4
% Passing of Each Sieve Size	1 in, 25 mm	100	100	100	100
	¾ in, 19mm	100	100	100	100
	½ in, 12.5mm	80	77	71	85
	3/8 in, 9.5mm	76	72	65	82
	No.4, 4.75mm	59	53	43	67
	No.8, 2.36 mm	46	40	31	53
	No.16, 1.18mm	35	30	23	41
	No.30, 0.6mm	24	21	16	28
	No.50, 0.3mm	12	10	8	13
	No.100, 0.15mm	3	3	2	4
	No.200, 0.075mm	1.4	1.2	1.1	1.5

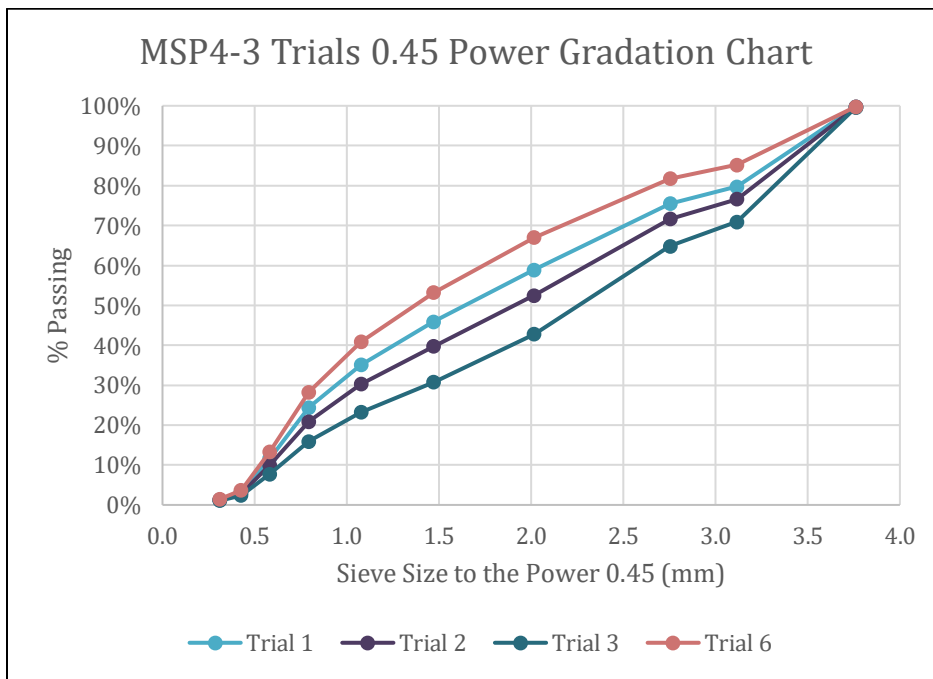


Figure 6.7 The 0.45 gradation chart for the trial blends of SP4-3.

Two gyratory specimens were compacted to the N_{design} , 30 gyrations, for each trial blend. The density, $\%G_{mm}$, for each compacted specimen were recorded in Table 6.11. The compaction curves for the six trials are shown in Figure 6.8.

Table 6.11 Compaction data for MSP4-3 trials

Trial #	1		2		3		4	
Specimen #	1	2	1	2	1	2	1	2
% G_{mm}	93.8	93.5	95.1	95.0	92.3	92.3	91.4	91.2

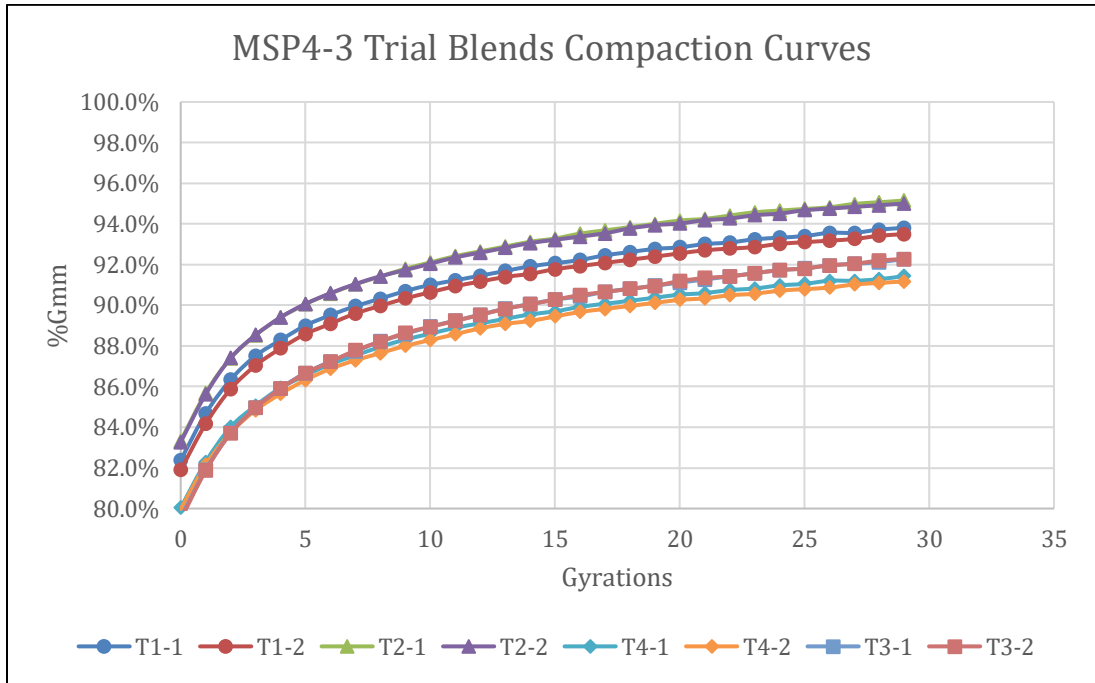


Figure 6.8 Compaction curves for MSP4-3 trial blend specimens.

It is seen that trial 2 was the only trial that met the requirements for a SP5 mix design with an air voids being 5%, and therefore it was selected as the candidate for the modified mix design MSP4-3. It is later validated by performance tests, as discussed in Chapter 6.3 and 6.4.

6.2.4 Project 4 (MSP4-4)

The Superpave 5 mix design for project 1 is denoted as MSP4-4. Four trial blends were designed for MSP4-4. The first trial blend was the original SP4-4 mix design. The weight percentages of aggregate sources and virgin binder for the trials are shown in Table 6.12. The aggregate gradations and packing fractions of the trial blends are shown in Table 6.13. Figure 6.9 shows the gradations of trials.

Table 6.12 Weight percentage of aggregate sources and virgin binder content for MSP4-4 trial blends

Trial #	Sand 1	Aggregate 1	Aggregate 2	Sand 2	Millings	Virgin AC
1	20%	5%	20%	35%	20%	4.8%
2	15%	8%	32%	25%	20%	4.8%
3	12%	9%	37%	22%	20%	4.8%
4	17%	7%	27%	29%	20%	4.8%

Table 6.13 Gradation and aggregate packing fraction for MSP4-4 trial blends

Trial #		1	2	3	4
% Passing of Each Sieve Size	1 in, 25 mm	100	100	100	100
	¾ in, 19mm	100	100	100	100
	½ in, 12.5mm	93	86	84	88
	3/8 in, 9.5mm	85	72	68	75
	No.4, 4.75mm	68	53	47	58
	No.8, 2.36 mm	53	40	36	44
	No.16, 1.18mm	38	29	26	32
	No.30, 0.6mm	26	18	17	20
	No.50, 0.3mm	15	10	9	12
	No.100, 0.15mm	7	4	4	5
	No.200, 0.075mm	4.4	1.3	1.2	1.5

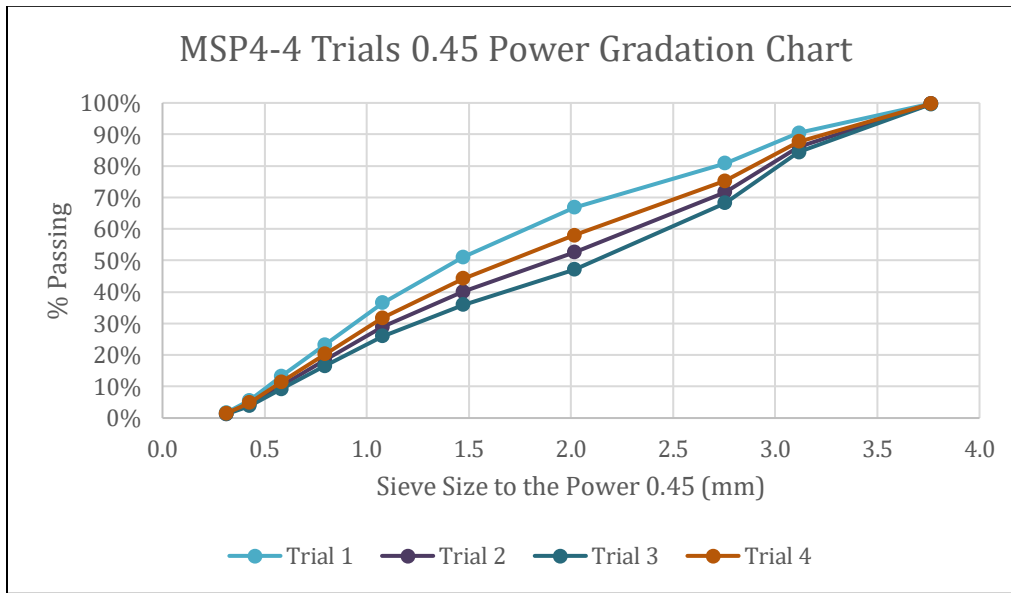


Figure 6.9 The 0.45 gradation chart for the trial blends of MSP4-4.

Two gyratory specimens were compacted to the N_{design} , 30 gyrations, for each trial blend. The density, $\%G_{mm}$, for each compacted specimen were recorded in Table 6.14. The compaction curves for the six trials are shown in Figure 6.10.

Table 6.14 Compaction data for MSP4-4 trials

Trial #	1		2		3		4	
Specimen #	1	2	1	2	1	2	1	2
% G_{mm}	96.0	96.2	98.0	98.2	98.3	98.4	96.9	97.3

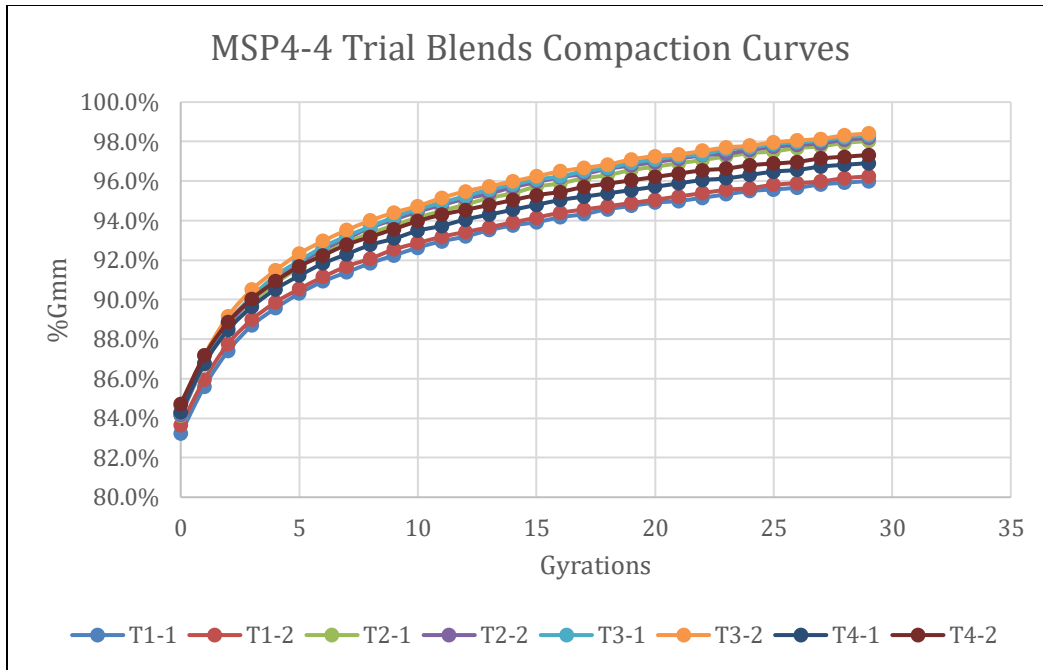


Figure 6.10 Compaction curves for MSP4-4 trial blend specimens.

It is seen that all trials reached air voids lower than 5% at the N_{design} . Among the trials, trial 3 is most compactable, which achieved the highest density %G_{mm} of 98.4 at the N_{design} . Therefore, trial 3 was selected as the candidate for the modified mix design, MSP4-4. It is later validated by performance tests, as discussed in Chapter 6.3 and 6.4. It is important to note that, the design air voids of the trial 3 is very low, about 1.6%, which may cause a potential for bleeding. The air voids can be increased by reducing the binder content. However, due to the lack of raw materials, extra trials with reduced binder contents were not investigated in this study.

6.2.5 Comparison of Bailey Method Parameters

In this section, the Bailey method parameters of the original mix designs (SP4) and modified mix designs (MSP4) are compared. As described in Task 4A, the Bailey method parameters the Coarse Aggregate (CA) ratio, the Fine Aggregate Coarse (FAC) ratio, and the Fine Aggregate Fine (FAF) ratio. The CA defines the fineness of the coarse aggregates, FAC defines the fineness of the coarse part of the fine aggregates, and the FAF defines the fineness of the fine part of the fine aggregates. More information on how the parameters are calculated can be found elsewhere (Vavrik et al., 2002).

The Bailey method parameters for SP4 and MSP4 mixtures are computed and listed in Table 6.15, and are compared in Figure 6.11, Figure 6.12, and Figure 6.13 for CA, FAC, and FAF, respectively. The recommended ranges of Bailey parameters are also shown in the figures. For CA ratio, the recommended range is 0.4~0.55 for N_{MAS}=9.5mm, and 0.5~0.65 for N_{MAS}=12.5mm. The recommended ranges for FAC and FAF are the same, which is 0.35~0.5.

Table 6.15 Bailey method parameters of the SP4 and MSP4 mix designs

Mixtures	NMAS, mm	CA	FAC	FAf
SP4-1	9.5	0.65	0.54	0.19
SP4-2	12.5	1.00	0.40	0.17
SP4-3	12.5	0.66	0.52	0.13
SP4-4	12.5	1.00	0.49	0.27
MSP4-1	9.5	0.54	0.54	0.24
MSP4-2	12.5	0.72	0.42	0.21
MSP4-3	12.5	0.60	0.53	0.14
MSP4-4	12.5	0.51	0.47	0.24

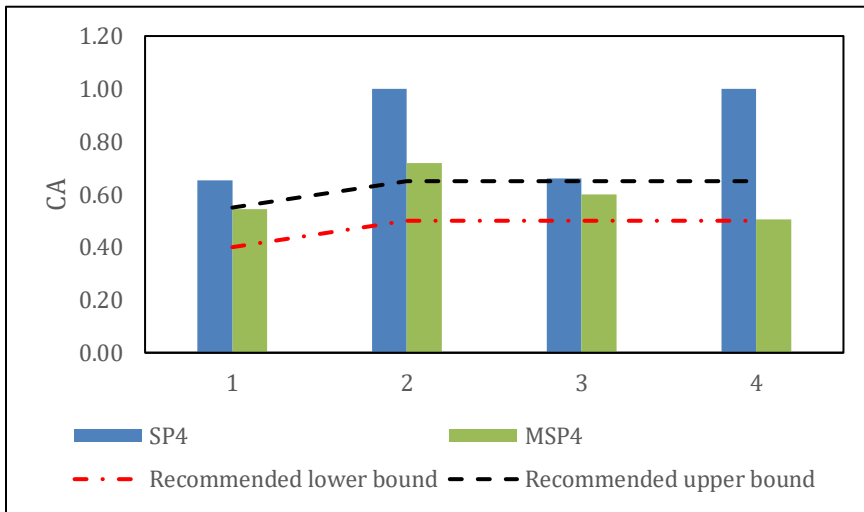


Figure 6.11 CA ratio of the SP4 and MSP4 mix designs

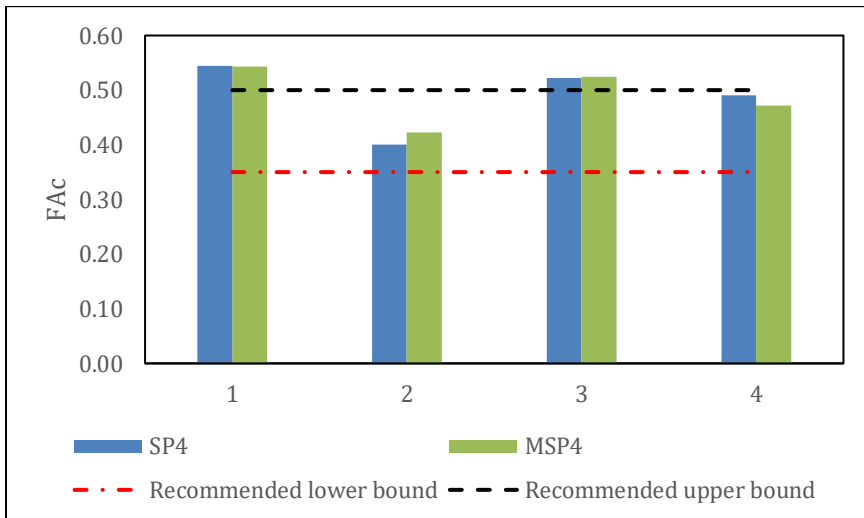


Figure 6.12 FAC ratio of the SP4 and MSP4 mix designs

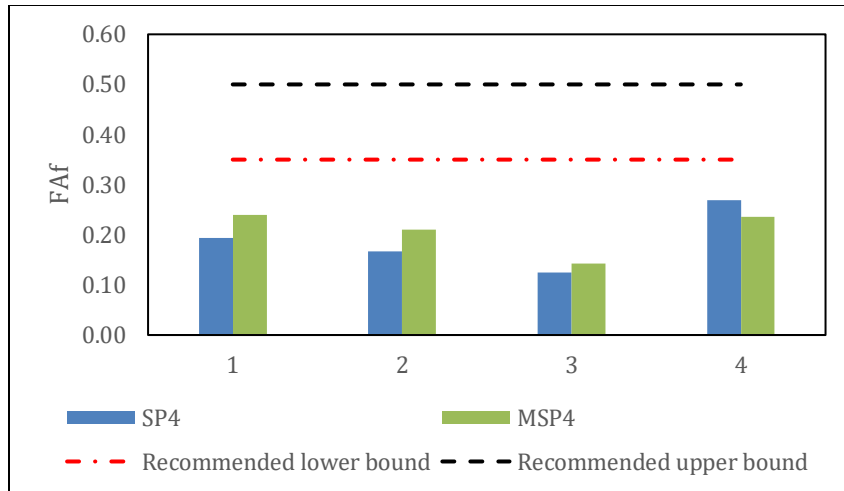


Figure 6.13 FAF ratio of the SP4 and MSP4 mix designs

It is seen that the SP4 mix designs have CA ratios higher than the recommended range. The CA ratios were reduced for MSP4 mix designs to either within or close to the recommended range. The MSP4 and SP4 mixtures have similar FAc and FAF values, because the two parameters are predominated by fine aggregate gradation and the SP4 and MSP4 mixtures used the same fine aggregates. It is seen that for both SP4 and MSP4 mixtures, their FAc values are close to the recommended range, while the FAF values are lower than the recommended range.

In conclusion, the modified mix designs have more preferable CA ratios than the original designs, while there is no significant difference of FAc and FAF between the modified and original mixtures. Therefore, overall, the modified mixture is also more preferable in terms of Bailey Method parameters.

6.3 PERFORMANCE TESTS AT UMN

Semi-Circular Bending (SCB), Diametral Dynamic Modulus (E^*), and Flow Number (FN) tests were conducted at the University of Minnesota (UMN) on the SP4 and MSP4 mixtures to validate the MSP4 mix designs. Performance tests were also conducted on mixtures from three Superpave 5 (SP5) projects already built in Minnesota. The basic information of the Minnesota SP5 mixtures are listed in Table 6.16. This section presents the test results of the three groups of mixtures: SP4, MSP4, and SP5. The comparison of these three groups of mixtures are detailed in Chapter 6 3.5 – 6.3.7

Table 6.16 Summary of the Superpave 5 mixtures

Mix ID	SP5-1	SP5-2	SP5-3
Traffic level	3	3	4
NMAS	12.5	12.5	9.5
Design Air voids	5.0	5.0	5.0
Binder PG	58S-28	58H-34	58H-34
RAP content	10%	17%	20%
N_{design}	30	30	50
%AC	5.5	5.2	5.5

6.3.1 Sample Preparation

The compacted specimens use for the performance testing were sawed and cored to fit the required dimensions of the corresponding performance test (AASHTO R83, 2017). For a certain mixture, the test temperature and the number of replicates at each temperature are shown in Table 6.17. The SCB tests were performed at two temperatures, the actual low temperature and -12 °C. The actual low temperatures are different for different projects, because they are at different locations in Minnesota. The actual low temperatures for SP4-1, SP4-2, SP4-3, and SP4-4 are -24, -20, -19, and -21°C, respectively. The MSP4 projects have the same respective actual low temperatures as the SP4 projects. The actual low temperatures for SP5-1, SP5-2, and SP5-3 are -19, -21, and -24 °C, respectively. The E* tests were performed at three different temperatures, -12, 12, and 36°C. The Flow number tests were performed at 49 °C. For all tests, three replicates were performed at each testing temperature.

Table 6.17 Test temperatures for performance tests

Tests	Temperature, °C	Replicates
SCB	Actual low temperature*	3
	-12	3
E*	-12	3
	12	3
	36	3
FN	49	3

6.3.2 The Semi-Circular Bending (SCB) Test

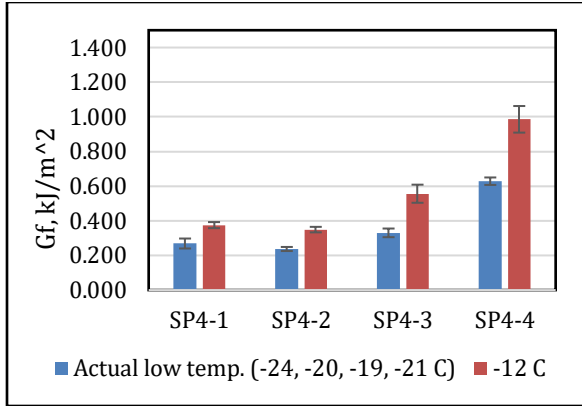
The Semi-Circular Bending (SCB) tests were performed in order to characterize the low temperature cracking performance of each group of mixtures. The tests were performed in accordance with AASHTO TP105 (2013). All projects were tested at two temperatures: the actual low temperature for the project and -12 °C. Three replicates were tested for each project tested at each temperature. The results of the fracture energy and fracture toughness are listed in Table 6.18 and Table 6.19, and are plotted in Figure 6.14 and Figure 6.15. The error bar indicates the standard error of the mean computed based on three replicates. The Coefficient of Variation (COV) is a measure of variation around the mean. A larger COV value represents a greater level of test result variations around the mean.

Table 6.18 SCB fracture energy

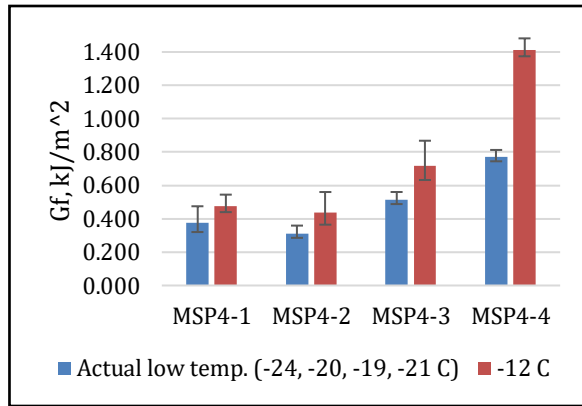
Mix ID	Gf @ actual lowest temp., kJ/m ²				Gf @ -12 °C, kJ/m ²		
	Actual Low Temperature (°C)	Ave.	Std.	COV	Ave.	Std.	COV
SP4-1	-24	0.269	0.050	0.19	0.375	0.030	0.08
SP4-2	-20	0.237	0.020	0.08	0.349	0.028	0.08
SP4-3	-19	0.330	0.043	0.13	0.556	0.091	0.16
SP4-4	-21	0.628	0.037	0.05	0.986	0.133	0.13
MSP4-1	-24	0.374	0.101	0.27	0.475	0.070	0.15
MSP4-2	-20	0.313	0.047	0.15	0.436	0.124	0.28
MSP4-3	-19	0.515	0.046	0.02	0.719	0.149	0.21
MSP4-4	-21	0.770	0.043	0.06	1.414	0.068	0.05
SP5-1	-19	0.445	0.098	0.22	0.684	0.129	0.19
SP5-2	-21	0.231	0.022	0.09	0.392	0.096	0.24
SP5-3	-24	0.444	0.048	0.11	0.596	0.067	0.11

Table 6.19 SCB fracture toughness

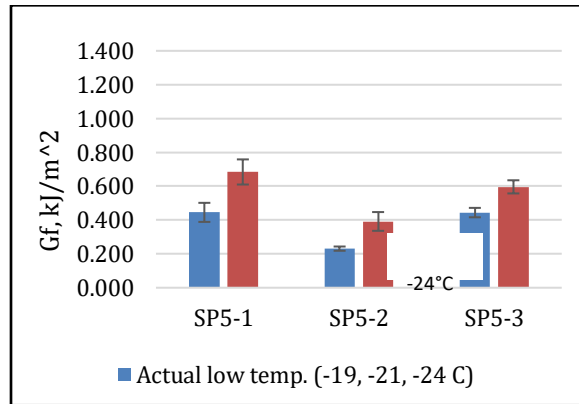
Mix ID	K _l c @ actual lowest temp., MPa*m ^{0.5}				K _l c @ -12 °C, MPa*m ^{0.5}		
	Actual Low Temperature (°C)	Ave.	Std.	COV	Ave.	Std.	COV
SP4-1	-24	0.683	0.040	0.06	0.612	0.057	0.09
SP4-2	-20	0.657	0.043	0.07	0.634	0.059	0.09
SP4-3	-19	0.841	0.067	0.08	0.761	0.122	0.16
SP4-4	-21	0.765	0.045	0.06	0.573	0.021	0.04
MSP4-1	-24	0.849	0.049	0.06	0.814	0.083	0.10
MSP4-2	-20	0.774	0.064	0.08	0.769	0.020	0.03
MSP4-3	-19	1.057	0.072	0.07	0.944	0.092	0.10
MSP4-4	-21	0.923	0.049	0.05	0.599	0.039	0.07
SP5-1	-19	0.859	0.077	0.09	0.685	0.030	0.04
SP5-2	-21	0.660	0.004	0.01	0.661	0.005	0.01
SP5-3	-24	0.895	0.055	0.06	0.764	0.027	0.04



(a)

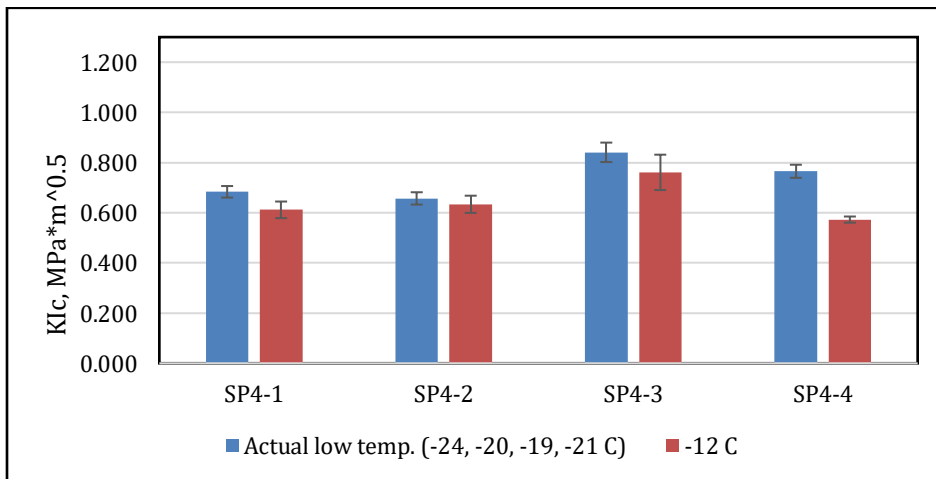


(b)

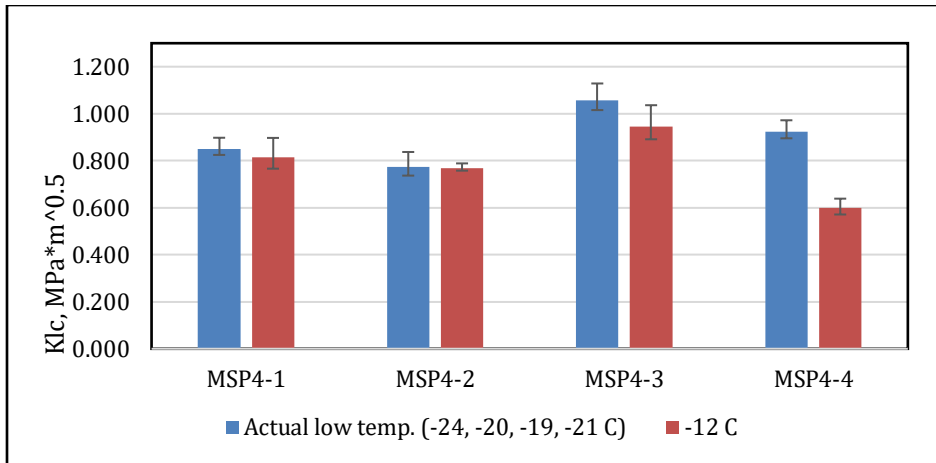


(c)

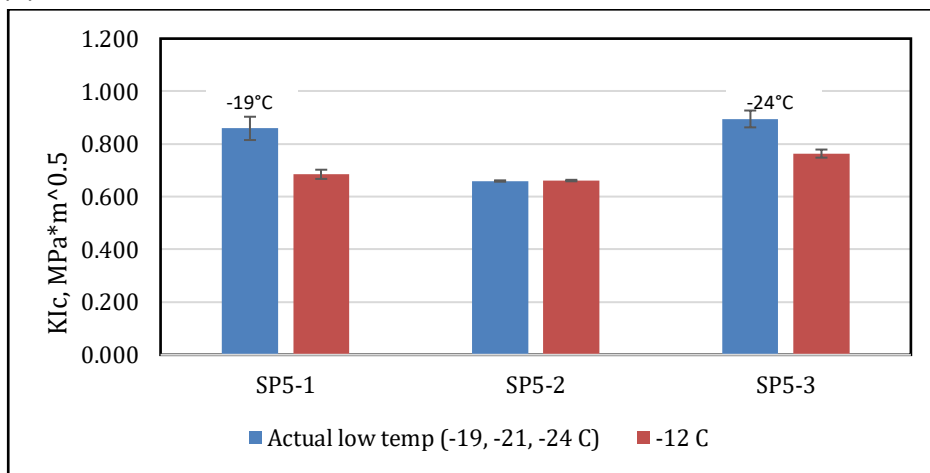
Figure 6.14 Comparison of fracture energy of the different mixture groups, SP4, MSP4, and SP5, at their respective actual low temperature and -12°C .



(a)



(b)



(c)

Figure 6.15 Comparison of fracture toughness of different mixture groups, SP4, MSP4, and SP5, at their respective actual low temperature and -12°C.

For all the mixture groups, the fracture energy increases as the temperature increases and the fracture toughness decreases as the temperature increases. In the SP4 and MSP4 mixture groups, SP4-4 and MSP4-4 had the largest fracture energy and SP4-3 and MSP4-3 had the highest fracture toughness. In the SP5 group, SP5-1 had the highest fracture energy while SP5-3 had the highest fracture toughness.

The criteria for fracture energy and fracture toughness are $0.4\text{kJ}/\text{m}^2$ and $0.8\text{MPa}\cdot\text{M}^{0.5}$, respectively, at the temperature $\text{PHGT}+10\text{ }^\circ\text{C}$ (the low temperature of binder performance grade plus $10\text{ }^\circ\text{C}$) (Marasteanu et al., 2012). The $\text{PGLT}+10\text{ }^\circ\text{C}$ is close to the actual lowest temperatures for all of the projects, so the values for fracture energy and fracture toughness at the actual low temperature can be inspected to see if they meet the criteria. The projects that meet these criteria, according to Figure 6.14 and Figure 6.15, are MSP4-3, MSP4-4, SP5-1, and SP5-3. None of the SP4 mixes meet the requirements for fracture energy and fracture toughness. Comparison between the three mixture groups SP4, MSP4, and SP5 is detailed in Chapter 6.3.5.

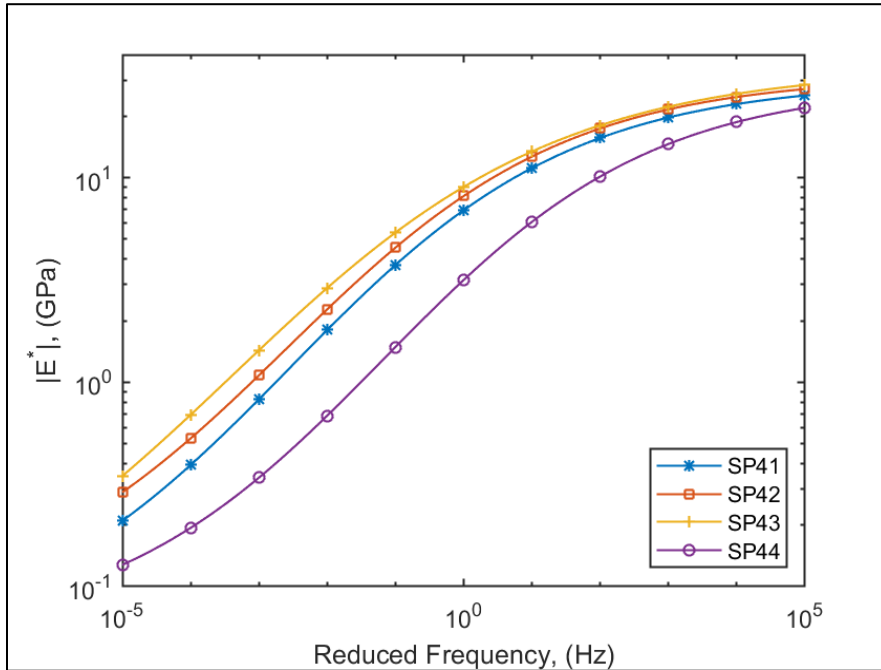
6.3.3 Diametral Dynamic Modulus (E^*) Test

In this study, the Diametral Dynamic modulus (E^*) test (Kim et al., 2004) was used to characterize the stiffness of asphalt mixtures. Three replicates were tested for each mixture with frequency sweeps ranging from 0.1 Hz to 25 Hz at 3 temperatures: -12, 12, and 36 °C. Table 6.20 lists the test results.

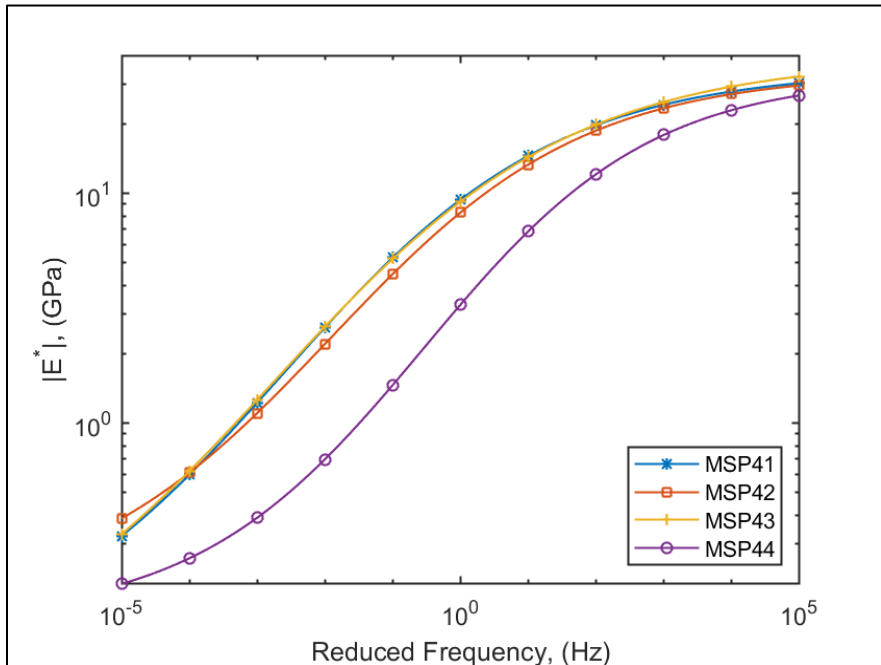
Table 6.20 | E^* | test results

Mix ID	Temperature, °C	AVG of $ E^* $, (GPa)							
		25 Hz	10 Hz	5 Hz	1 Hz	0.5 Hz	0.1 Hz	0.05 Hz	0.01 Hz
SP4-1	-12	26.13	25.35	24.59	22.39	21.36	18.77	17.65	14.92
	12	12.55	10.77	9.60	6.87	5.87	3.83	3.11	1.80
	36	2.71	1.98	1.52	0.83	0.66	0.40	0.33	0.23
SP4-2	-12	28.24	27.11	26.01	23.86	22.80	20.20	19.09	16.27
	12	14.20	12.27	10.99	8.09	6.98	4.64	3.87	2.25
	36	3.22	2.35	1.84	1.05	0.84	0.52	0.43	0.30
SP4-3	-12	29.57	28.21	27.29	24.91	23.83	21.18	19.95	17.20
	12	15.12	13.08	11.71	8.99	7.76	5.45	4.63	2.92
	36	3.63	2.68	2.17	1.26	1.01	0.61	0.50	0.33
SP4-4	-12	22.24	20.74	19.46	16.50	15.23	12.25	10.95	8.15
	12	7.47	6.01	5.00	3.17	2.56	1.48	1.19	0.69
	36	1.15	0.79	0.60	0.36	0.29	0.22	0.19	0.14
MSP4-1	-12	31.37	30.81	29.72	27.19	26.05	23.25	21.92	19.09
	12	15.65	14.32	12.76	9.32	8.17	5.44	4.41	2.60
	36	3.67	2.70	2.08	1.16	0.93	0.58	0.48	0.34
MSP4-2	-12	31.88	29.64	28.13	25.73	24.66	21.74	20.65	17.96
	12	15.44	12.75	11.34	8.21	7.04	4.59	3.77	2.21
	36	3.63	2.61	2.01	1.18	0.96	0.65	0.56	0.44
MSP4-3	-12	34.45	31.97	30.60	27.86	26.55	23.61	22.18	19.12
	12	16.79	14.03	12.37	9.12	8.02	5.28	4.37	2.63
	36	3.52	2.67	2.08	1.20	0.98	0.59	0.49	0.34
MSP4-4	-12	27.33	24.95	23.33	19.67	18.00	14.33	12.60	9.02
	12	8.74	6.78	5.56	3.29	2.59	1.46	1.16	0.72
	36	1.16	0.79	0.64	0.40	0.35	0.28	0.26	0.22
SP5-1	-12	30.83	29.31	28.07	25.17	23.85	20.85	19.15	15.75
	12	14.24	12.16	10.74	7.43	6.20	3.87	3.08	1.76
	36	2.82	1.96	1.52	0.89	0.73	0.50	0.44	0.34
SP5-2	-12	29.49	27.97	27.02	24.78	23.67	20.99	19.87	16.95
	12	14.61	12.34	11.14	8.19	7.01	4.56	3.74	2.15
	36	3.17	2.28	1.73	0.92	0.72	0.44	0.37	0.26
SP5-3	-12	27.15	25.45	24.29	21.79	20.69	18.11	16.91	14.20
	12	11.82	10.18	9.07	6.56	5.63	3.79	3.11	1.92
	36	2.79	2.11	1.68	1.01	0.84	0.55	0.47	0.35

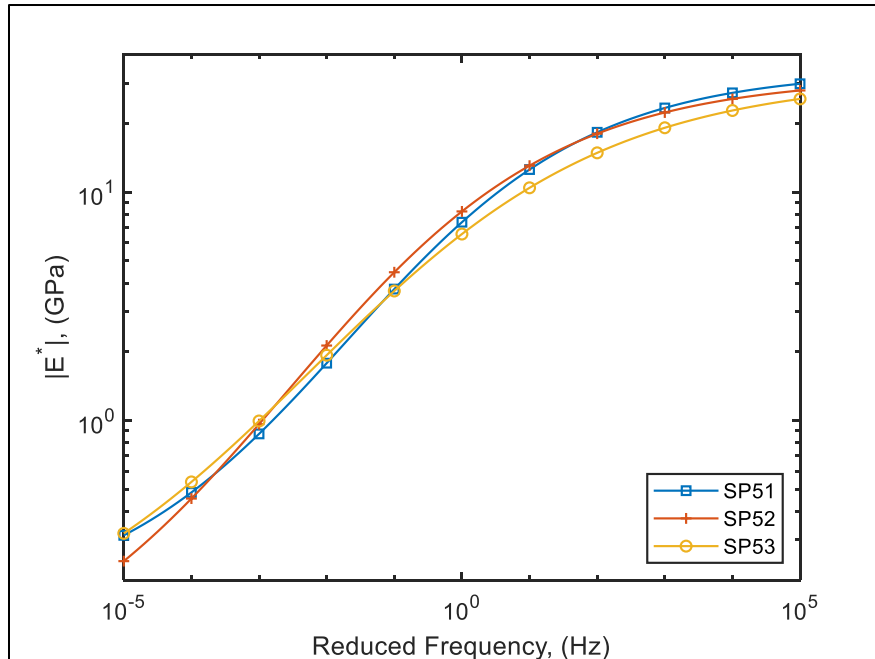
Using AASHTO R62 (2013), $|E^*|$ values were used to construct master curves with a reference temperature chosen to be 12 °C. A summary of the master curves for each of the three mixture groups are found in Figure 6.16.



(a)



(b)



(c)

Figure 6.16 Master curves for each mixture group at the reference temperature of 12°C.

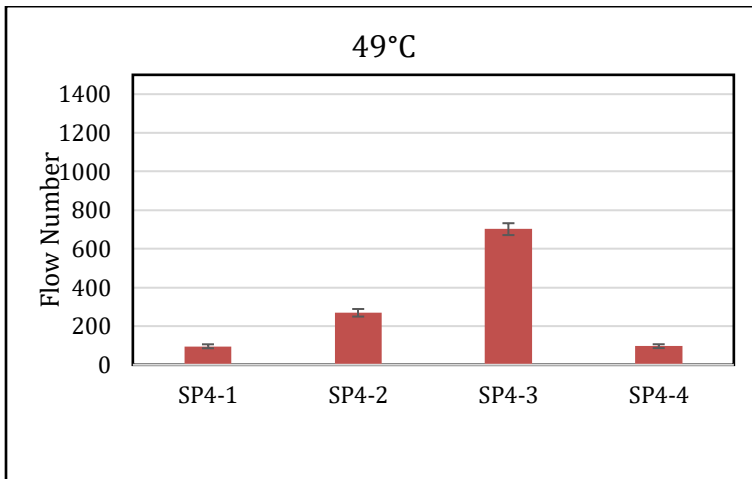
As shown in Figure 6.16(a) and (b), the project 1, 2, and 3 have similar master curves, while the project 4 (SP4-4 and MSP4-4) has significantly lower $|E^*|$ values than the other 3 projects, which indicates that the project 4 may have a good low temperature cracking resistance and a poor rutting resistance. This inference is confirmed by the SCB and FN testing results. As shown in Figure 6.16(c), among the SP5 mixtures, SP5-3 has the most desired stiffness which are higher at low frequency (high temperature) and the lower at high frequency (low temperature). The SCB and FN test results also confirmed that the SP5-3 mixture has better rutting and cracking than the other two SP5 mixtures. Comparison between the three mixture groups SP4, MSP4, and SP5 are detailed in Chapter 6.3.5.

6.3.4 Flow Number Test

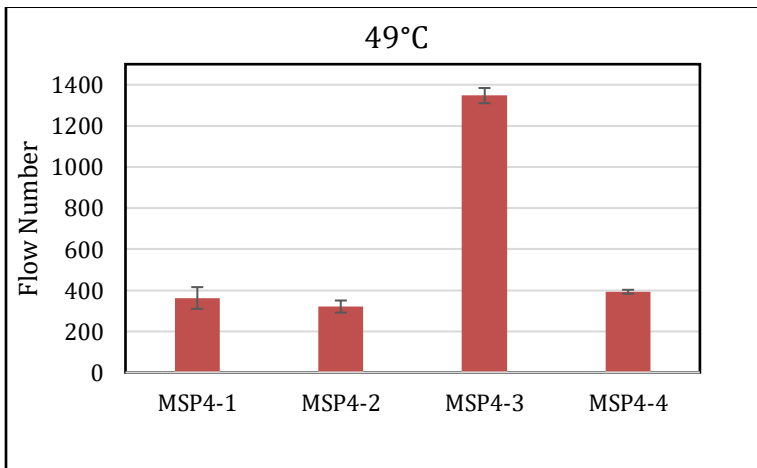
Flow Number (FN) tests were conducted according to AASHTO T378 (2017) to measure the resistance of asphalt mixture to permanent deformation (rutting). All mixtures were tested at 49 °C. The flow numbers for all of the projects are listed in Table 6.21 and plotted in Figure 6.17. In Figure 6.17, the values indicate the mean value of the three replicates that were tested at each temperature, and the error bar indicates the standard error of the mean computed based on three replicates.

Table 6.21 Flow number

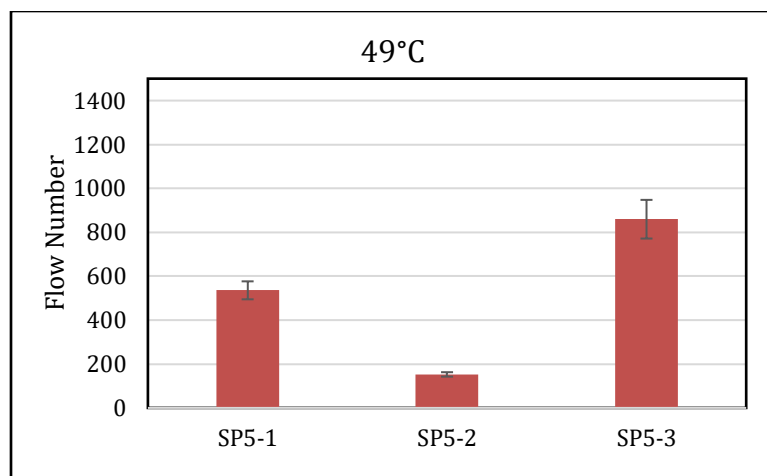
Mix ID	Flow number @ 49 °C		
	Ave.	Std.	COV
SP4-1	95.7	17.6	0.18
SP4-2	269.0	33.9	0.13
SP4-3	701.7	53.1	0.08
SP4-4	96.30	17.0	0.18
MSP4-1	362.0	74.9	0.21
MSP4-2	320.5	41.7	0.13
MSP4-3	1347.0	52.3	0.04
MSP4-4	392.5	13.4	0.03
SP5-1	535.7	70.9	0.13
SP5-2	152.7	17.5	0.11
SP5-3	859.7	152.6	0.18



(a)



(b)



(c)

Figure 6.17 Comparison of the flow numbers of the different mixture groups at 49°C.

As shown in Figure 6.17(a) and (b), the mix designs of project 3 (traffic level 4), both the original mix design (SP4-3) and modified mix designs (MSP4-3), have the highest flow number in the SP4 and MSP4 groups. It is interesting to note that the SP4-4 and MSP4-4, a traffic level 5, have about the same or lower flow number compared to the traffic level 3 mixes (project 1 and 2). As shown in Figure 6.17(c), SP5-3 has the highest flow number among SP5 mixtures, which make sense since SP5-3 is a traffic level 4 mixture while other SP5 mixtures are traffic level 3 mixtures. Except for SP4-4, all mixtures meet the minimum FN requirements: FN>50 for traffic level 4 and FN>190 for traffic level 5. (AASHTO T378, 2017). Comparison between the three mixture groups SP4, MSP4, and SP5 are detailed in the following sections.

6.3.5 Comparison between SP4 and MSP4

The performance test results for SP4 and MSP4 groups are compared in this section to validate the MSP4 mix designs. The MSP4 group uses the same aggregate and binder as the SP4 group. MSP4 changed aggregate gradation of SP4 to make it more compactable. The detailed mix design processes have been described in Chapter 6.2.

6.3.5.1 SCB Results

The fracture energy and toughness results of the SP4 and MSP4 mixtures are compared in Figure 6.18 and Figure 6.19. The height of each bar represents the mean value of three replicates, and the error bar indicates the standard error of the mean.

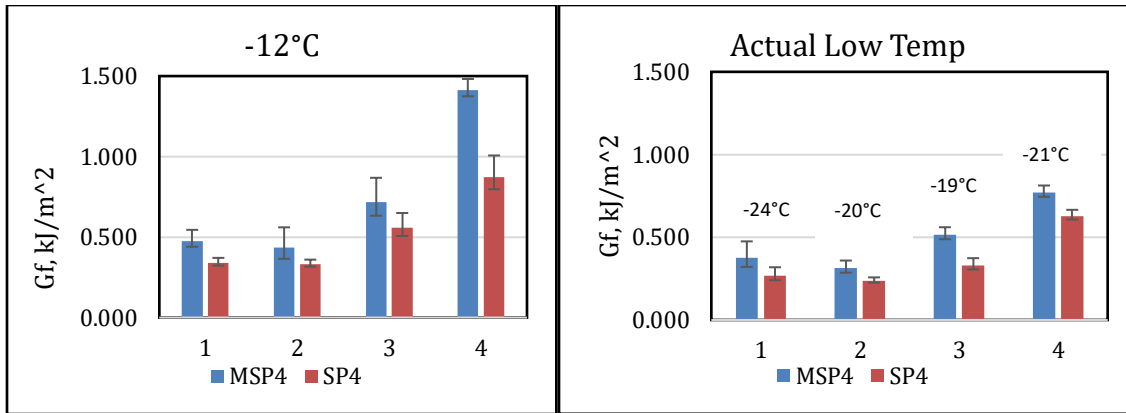


Figure 6.18 Comparison of fracture energy between SP4 and MSP4 at -12°C and the lowest temperature.

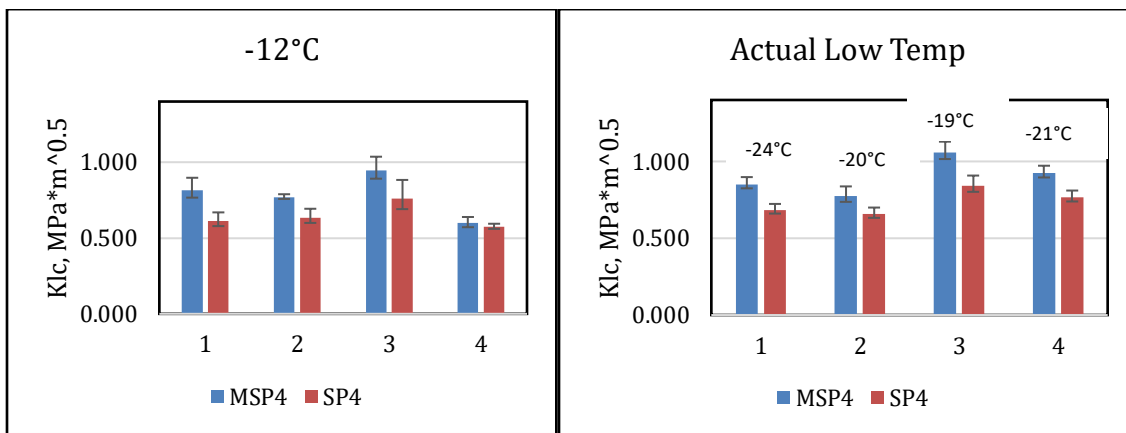


Figure 6.19 Comparison of fracture toughness between SP4 and MSP4 at -12°C and the lowest temperature.

It can be seen that MSP4 mixtures have higher values of fracture energy and fracture toughness for each project at each testing temperature compared to the traditional mixtures in the SP4 group. This result validates that every MSP4 mixture has better low temperature cracking resistance than the corresponding SP4 mixture.

6.3.5.2 | E* | Results

The E* results for SP4 and MSP4 mixtures are shown in Figure 6.20.

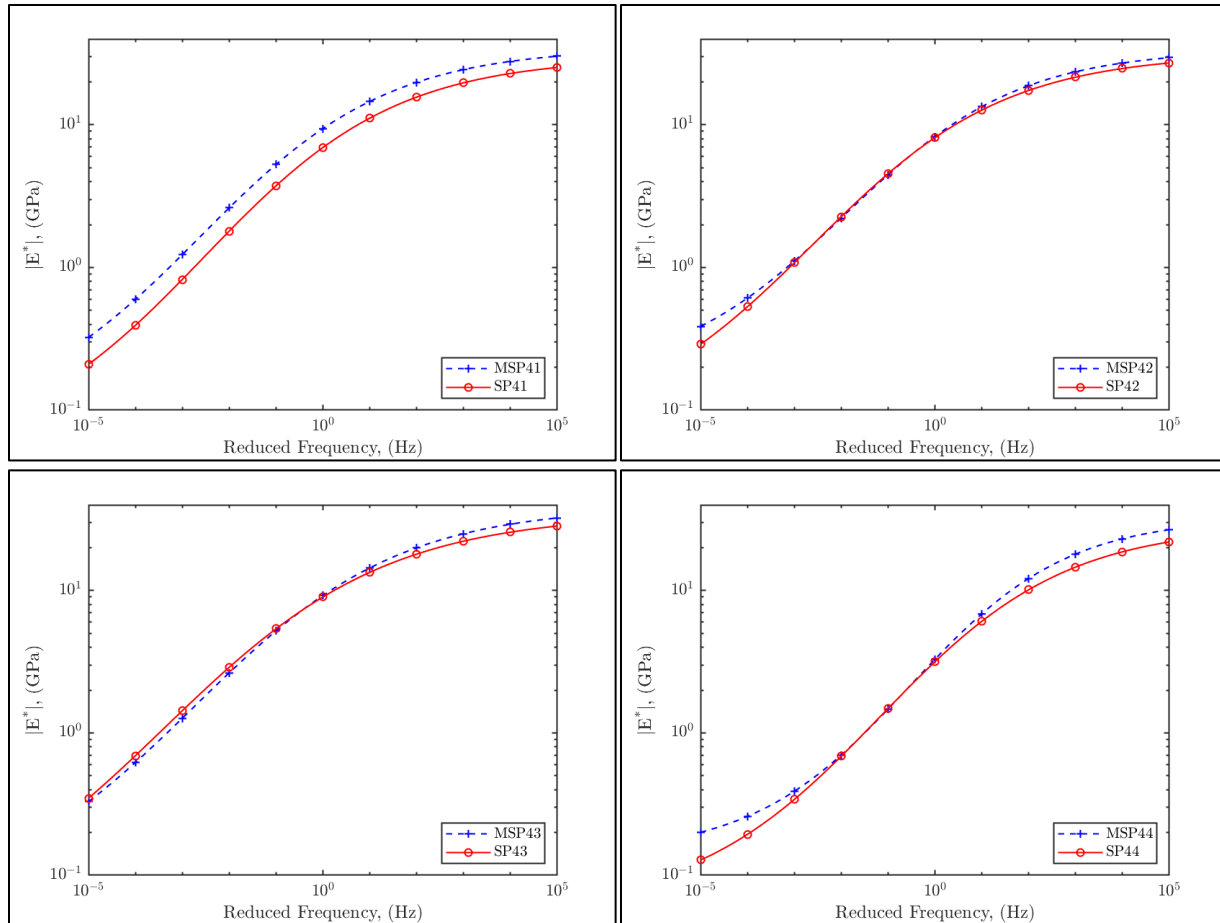


Figure 6.20 Comparison of $|E^*|$ values between SP4 and MSP4 groups. 12°C was the reference temperature that was chosen.

It can be observed that, in general, the MSP4 mixtures have slightly higher stiffness values than the corresponding traditional SP4 mixtures.

6.3.5.3 Flow Number Results

The comparison of flow number results for SP4 and MSP4 mixtures are shown in Figure 6.21. The flow number values represent the mean value of the three replicates, and the error bar indicates the standard error of the mean.

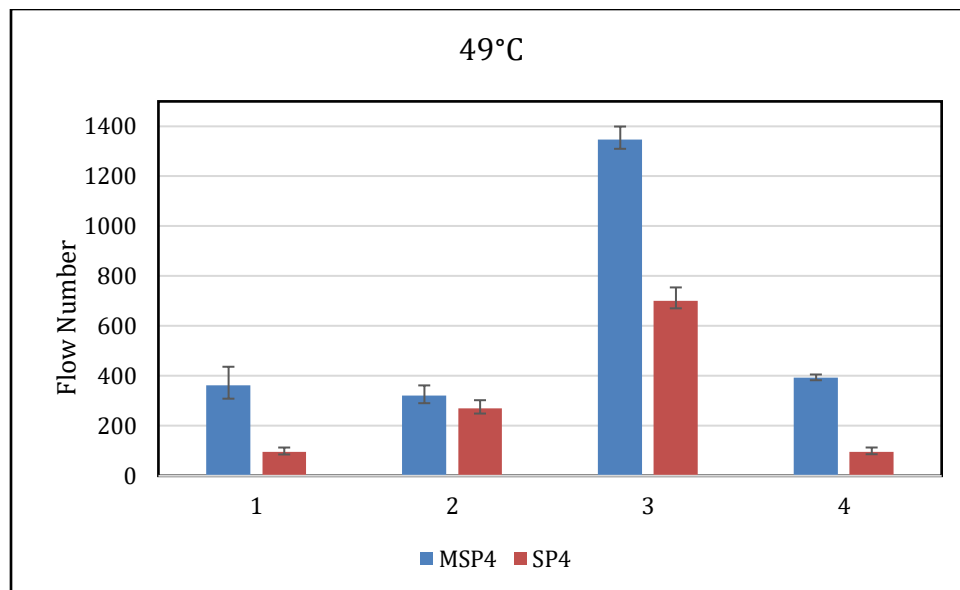


Figure 6.21 Comparison of flow numbers between SP4 and MSP4 group at 49°C.

It can be seen that each MSP4 mixture has a higher flow number than the corresponding SP4 mixture. The higher flow numbers indicate a higher rutting resistance of the mixture.

In conclusion, all the modified mix designs (MSP4) have improved rutting and low temperature cracking resistance than the original mix designs (SP4). Therefore, the MSP4 mix designs are validated.

6.3.6 Comparison between MSP4 and SP5

The performance test results of Superpave 5 mixtures designed by University of Minnesota (denoted by MSP4 mixture) are compared with that of the Superpave 5 mixtures designed by contractors (denoted by SP5).

Only the first three MSP4 projects were used. The first three MSP4 projects have project levels of 3, 3, and 4, respectively, and the three SP5 projects had traffic levels of 3, 3, and 4, respectively. Since each group has the same traffic level for their respective project, a general comparison can be made. However, different aggregate sources and binders were used in each group, so a one-to-one comparison cannot be made.

6.3.6.1 SCB Results

All mixtures were tested at -12°C. The second test temperature, that represents the lowest test temperature, were -24, -20, -19, and -21°C, for MSP4-1, MSP4-2, MSP4-3, and MSP4-4, respectively, and -19, -21, and -24 °C for SP5-1, SP5-2, and SP5-3, respectively.

The fracture energy values, shown in Figure 6.22 and Figure 6.23, represent the mean value of the three replicates that were tested at each temperature, and the error bar indicates the standard error of the mean computed based on three replicates.

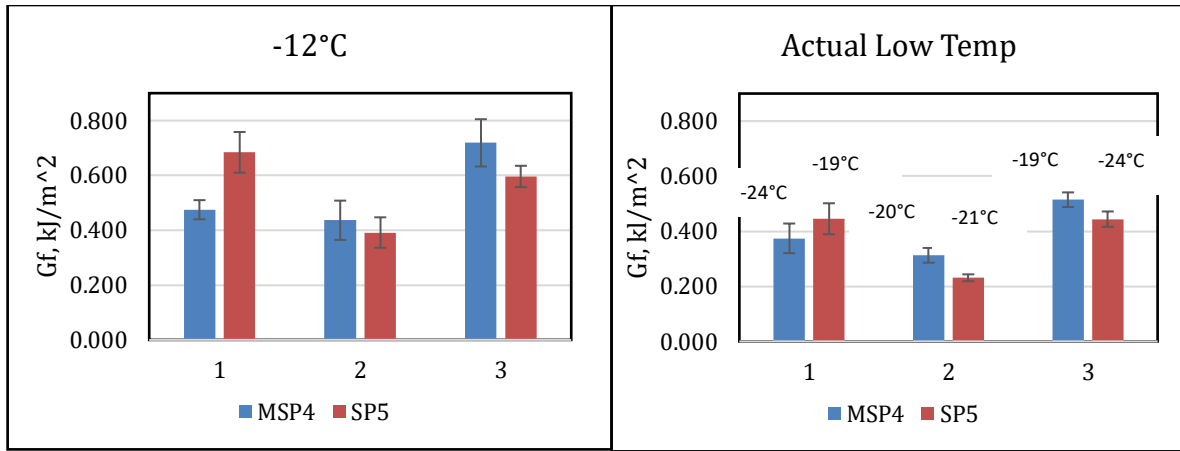


Figure 6.22 Comparison of fracture energy between MSP4 and SP5 at -12°C and the lowest temperature.

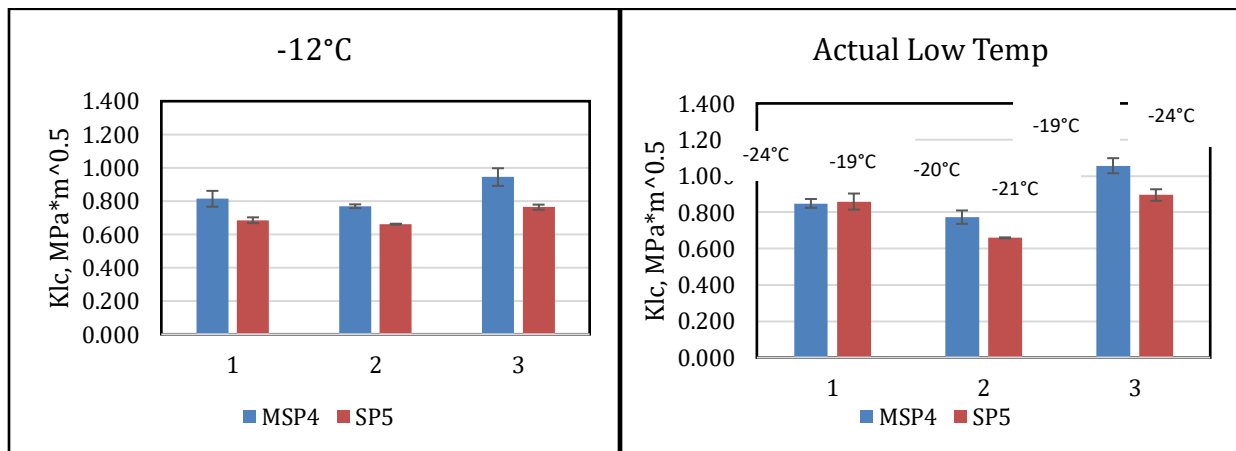


Figure 6.23 Comparison of fracture toughness between MSP4 and SP5 at -12°C and the lowest temperature.

MSP4 has higher values for fracture energy and fracture toughness for projects 2 and 3 for both temperatures compared to SP5. For project 1, SP5 had higher values for fracture energy at -12°C and the actual low temperature and for fracture toughness at the actual low temperature. Overall, the cracking resistance of MSP4 is very similar to that of SP5.

6.3.6.2 |E*| Results

The comparison of E* results for groups SP4 and MSP4 are shown in Figure 6.24.

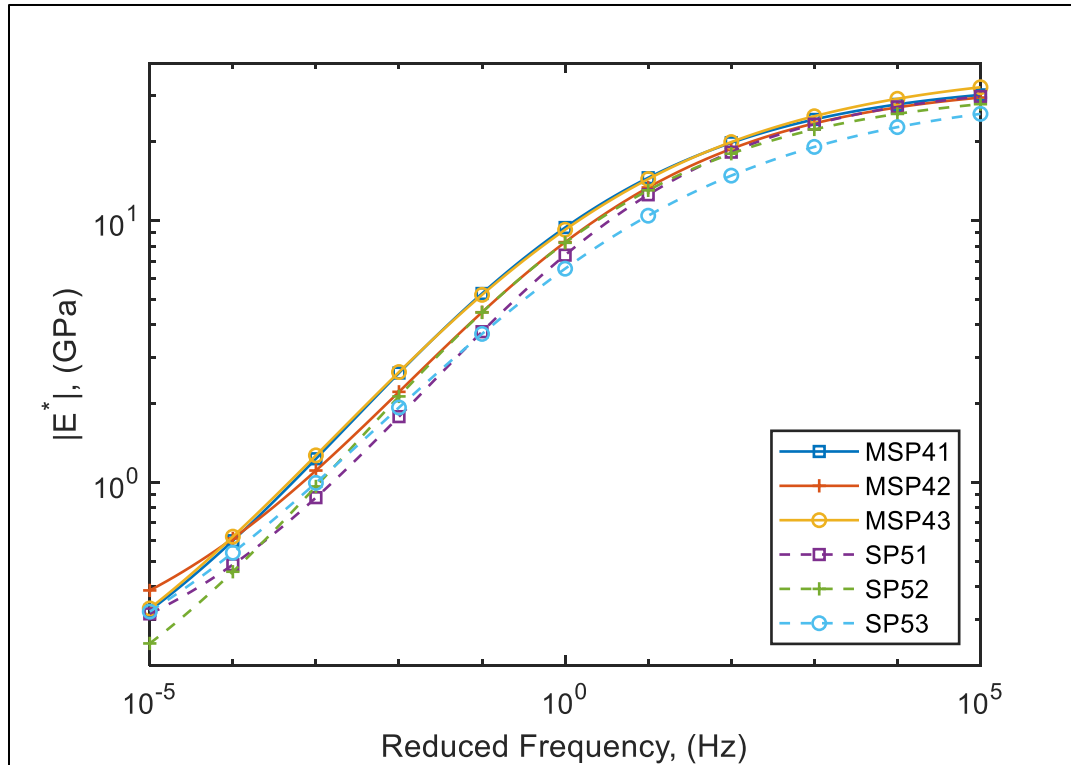


Figure 6.24 Comparison of $|E^*|$ values between MSP4 and SP5 groups. 12°C was the reference temperature that was chosen.

Since MSP4 and SP5 are composed of different aggregates and binder, a one-to-one comparison between the $|E^*|$ values of the two groups cannot be made. Although MSP4 and SP5 are made from different materials, the results of the MSP4 projects are similar to the SP5 projects. In general, the MSP4 group mixtures have slightly higher stiffness values compared to the SP5 mixtures.

6.3.6.3 Flow Number Results

The comparison of flow number results for groups MSP4 and SP5 are shown in Figure 6.25. The flow number values represent the mean value of the three replicates that were tested at each temperature, and the error bar indicates the standard error of the mean computed based on three replicates.

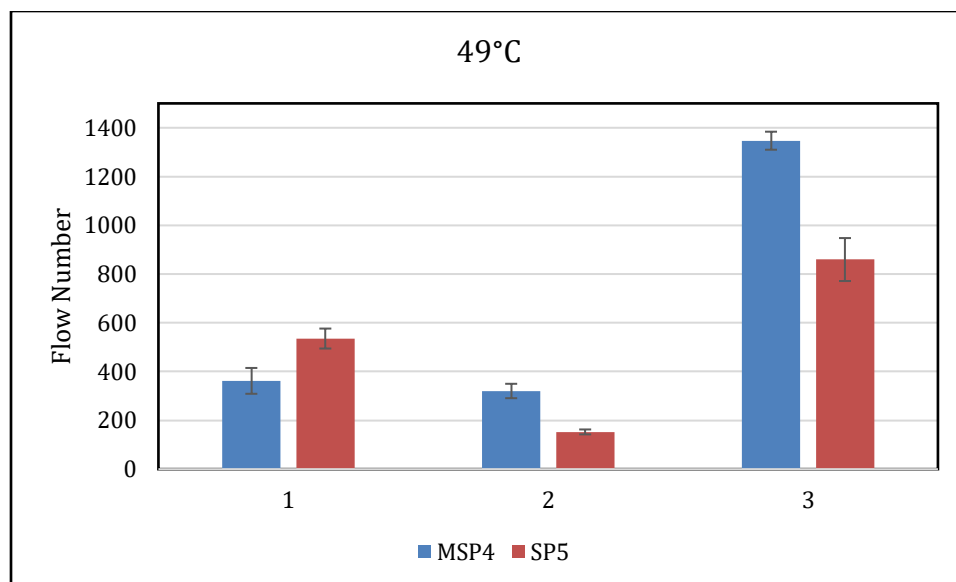


Figure 6.25 Comparison of flow numbers between the MSP4 and SP5 groups at 49°C.

MSP4 had higher flow number values for projects 2 and 3 while SP5 had a higher flow number for project 1.

In conclusion, there is no systematic difference between the MSP4 and SP5 mixtures.

6.3.7 Comparison between SP4 and SP5

The performance test results for SP4 and SP5 are compared in this section. Since SP4 and SP5 projects use different materials, one to one comparison is not possible. Instead, a general comparison is made between the two groups.

Only the first three projects of SP4 were compared to SP5 because there was only three SP5 projects that were tested. The first three SP4 projects have project levels of 3, 3, and 4, respectively, and the three SP5 projects had traffic levels of 3, 3, and 4, respectively. Since each group has the same traffic level for their respective project, a general comparison is made. Different aggregate sources and binders were used in each group, so an equal comparison cannot be made.

6.3.7.1 SCB Results

All mixtures were tested at -12°C. The second test temperature, that represents the lowest test temperature, were -24, -20, -19, and -21°C, for SP4-1, SP4-2, SP4-3, and SP4-4, respectively, and -19, -21, and -24 °C for SP5-1, SP5-2, and SP5-3, respectively.

The fracture energy and toughness values, shown in Figure 6.26 and Figure 6.27, represent the mean value of the three replicates that were tested at each temperature, and the error bar indicates the standard error of the mean computed based on three replicates.

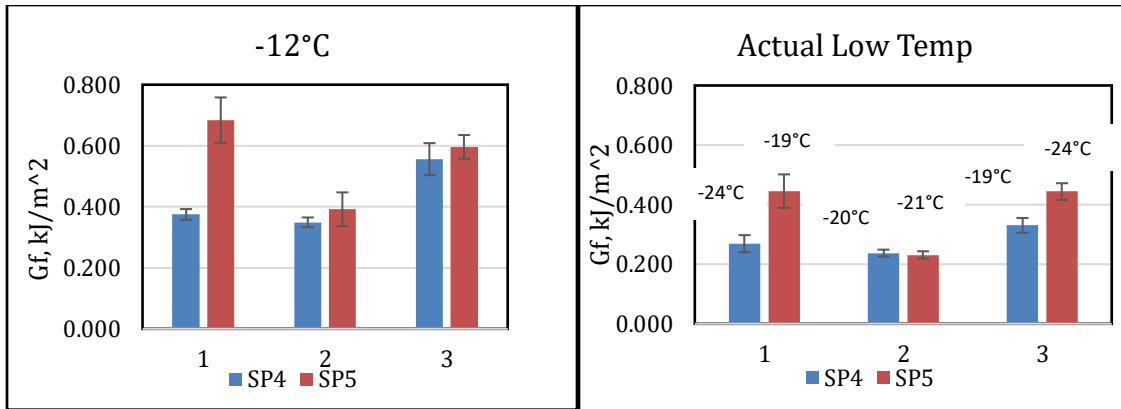


Figure 6.26 Comparison of fracture energy between SP4 and SP5 at -12°C and the lowest temperature.

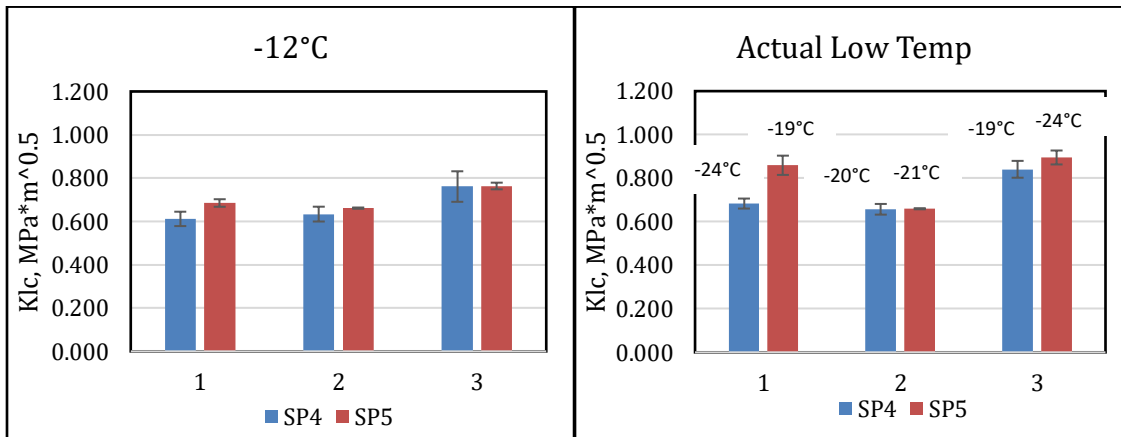


Figure 6.27 Comparison of fracture toughness between SP4 and SP5 at -12°C and the lowest temperature.

SP5 has higher values for the fracture energy and fracture toughness for every project, except for the fracture energy of project 2 at the lowest temperature.

6.3.7.2 |E*| Results

The comparison of E* results for groups SP4 and SP5 are shown in Figure 6.28.

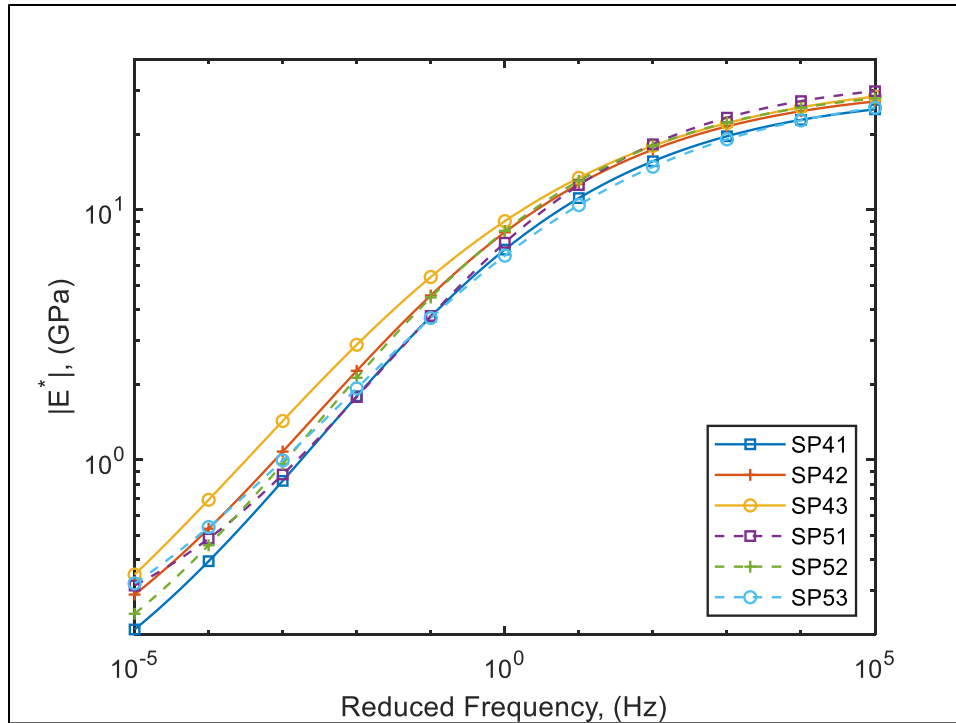


Figure 6.28 Comparison of $|E^*|$ values between SP4 and SP5 groups. 12°C was the reference temperature that was chosen.

Since SP4 and SP5 are composed of different aggregates and binder, a one-to-one comparison between the $|E^*|$ values of the two groups cannot be made. Although SP4 and SP5 are made from different materials, the $|E^*|$ results for SP4 and SP5 are very similar. In general, SP4 and SP5 have approximately the same stiffness at all frequencies.

6.3.7.3 Flow Number Results

The comparison of flow number results for groups SP4 and SP5 are shown in Figure 6.29. The flow number values represent the mean value of the three replicates that were tested at each temperature, and the error bar indicates the standard error of the mean computed based on three replicates.

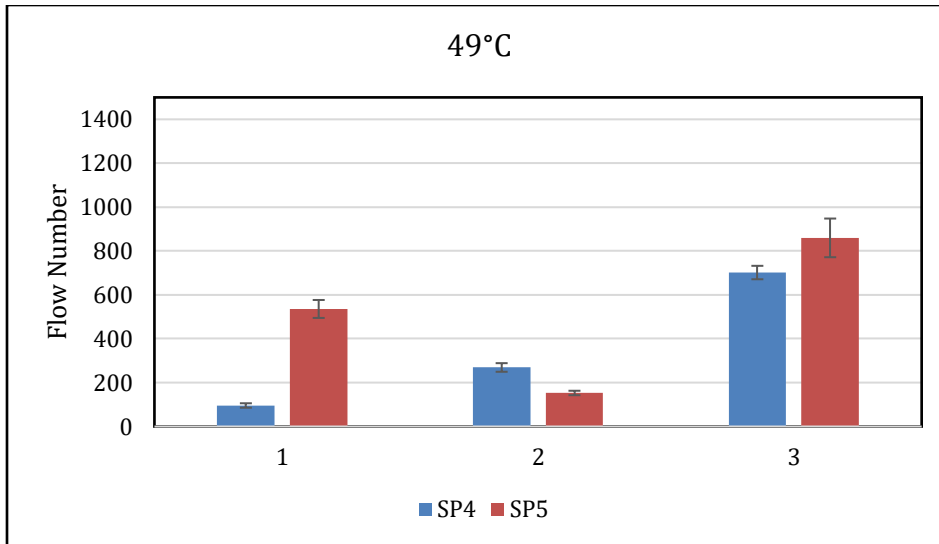


Figure 6.29 Comparison of flow numbers between the MSP4 and SP5 groups at 49°C.

SP5 had higher flow numbers for projects 1 and 3 while SP4 had a higher flow number for project 2.

In conclusion, except for the low rutting resistance of SP5-2, the SP5 group overall has better low temperature cracking and rutting resistance than the SP4 group.

6.4 PERFORMANCE TESTS AT OMRR

IDEAL CT, Hamburg Wheel Tracking Test, and Disc-shaped compact tension test (DCT) were performed at the Office of Materials and Road Research (OMRR) to check the laboratory performance of the original (SP4) and modified (MSP4) mixtures.

6.4.1 IDEAL-CT

The IDEAL-CT tests were performed at 25°C. For each mixture, 4 to 7 replicates were tested. Figure 6.30 shows the test result of displacement vs stability curve of SP41. From the displacement vs. stability curve, CT index and fracture energy can be calculated. The results for all mixtures are listed in Table 6.22. The comparison between SP4 and MSP4 mixtures were made in Figure 6.31 and Figure 6.32 for fracture energy and CT-index, respectively. The error bars in the figures represents the standard error of the mean values.

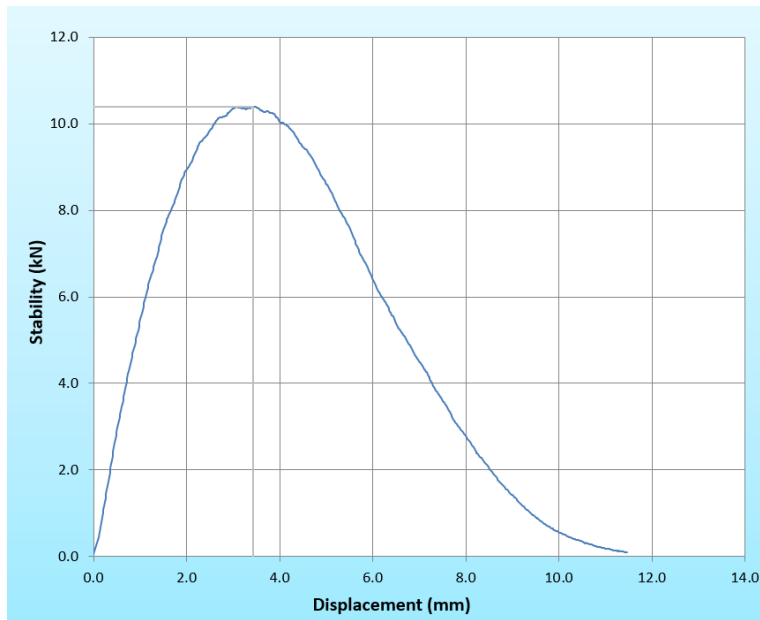


Figure 6.30 Displacement vs. stability results of a replicate of SP41.

Table 6.22 IDEAL- CT results

Mixture	Indices	Replicates						Ave.	Std. error		
MSP41	CT index	24.3	17.3	23.3	24.6	12.4		20.4	2.4		
	Gf (J/m ²)	9130.9	7934.4	8852.0	8830.6	7372.1		8424.0	331.2		
SP41	CT index	106.7	88.2	114.5	103.8	92.2	101.4	105.2	101.7	3.4	
	Gf (J/m ²)	6418.4	6314.8	6532.7	6240.3	6527.9	6206.6	4148.3	6055.6	321.6	
MSP42	CT index	81.6	102.5	92.6	137.5	94.5			101.7	9.5	
	Gf (J/m ²)	7766.0	9017.6	8612.2	8681.8	8671.6			8549.8	208.5	
SP42	CT index	76.9	64.8	65.7	84.9	96.8	75.4		77.4	4.9	
	Gf (J/m ²)	6749.6	7106.1	7398.0	6932.9	7305.9	7331.9		7137.4	104.5	
MSP43	CT index	67.9	41.6	51.5	44.5	44.8			50.1	4.7	
	Gf (J/m ²)	9782.1	8312.0	9720.4	9691.2	9445.2			9390.2	275.6	
SP43	CT index	48.4	56.9	55.2	108.8	112.6	74.9		76.1	11.5	
	Gf (J/m ²)	7955.5	8360.3	8466.4	8254.2	9189.8	8212.0		8406.4	171.6	
MSP44	CT index	183.6	143.3	128.8	111.6				141.8	15.4	
	Gf (J/m ²)	6170.4	6104.9	6661.5	6268.3				6301.3	124.7	
SP44	CT index	73.9	66.8	69.6	66.0	59.3	67.7	79.0	59.3	67.7	2.4
	Gf (J/m ²)	5723.4	5801.0	5798.5	5944.8	6114.7	5957.8	6385.7	5852.2	5947.3	76.0

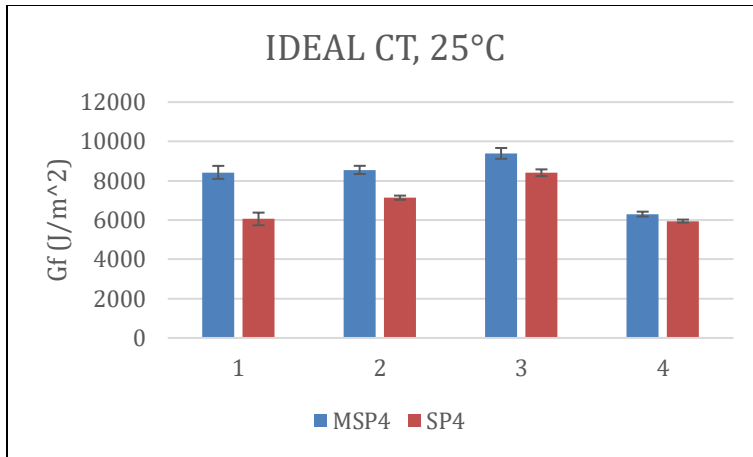


Figure 6.31 Comparison of fracture energy of SP4 and MSP4 mixtures.

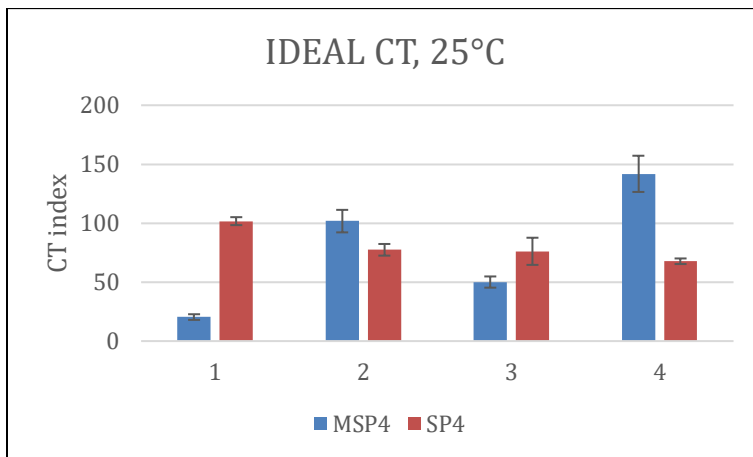


Figure 6.32 Comparison of CT-index of SP4 and MSP4 mixtures.

As shown in Figure 6.31, all the modified (MSP4) mixtures have improved intermedium-temperature (25°C) fracture energies compared to the original (SP4) mixtures, which is consistent with the fracture energy results at lower temperatures tested by SCB, as discussed in Section 5.3.2. However, the CT index results in Figure 6.32 show that, MSP41 and MSP43 have lower CT index values than the corresponding original mixtures, indicating that the MSP41 and MSP43 may have lower intermedium temperature cracking resistance than the corresponding original mixtures. The discrepancy between the fracture energy and CT index results is due to the fact that the CT index considers not only the fracture energy but also the post-peak slope and strain.

6.4.2 Hamburg Wheel Tracking Test

The Hamburg wheel tracking test were performed at 50°C. For each mixture 2 replicates were performed. Figure 6.30 shows the results of the two replicates of the mixture SP41. As shown, the stripping inflection point (SIP) were calculated from the rut depth vs. number of passes plot. The results for all mixtures are summarized in Table 6.23.

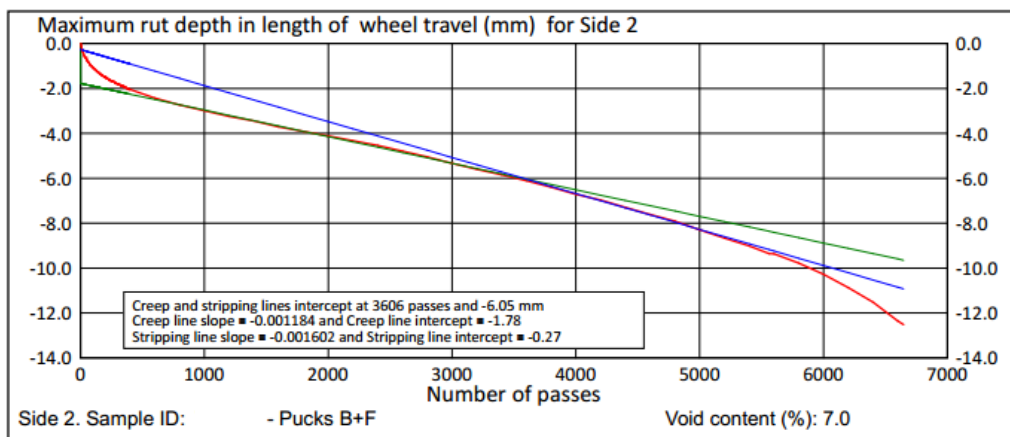
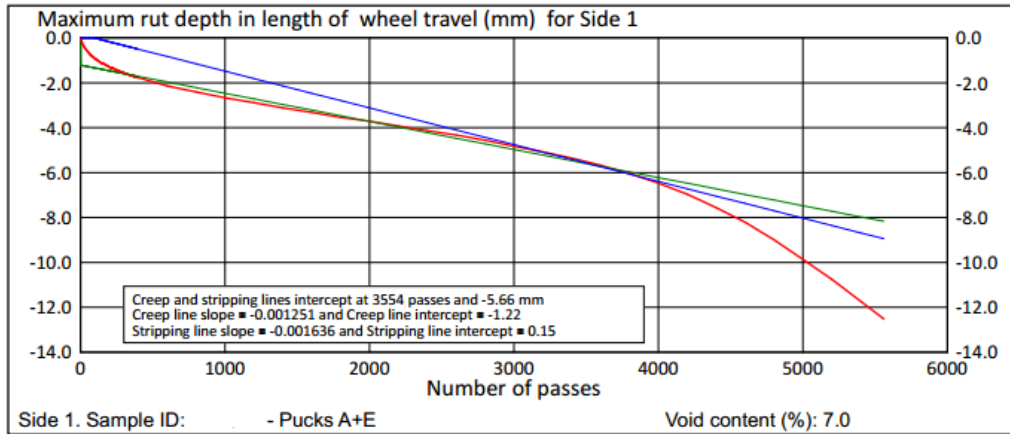


Figure 6.33 Hamburg wheel tracking test results of SP41.

Table 6.23 Hamburg wheel tracking test results

Mixture	Replicate	rut depth at number of passes				SIP	Ave. SIP
		5000	10000	15000	20000		
MSP41	#1	1.12	1.39	1.6	1.74	NA	NA
	#2	0.96	1.22	1.41	1.63	NA	
SP41	#1	9.86	NA	NA	NA	3554	3580
	#2	8.29	NA	NA	NA	3606	
MSP42	#1	2.4	3.92	7.79	NA	10229	11299.5
	#2	2.57	3.54	5.63	11.43	12370	
SP42	#1	2.990	5.1	9.5	NA	9713	10586
	#2	2.61	3.81	7.46	NA	11459	
MSP43	#1	1.27	1.57	1.74	1.9	NA	NA
	#2	0.91	1.08	1.2	1.29	NA	
SP43	#1	2.25	2.8	3.19	3.54	NA	NA
	#2	1.98	2.53	2.9	3.13	NA	

MSP44	#1	2.64	7.91	NA	NA	6068	4916
	#2	4.17	11.28	NA	NA	3764	
SP44	#1	2.66	4.17	8.38	NA	10413	11716.5
	#2	2.48	3.54	5.84	10.46	13020	

Note: NA for SIP means the SIP was not detected within the 20000 loading cycles, which indicating a good rutting resistance.

It is seen from Table 6.23 that, except for the MSP44, all modified mixtures have improved rutting resistance compared to the corresponding original mixtures. The lower rutting resistance of MSP44 compared to SP44 might be because the excessive low air-void ratio (about 2%) of MSP44, as discussed in Chapter 6.2.4.

It is important to note that the Hamburg wheel tracking test results of MSP44 and SP44 are inconsistent with their Flow Number test results as shown in Chapter 6.3.4, where MSP44 was shown having a higher flow number than SP44. These results indicate that the two rutting test method are not equivalent. Hamburg wheel tracking test is general considered as superior to the flow number test, since its loading condition is closer to the realistic traffic loading condition in the field. The discrepancy between Hamburg wheel tracking test and Flow Number test might be due to the uniaxial loading condition of the Flow Number test, which is incapable to capture, for example, the shear stress introduced near the edge of the wheel.

6.4.3 Disc-shaped Compact Tension Test

Due to the lack of raw material, the DCT tests were only performed on the project 4, i.e., on MSP44 and SP44. DCT tests were performed at -21 °C. The fracture energy results were shown in Figure 6.34. It is seen that the modified mixture MSP44 has higher fracture energy (low-temperature cracking-resistance) than the original mixture SP44. The results are consistent with the SCB test results discussed in Section. 5.3.2

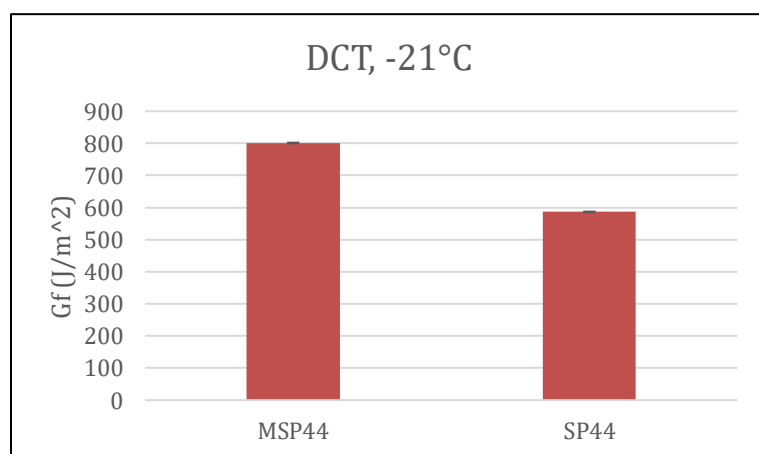


Figure 6.34 DCT fracture energy of MSP44 and SP44 mixtures.

6.5 CONSISTENCE OF SAMPLE PREPARATION BETWEEN THE TWO LABORATORIES

To check the consistency between the two laboratories, the SP44 mixture was selected as the duplicated mixture. Additional samples of this mixture were prepared by each laboratory and tested by the other laboratory. If the test results at the two laboratories are consistent, then we can conclude that the two laboratories are consistent in terms of sample preparation.

6.5.1 UMN Test OMRR Samples

Additional gyratory samples were prepared for SP44 at OMRR laboratory. The additional samples were then sent to and tested by UMN laboratory. Diametral E^* , Flow number, and low temperature SCB tests were conducted. The test results of OMRR and UMN samples were compared.

As shown in Figure 6.35, the OMRR samples has slightly higher stiffness at the low frequency than the UMN samples, but in general, the master curves of UMN and OMRR samples of SP44 are very close, indicating the consistence between UMN and OMRR samples.

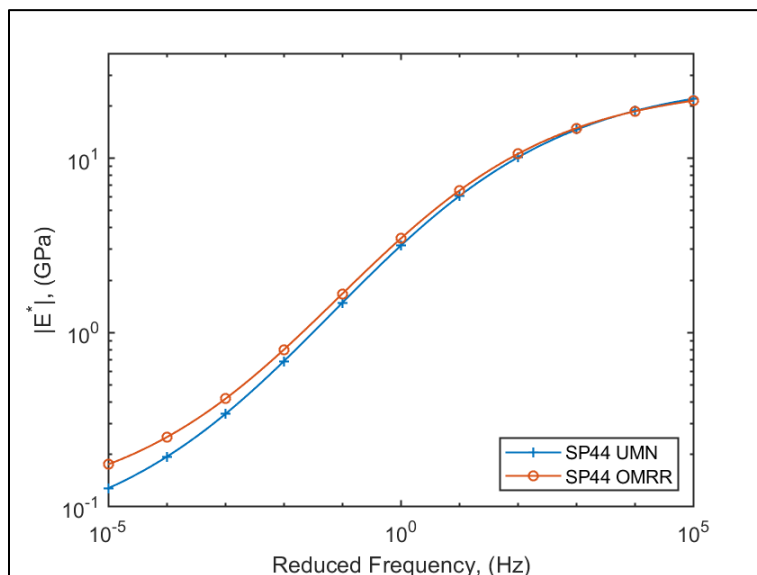


Figure 6.35 Comparison of E^* master curves of UMN and OMRR samples of SP44.

Figure 6.36 shows the flow number results of the OMRR and UMN prepared samples. It is seen that, the OMRR samples have lower flow number than the UMN samples. However, in general, the flow numbers of OMRR and UMN samples are in the same order of magnitude.

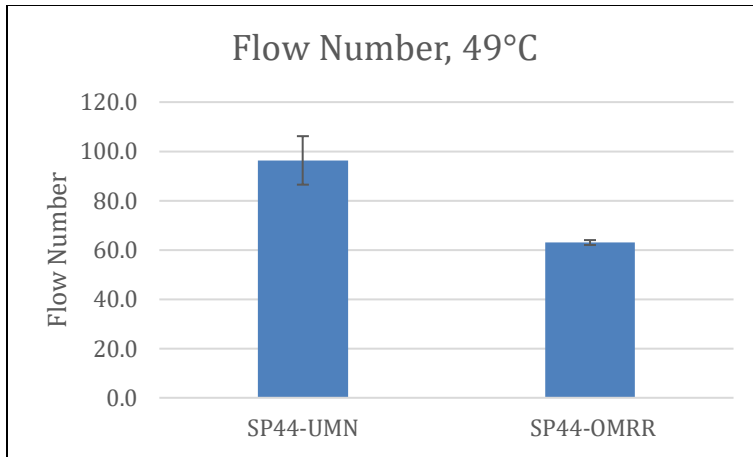


Figure 6.36 Comparison of flow numbers of UMN and OMRR samples of SP44.

Figure 6.37 compares the SCB fracture energy (Gf) and fracture toughness (K_{Ic}) results of the UMN and OMRR samples. It is seen that the both the Gf and K_{Ic} are similar for the OMRR and UMN samples at the two testing temperatures.

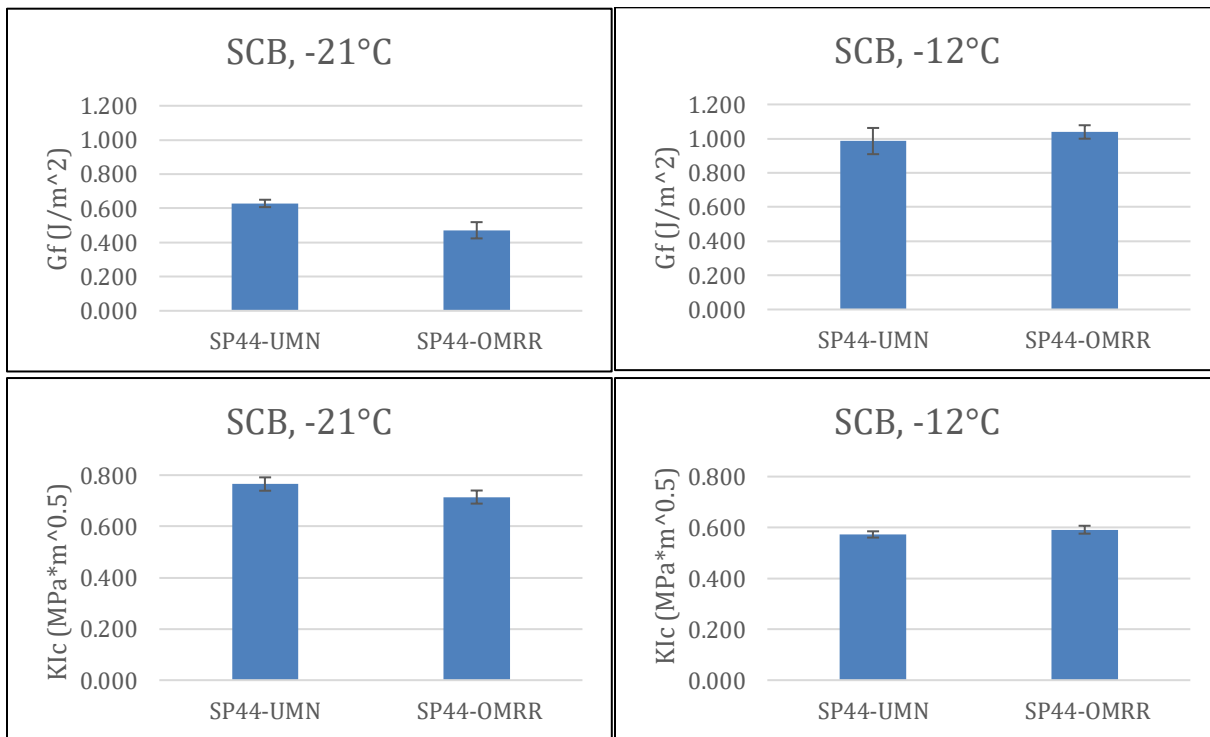


Figure 6.37 Comparison of the SCB Gf and K_{Ic} of UMN and OMRR samples of SP44.

In conclusion, the diametral E*, flow number, and SCB tests at UMN showed the consistence between the samples prepared by the two laboratories.

6.5.2 OMRR Test UMN Samples

Additional gyratory samples of SP44 were also prepared by UMN laboratory and were sent to OMRR laboratory to perform the IDEAL-CT, DCT and Hamburg Wheel Tracking Test. The test results of OMRR and UMN samples were compared to check the consistence of the samples preparation between the two laboratories.

Figure 6.14 shows the IDEAL CT test results. It is seen that the CT index results are in the same order of magnitude for the OMRR and UMN samples, with the values for OMRR slightly higher than that of the UMN samples.

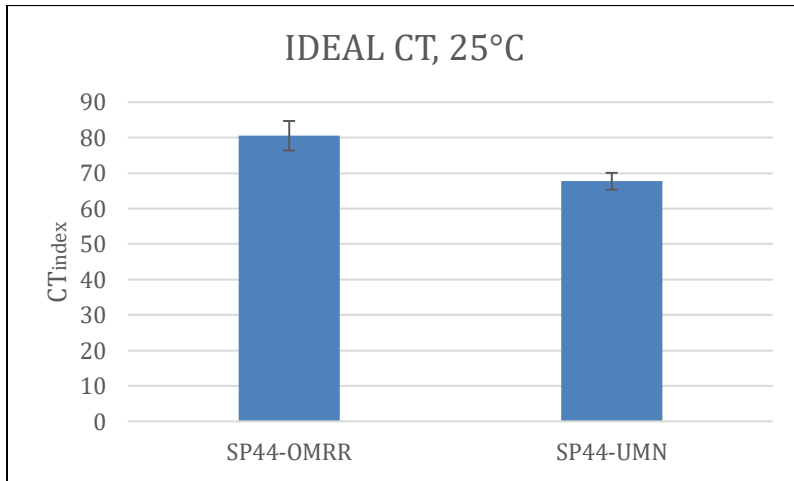


Figure 6.38 Comparison of the CT_{index} of UMN and OMRR samples of SP44.

Figure 6.39 compares the DCT test results. It is seen that the fracture energy, G_f , are consistent for the OMRR and UMN samples.

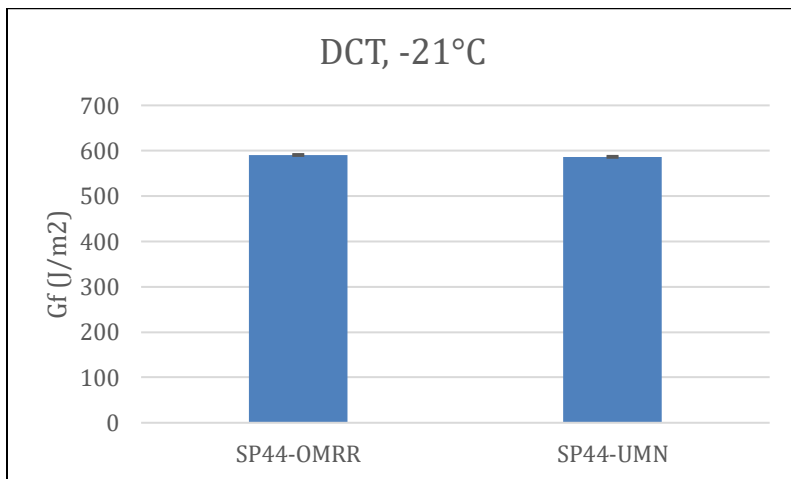


Figure 6.39 Comparison of the DCT G_f of UMN and OMRR samples of SP44.

The results of Hamburg wheel track tests are shown in Figure 6.40 and Figure 6.41, respectively, for the OMRR and UMN samples. The stripping inflection point (SIP) for the two OMRR samples are 6753 and 12196 respectively. The SIP values for the two UMN samples are 10413 and 13020 respectively. It is seen that SIP are in the same order of magnitude for the OMRR and UMN samples. As shown in Figure 6.40 and Figure 6.41, the development of rutting depth is also similar between the OMRR and UMN samples.

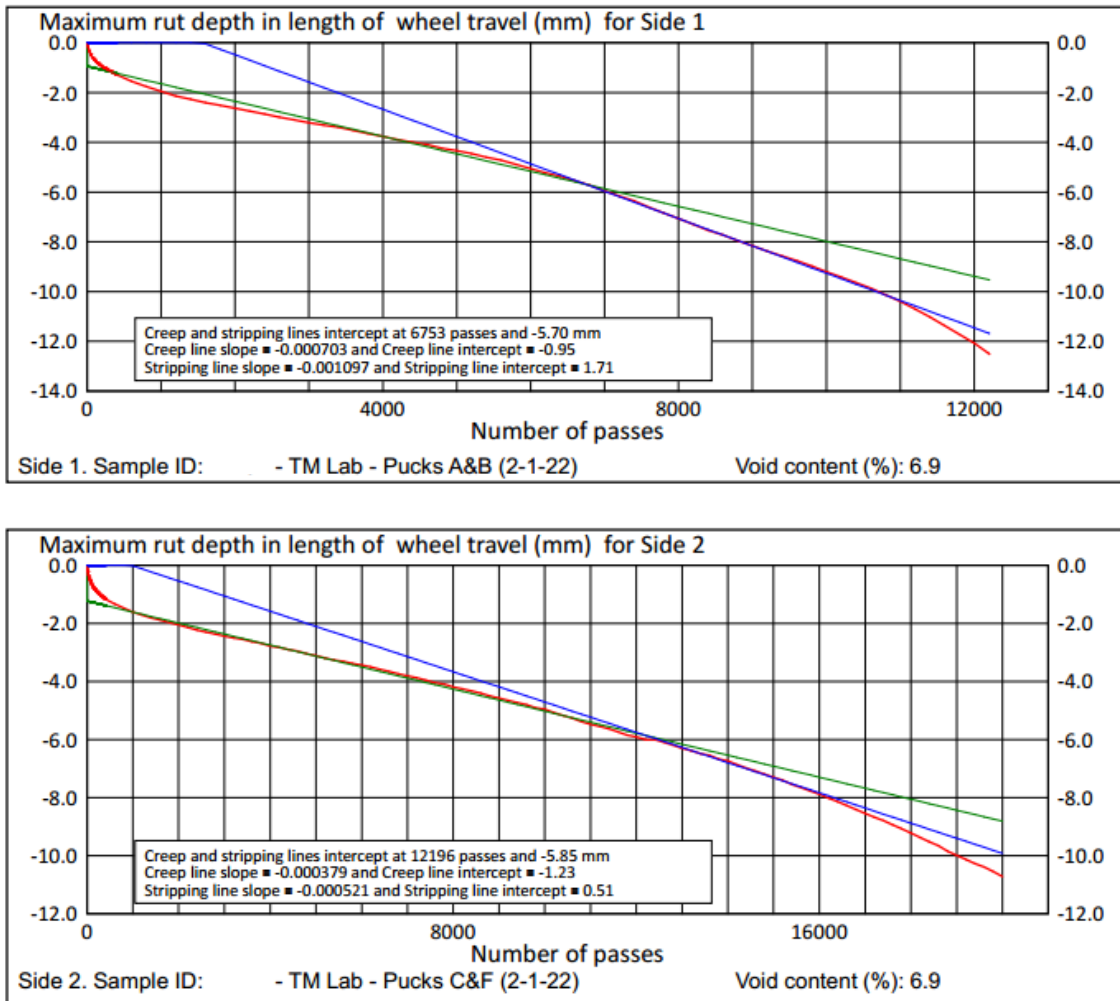


Figure 6.40 Hamburg wheel track test results of the OMRR samples of SP44.

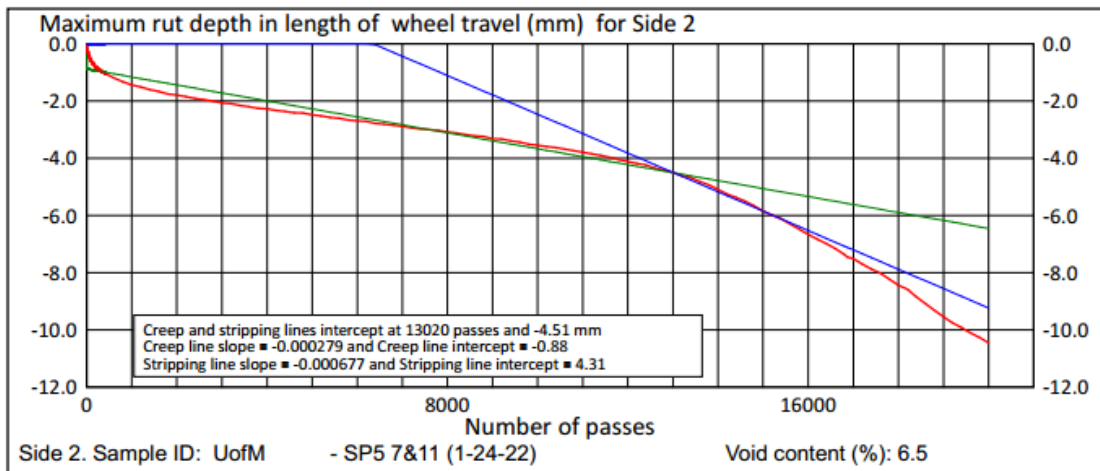
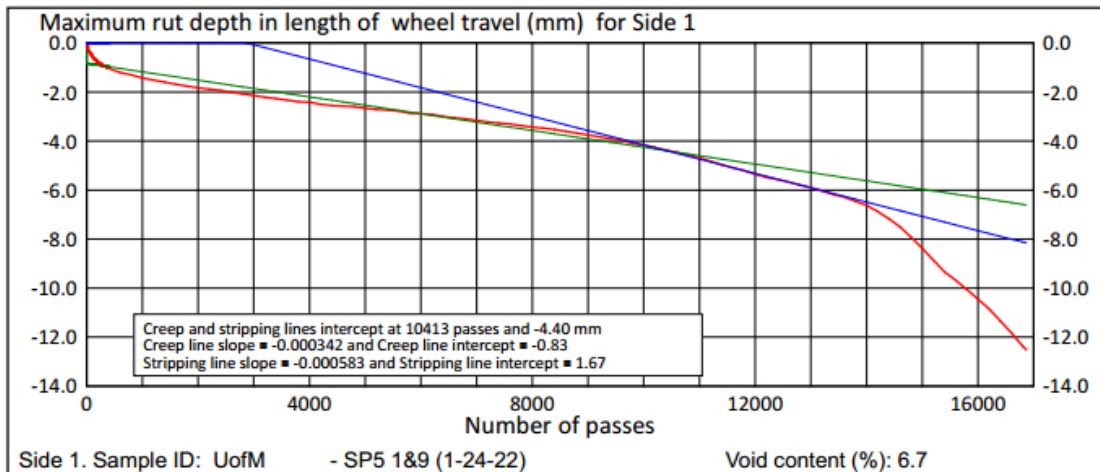


Figure 6.41 Hamburg wheel track test results of the UMN samples of SP44.

In conclusion, the IDEAL-CT, DCT and Hamburg Wheel Tracking Test results at the OMRR laboratory showed the consistence between the samples of the two laboratories.

6.6 CONCLUSIONS

Four traditional Superpave 4 (SP4) asphalt mixtures were modified to Superpave 5 mixtures (MSP4) by changing their aggregate gradations while not increasing their binder contents. Performance tests were conducted by UMN and OMRR on the SP4 and MSP4 mixtures to check the Superpave 5 mix designs. For comparison purposes, asphalt mixtures from three Superpave 5 (SP5) mixtures already used in construction projects in Minnesota, were also included in the investigation. The main conclusions of this task are summarized as follows:

1. Aggregate gradation has a strong effect on the compactability of asphalt mixture. For the four projects studied, it is possible to improve the compactability (reduce the air voids) of a

- Superpave 4 mixture to satisfy the design requirement of Superpave 5 by adjusting the aggregate gradation and without increasing the binder content.
2. Compared to the original mix designs, the developed Superpave 5 (MSP4) mix designs have gradation curves closer to the maximum density line, and have CA ratios closer to the Bailey method recommended range.
 3. The laboratory testing results at UMN (Flow number, SCB, and diametral E*) indicate that the MSP4 mixtures have higher stiffness and rutting and low-temperature cracking resistance than the original SP4 mixtures.
 4. The laboratory testing results at UMN (Flow number, SCB, and diametral E*) indicate that there were no major differences in the rutting and cracking performance between the laboratory designed Superpave 5 mixtures (MSP4) and the current Minnesota Superpave 5 (SP5) mixtures.
 5. The Hamburg wheel tracking tests at OMRR show that, except for the MSP44, all other modified mixtures have better rutting resistance than the original SP4 mixtures. The lower rutting resistance of MSP44 might be due to its excessive low air-void ratio, which can be solved by reducing binder content. The IDEAL CT tests at OMRR show that the two of the four modified mixtures (MSP42 and MSP44) have higher CT index values (intermedium-temperature cracking resistance) than the corresponding original mixtures, while the other two modified mixtures (MSP41 and MSP43) have lower CT index values than the corresponding original mixtures.
 6. The laboratory test results of the duplicated mixture (SP44) showed the consistence of the sample preparation between the UMN and OMRR.
 7. Based on the limited laboratory results, the Superpave 5 mix designs, both the MSP4 and SP5 mixtures, in general, performed better in laboratory testing than the traditional Superpave 4 (SP4) mixtures.

Based on the results of this study, Superpave 5 mixtures are expected to perform better compared to the traditional Superpave mixtures, and to have increased resistance to both durability and permanent deformation distresses.

CHAPTER 7: SUMMARY, CONCLUSIONS, AND RECOMMENDATIONS

In this research, Superpave 5 mix designs were developed using locally available materials to improve the field density of asphalt pavements in Minnesota. The field density and material properties of previous projects constructed in 2018 to 2020 were investigated to reveal the current situation of field density in Minnesota. Correlations between field density and material properties were identified from the data. Four traditional mixtures were selected and modified to be Superpave 5 mixtures by adjusting their aggregate gradations. Laboratory performance tests were conducted to check the mechanical properties of the modified mixtures.

In Chapter 2, a comprehensive literature review was performed on the compaction and field density of asphalt mixtures. Factors affecting the compaction of asphalt mixtures and mix design techniques on improving compactability were summarized. Particular attention was given to the Superpave 5 mix design method developed in Indiana. The current specification in Indiana was inspected to identify what changed to make it a Superpave 5 mix design.

In Chapter 3 and 4, field density and material properties data of previous projects were investigated. It was found that field densities of these projects exhibited considerable randomness. They approximately followed normal distributions, while more specifically they exhibited left-skewed and leptokurtic features. The mean field density and standard deviation of the previous projects were about 93.5 % G_{mm} and 1.5 % G_{mm} , respectively. The correlation analysis showed that 1) mixtures with a higher traffic level tended to have lower field density; 2) mixtures with larger aggregate size (NMAS) tended to have lower field density; 3) mixtures harder to compact in the laboratory (designed by higher N_{design}) tended to have lower field density; and 4) mixtures with higher fine aggregate angularity (FAA) tended to have lower field density.

The gyratory compaction tests of loose mixtures from construction projects showed that, regardless of the traffic level, 30 gyrations approximately represented the field compaction effort in Minnesota, and thus can be used as the N_{design} for the Superpave 5 mix design.

In Chapter 5, field density and material properties data of three Superpave 5 projects in Minnesota were studied. It was found that the mean field density of Superpave 5 projects (94.2% G_{mm}) was significantly higher than that of the traditional Superpave mixtures studied in Chapters 3 and 4 (93.5% G_{mm}).

In Chapter 6, four traditional Superpave mixtures were modified to be Superpave 5 mixtures by changing their aggregate gradations, while not increasing their binder contents. Performance tests were conducted by both the University of Minnesota and OMRR on both the original and modified mixtures. It was found that aggregate gradation has a strong effect on the compactability of asphalt mixtures. For the four mixtures studied, it was possible to improve their compactability (reduce the air voids) by increasing the proportion of coarse aggregates without increasing the binder content. Compared to the original Superpave mix designs, the corresponding Superpave 5 mix designs have gradation curves closer to the maximum density line and CA ratios closer to the Bailey method recommended range. The

laboratory tests at the University of Minnesota (Flow number, SCB, and diametral E*) indicated that all the Superpave 5 mixtures have higher rutting and low-temperature cracking resistance than the corresponding original Superpave mixtures. The Hamburg wheel tracking tests at OMRR showed that one of the Superpave 5 mixtures (MSP44) had lower rutting resistance than the corresponding original Superpave mixture (SP44), which was inconsistent with the flow number test results at the University of Minnesota. All other Superpave 5 mixtures performed better in the Hamburg wheel track test than the corresponding original Superpave mixtures. The IDEAL CT tests (at 25 °C) at OMRR showed that two of the four Superpave 5 mixtures (MSP42 and MSP44) had lower CT index values (intermedium-temperature cracking resistance) than the corresponding original Superpave mixtures. In summary, the laboratory testing results showed that in general the Superpave 5 mixtures performed better than the traditional Superpave mixtures.

This research effort validated that mixtures can be designed to be more compactable to become Superpave 5 mixtures by adjusting aggregate gradations. The improved compactability of the mixture did not necessarily adversely affect other mixture performances, e.g., rutting, stiffness, and cracking resistance. In fact, as shown in this study, the other performances, in most cases, also improved with the increase in the compactability of the mixture. Therefore, it was expected that Superpave 5 mixtures can increase field density, as well as other performances (e.g., rutting, stiffness and cracking) of asphalt pavements if implemented.

Although this research demonstrates a feasible approach for designing Superpave 5 mixtures and the potential benefits of implementing the Superpave 5 mix design, we suggest additional future research directions. In terms of the mix design method, the industry is moving toward the performance-based mix design, so it is worth exploring incorporating the Superpave 5 mix design (remaining a volumetric mix design method) into the performance-based mix design method (e.g., the balanced mix design). The performance test results in this study showed discrepancy between the flow number test and the Hamburg wheel tracking test. Therefore, it is worth exploring how to better interpret the results of these test methods.

REFERENCES

- AASHTO R9. (2005). *Standard practice for acceptance sampling plans for highway construction*. Washington, DC: American Association of State Highway and Transportation Officials.
- AASHTO R35. (2019). *Standard practice for superpave volumetric design for asphalt mixtures*. Washington, DC: American Association of State Highway and Transportation Officials.
- AASHTO R62. (2013). *Standard practice for developing dynamic modulus master curves for asphalt mixtures*. Washington, DC: American Association of State Highway and Transportation Officials.
- AASHTO R83. (2017). *Standard practice for preparation of cylindrical performance tests specimens using the superpave gyratory compactor (SGC)*. Washington, DC: American Association of State Highway and Transportation Officials.
- AASHTO T166. (2015). *Standard method of test for bulk specific gravity (G_{mb}) of compacted asphalt mixtures using saturated surface-dry specimens*. Washington, DC: American Association of State Highway and Transportation Officials.
- AASHTO T209. (2011). *Theoretical maximum specific gravity and density of hot mix asphalt (HMA)*. Washington, DC: American Association of State Highway and Transportation Officials.
- AASHTO T304. (2017). *Uncompacted void content of fine aggregate*. Washington, DC: American Association of State Highway and Transportation Officials.
- AASHTO T312. (2017). *Standard method of test for preparing and determining the density of asphalt mixture specimens by means of the superpave gyratory compactor*. Washington, DC: American Association of State Highway and Transportation Officials.
- AASHTO T378. (2017). *Standard method of test for determining the dynamic modulus and flow number for asphalt mixtures using the asphalt mixture performance tester (AMPT)*. Washington, DC: American Association of State Highway and Transportation Officials.
- AASHTO TP105. (2013). *Standard method of test for determining the fracture energy of asphalt mixtures using the semicircular bend geometry (SCB)*. Washington, DC: American Association of State Highway Transportation Officials.
- Anderson, R.M. (2002). *Relationship of superpave gyratory compaction properties to HMA rutting behavior* (Vol. 478). Washington, DC: Transportation Research Board.
- Aschenbrener, T. & Tran, N. (2020). Optimizing in-place density through improved density specifications. *Transportation Research Record*, 2674(3), 211–218.
- Asphalt Institute. (1962). *Mix design methods for asphalt concrete and other hot-mix types*, series No.1. Lexington, KY: Asphalt Institute.

- Asphalt Institute. (1974). *Mix design methods for asphalt concrete and other hot-mix types*, Manual Series No. 2. Lexington, KY: Asphalt Institute.
- ASTM C-29. (2017). *Standard test method for bulk density ("unit weight") and voids in aggregate*, West Conshohocken, PA: American Society for Testing and Materials.
- ASTM D1188. (2015). *Standard test method for bulk specific gravity and density of compacted bituminous mixtures using coated samples*. West Conshohocken, PA: ASTM International.
- ASTM D5821. (2017) *Standard test method for determining the percentage of fractured particles in coarse aggregate*. West Conshohocken, PA: American Society for Testing and Materials.
- Bahia, H. U., & Paye, B. C. (2001). *Minimum pavement lift thickness for superpave mixtures* (No. WHRP 03-02). Madison, WI: Wisconsin Department of Transportation.
- Bahia, H., Fahim, A., & Nam, K. (2006). Prediction of compaction temperatures using binder rheology. *Proc. of the 84th Annual Meeting of the Transportation Research Board*, pp. 3-17.
- Bahia, H., Hanson, D., Zeng, M., Zhai, H., Khatri, M., & Anderson, R. (2001). *Characterization of modified asphalt binders in superpave mix design (NCHRP Report 459)*. Washington, DC: Transportation Research Board. National Research Council.
- Blankenship, P. B., Mahboub, K. C., & Huber, G. A. (1994). Rational method for laboratory compaction of hot-mix asphalt. *Transportation Research Record*, 1454(8), 144–153.
- Brown, E. (1990). Density of asphalt concrete-how much is needed? *Transportation Research Record*, 1282, 27-32.
- Brown, E. R. (1984). Experiences of Corps of Engineers in compaction of hot asphalt mixtures. In *Placement and compaction of asphalt mixtures*. West Conshohocken, PA: ASTM International.
- Brown, E. R., Hainin, M. R., Cooley, L. A., & Hurley, G. (2004). *Relationship of air voids, lift thickness, and permeability in hot mix asphalt pavements* (NCHRP Report 531). Washington, DC: Transportation Research Board. National Research Council.
- Brown, E. R., Prowell, B., Cooley, A., Zhang, J., & Powell, R. B. (2004). Evaluation of rutting performance on the 2000 NCAT test track (with discussion). *Journal of the Association of Asphalt Paving Technologists*, 73, 287-336.
- Burati, J. L., Weed, R. M., Hughes, C. S., & Hill, H. S. (2003). *Optimal procedures for quality assurance specifications*. McLean, VA: Turner- Fairbank Highway Research Center.
- Canestrari, F., Ingrassia, L., Ferrotti, G., & Lu, X. (2017). State of the art of tribological tests for bituminous binders. *Construction and Building Materials*, 157, 718-728.
- Chang, G., Xu, Q., Rutledge, J., Garber, S., & TranstecGroup. (2014). *A Study on intelligent compaction and in-place asphalt density (FHWA-HIF-14-017)*. Washington, DC: Federal Highway Administration.

- Chen, J. (2011). *Discrete element method (DEM) analyses for hot-mix asphalt (HMA) mixture compaction*. PhD diss., Knoxville, TN: University of Tennessee.
- Choubane, B., Gokhale, S., Sholar, G., & Moseley, H. (2006). Evaluation of coarse-and fine-graded superpave mixtures under accelerated pavement testing. *Transportation Research Record, 1974*(1), 120-127.
- Cooley Jr, L., Brown, E. R., & Maghsoodloo, S. (2001). Developing critical field permeability and pavement density values for coarse-graded superpave pavements. *Transportation Research Record, 1761*(1), 41-49.
- Cox, B. C., Howard, I. L., Williams, K. L., & Cooley Jr, L. A. (2015). Asphalt concrete field compactibility models focusing on aggregate properties and moisture. *Transportation Research Record, 2509*(1), 18-28.
- Dessouky, S. (2015). Laboratory and field evaluation of asphalt concrete mixture workability and compactability. In *Airfield and highway pavements* (pp. 97-106). Miami, Florida: American Society of Civil Engineers.
- Dessouky, S., Masad, E., & Bayomy, F. (2004). Prediction of hot mix asphalt stability using the superpave gyratory compactor. *Journal of Materials in Civil Engineering, 16*(6), 578-587.
- Epps, J. A., Gallaway, B. M., & Scott Jr, W. W. (1970). Long-term compaction of asphalt concrete pavements. *Highway Research Record, 313*, 79-91.
- Faheem, A.F., & Bahia, H.U., (2004). *Using the gyratory compactor to measure the mechanical stability of asphalt mixtures* (doctoral dissertation), University of Wisconsin-Madison.
- Federal Aviation Administration. (2013). *Hot mix asphalt paving handbook* (advisory circular 150/5370-14B). Washington, DC: Federal Aviation Administration.
- FHWA. (2000). *Superpave fundamentals reference manual* (NHI Course #131053). Retrieved from <http://www.dot.state.il.us/blr/p028.pdf>
- FHWA. (2010). *Superpave mix design and gyratory compaction levels*. Washington, DC: FHWA.
- Finn, F. N., & Epps, J. A. (1980). *Compaction of hot mix asphalt concrete*. College Station, TX: Texas Transportation Institute, Texas A&M University.
- Gong, F., Liu, Y., Zhou, X., & You, Z. (2018a). Lab assessment and discrete element modeling of asphalt mixture during compaction with elongated and flat coarse aggregates. *Construction and Building Materials, 182*, 573-579.

- Gong, F., Zhou, X., You, Z., Liu, Y., & Chen, S. (2018b). Using discrete element models to track movement of coarse aggregates during compaction of asphalt mixture. *Construction and Building Materials*, *189*, 338-351.
- Graziani, A., Ferrotti, G., Pasquini, E., & Canestrari, F. (2012). An application to the European practice of the Bailey method for HMA aggregate grading design. *Procedia-Social and Behavioral Sciences*, *53*, 990-999.
- Gudimettla, J., Cooley, L., & Brown, E. (2003). *Workability of hot mix asphalt*. Auburn, AL: NCAT.
- Guler, M., Bahia, H. U., Bosscher, P. J., & Plesha, M. E. (2000). Device for measuring shear resistance of hot-mix asphalt in gyratory compactor. *Transportation Research Record*, *1723*(1), 116-124.
- Haddock, J., Rahbar-Rastegar, R., Pouranian, M. R., Montoya, M., & Patel, H. (2020). *Implementing the Superpave 5 asphalt mixture design method in Indiana*. West Lafayette, IN: Purdue University.
- Hanz, A., & Bahia, H. (2013). Asphalt binder contribution to mixture workability and application of asphalt lubricity test to estimate compactability temperatures for warm-mix asphalt. *Transportation Research Record*, *2371*, 87-95.
- Harmelink, D. S., & Aschenbrener, T. (2002). *In-place voids monitoring of hot mix asphalt pavements* (No. CDOT-DTD-R-2002-11). Denver, CO: Colorado Department of Transportation, Research Branch.
- Hekmatfar, A., McDaniel, R. S., Shah, A., & Haddock, J. E. (2015). *Optimizing laboratory mixture design as it relates to field compaction to improve asphalt mixture durability*. Retrieved from <https://doi.org/10.5703/1288284316010>
- Hesami, E., Jelagin, D., Kringos, N., & Birgisson, B. (2012). An empirical framework for determining asphalt mastic viscosity as a function of mineral filler concentration. *Construction and Building Materials*, *35*, 23–29. <https://doi.org/10.1016/j.conbuildmat.2012.02.093>
- Huber, G. (2013). History of asphalt mix design in North America, Part II: Superpave. *Asphalt*, *28*(2), 25-29.
- Huber, G., Haddock, J., Wielinski, J., Kriech, A., & Hekmatfar, A. (2016). Adjusting design air void levels in superpave mixtures to enhance durability. Retrieved from <https://doi.org/10.14311/EE.2016.348>
- Hughes, C.S., (1989). *Compaction of asphalt pavement* (No. 152). Washington, DC: Transportation Research Board. National Research Council.
- Indiana DOT. (2019). *Standard specifications 2020*. Retrieved from: <https://www.in.gov/dot/div/contracts/standards/book/sep19/2020%20INDOT%20Standard%20Specifications.pdf>
- Ingrassia, L., Lu, X., Canestrari, F., & Ferrotti, G. (2018). Tribological characterization of bituminous binders with warm mix asphalt additives. *Construction and Building Materials*, *172*, 309-318.

- Kallas, B., Puzinauskas, V., & Krieger, H. (1962). Mineral fillers in asphalt paving mixtures. *Highway Research Board Bulletin*, 329, 6-29.
- Kataware, A., & Singh, D. (2018). Effects of wax-based, chemical-based, and water-based warm-mix additives on mechanical performance of asphalt binders. *Journal of Materials in Civil Engineering*, 30(10), 4018237.
- Kavehpour, H., & McKinley, G. (2004). Tribo-rheometry: From gap-dependent rheology to tribology. *Tribology Letters*, 17(2), 327-335.
- Khatri, A., Bahia, H., & Hanson, D. (2001). Mixing and compaction temperatures for modified binders using the superpave gyratory compactor (with discussion). *Journal of the Association of Asphalt Paving Technologists*, 70, 368-402.
- Kim, Y., Seo, Y., King, M., & Momen, M. (2004). Dynamic modulus testing of asphalt concrete in indirect tension mode. *Transportation Research Record*, 1891, 163-173.
- Leiva, F., & West, R. C. (2008). Analysis of hot-mix asphalt lab compactability using lab compaction parameters and mix characteristics. *Transportation Research Record*, 2057(1), 89–98. <https://doi.org/10.3141/2057-11>
- Linden, R. N., Mahoney, J. P., & Jackson, N. C. (1989). Effect of compaction on asphalt concrete performance. *Transportation Research Record*, 1217, 20-28.
- Liu, W., Gao, Y., Huang, X., & Li, L. (2020). Investigation of motion of coarse aggregates in asphalt mixture based on virtual simulation of compaction test. *International Journal of Pavement Engineering*, 21, 144-156.
- Marasteanu, M., Buttlar, W., Bahia, H., Williams, C., Moon, K. H., Teshale, E. Z., ... & Kvasnak, A. (2012). *Investigation of low temperature cracking in asphalt pavements national pooled fund study—phase II*. St. Paul, MN: Minnesota Department of Transportation.
- Marasteanu, M., Le, J.-L., Hill, K., Yan, T., Man, T., Turos, M., Barman, M., Arepalli, U. M., & Munch, J. (2019). *Experimental and computational investigations of high-density asphalt mixtures*. St. Paul, MN: Minnesota Department of Transportation.
- McDaniel, R. S. (2019). *Impact of asphalt thickness on pavement quality. Impact of asphalt thickness on pavement quality*. Retrieved from <https://doi.org/10.17226/25498>
- McDaniel, R. S., Leahy, R. B., Huber, G. A., Moulthrop, J. S., & Ferragut, T. (2011). *The superpave mix design system: Anatomy of a research program*. Retrieved from <https://doi.org/10.17226/22812>
- Minnesota DOT. (2018). *Standard specification for construction 2360, 2018 edition*. St. Paul, MN: MnDOT.

- Mo, L., Li, X., Fang, X., Huurman, M., & Wu, S. (2012). Laboratory investigation of compaction characteristics and performance of warm mix asphalt containing chemical additives. *Construction and Building Materials*, 37, 239-247.
- Moutier, F. (1974). La presse a cisaillement giratoire-modele de eerie. *Bull Liaison Lab Ponts Chauss*, 74, 37-48.
- Pine, W.J. (1997). *Superpave gyratory compaction and the N_{design} table*. Springfield, IL: Illinois Department of Transportation.
- Prowell, B. D., & Brown, E. R. (2007). *Superpave mix design: Verifying gyration levels in the N_{design} table* (Vol. 573). Washington, DC: Transportation Research Board.
- Prowell, B. D., Zhang, J., & Brown, E. R. (2005). *Aggregate properties and the performance of superpave-designed hot mix asphalt* (Vol. 539). Washington, DC: Transportation Research Board.
- Retzer, N. (2008). *Permeability research with the ROMUS air permeameter* (Report CDOT-2008-5). Denver, CO: Colorado Department of Transportation.
- Shamsi, K., & Mohammad, L.N. (2010). Estimating optimum compaction level for dense-graded hot-mix asphalt mixtures. *The Journal of Engineering Research*, 7(1), 11-21.
- Shenoy, A. (2001). Determination of the temperature for mixing aggregates with polymer-modified asphalts. *International Journal of Pavement Engineering*, 2(1), 33-47.
- Stakston, A., Bahia, H., & Bushek, J. (2002). Effect of fine aggregate angularity on compaction and shearing resistance of asphalt mixtures. *Transportation Research Record*, 1789, 14-24.
- Stakston, A. D., & Bahia, H. U. (2003). *The effect of fine aggregate angularity, asphalt content and performance graded asphalts on hot mix asphalt performance* (Vol. 92, No. 45-98). Madison, WI: Wisconsin Highway Research Program.
- Stroup-Gardiner, M., Newcomb, D. E., Olson, R., & Teig, J. (1997). Traffic densification of asphalt concrete pavements. *Transportation Research Record*, 1575(1), 1-9.
- Tang, Y., & Haddock, J. (2006). Field testing of the zero-shear viscosity method. *Factors Affecting Compaction of Asphalt Pavements, Transportation Research Circular, Number E-C105*, 18-26.
- Tarefder, R., & Zaman, M. (2002). Evaluation of rutting potential of hot mix asphalt using the asphalt pavement analyzer. Oklahoma City, OK: Oklahoma Department of Transportation.
- US Army Corps of Engineers. (2000). *Hot-mix asphalt paving handbook 2000*. Washington DC: U.S. Army Corps of Engineers. Retrieved from <http://www.worldcat.org/title/hot-mix-asphalt-paving-handbook-2000/oclc/47222499>

- Vavrik, W. R., Huber, G., Pine, W. J., Carpenter, S. H., & Baliey, R. (2002). Bailey method for gradation selection in hot-mix asphalt mixture design (Transportation research e-circular). Washington, DC: Transportation Research Board.
- Vavrik, W. R., & Carpenter, S. H. (1998). Calculating air voids at specified number of gyrations in Superpave gyratory compactor. *Transportation Research Record*, 1630(1), 117-125.
- Vivar, E. D. P., & Haddock, J.E. (2006). *HMA pavement performance and durability* (No. FHWA/IN/JTRP-2005/14). West Lafayette, IN: Joint Transportation Research Program, Indiana Department of Transportation and Purdue University
- VÖGELE. (2018). Retrieved from <https://www.voegele.info/en/technologies/screed-technology/hochverdichtungstechnologie.html>
- Wang, H., Al-Qadi, I., Faheem, A., Bahia, H., Yang, S.-H., & Reinke, G. (2011). Effect of mineral filler characteristics on asphalt mastic and mixture rutting potential. *Transportation Research Record*, 2208(1), 33-39.
- West, R., Rodezno, C., Leiva, F., & Taylor, A. (2018). *Regressing air voids for balanced HMA mix design*. Madison, WI: Wisconsin Highway Research Program.
- West, R., Rodezno, C., Leiva, F., & Yin, F. (2018). *Development of a framework for balanced mix design* (Project NCHRP, 20-07). Washington, DC: Transportation Research Board. National Research Council.
- White, T. D. (1985). Marshall procedures for design and quality control of asphalt mixtures. In *Association of Asphalt Paving Technologists Proceedings, Vol. 54*.
- Williams, K. L., Cox, B. C., Howard, I. L., & Cooley Jr, L. A. (2015). Models of asphalt concrete field compactibility with focus on lift thickness. *Transportation Research Record*, 2504(1), 135-147.
- Willoughby, K., & Mahoney, J. P. (2007). *An assessment of WSDOT's hot-mix asphalt quality control and assurance requirements* (WA-RD 517.2). Olympia, WA: Washington State Department of Transportation.
- Yan, T., Ingrassia, L. P., Kumar, R., Turos, M., Canestrari, F., Lu, X., & Marasteanu, M. (2020). Evaluation of graphite nanoplatelets influence on the lubrication properties of asphalt binders. *Materials*, 13(3), 772.
- Yan, T., Marasteanu, M., & Le, J.-L. (2021a). Mechanism-based evaluation of compactability of asphalt mixtures. *Road Materials and Pavement Design*, 22(sup1), S482–S497.
- Yan, T., Marasteanu, M., & Le, J.-L. (2022a). One-dimensional nonlocal model for gyratory compaction of hot asphalt mixtures. *Journal of Engineering Mechanics*, 148(2), 04021144.
- Yan, T., Marasteanu, M., Bennett, C., & Garrity, J. (2021b). Field density investigation of asphalt mixtures in Minnesota. *Transportation Research Record*, 2675, 1670–1680.

- Yan, T., Turos, M., Bennett, C., Garrity, J., & Marasteanu, M. (2022b). Relating Ndesign to field compaction: A case study in Minnesota. *Transportation Research Record*, 2676:192-201.
- Yan, T., Le, J.-L., Marasteanu, M., & Turos., M. (2022c). A probabilistic model for field density distribution of asphalt pavements. *International Journal of Pavement Engineering* (under review).
- Yeung, E., Braham, A. and Barnat, J. (2016). Exploring the effect of asphalt-concrete fabrication and compaction location on six compaction metrics. *Journal of Materials in Civil Engineering*, 28(12), 04016163
- Yildirim, Y., Ideker, J., & Hazlett, D. (2006). Evaluation of viscosity values for mixing and compaction temperatures. *Journal of Materials in Civil Engineering*, 18(4), 545-553.
- Yildirim, Y., Solaimanian, M., & Kennedy, T. (2000). Mixing and compaction temperatures for superpave mixes. *Asphalt Paving Technology: Association of Asphalt Paving Technologists-Proceedings of the Technical Sessions*, 69, 34-71.